THERMODYNAMIC CALCULATION OF MULTICOMPONENT PHASE COMPOSITIONS

by

Rong Liu

Submitted in partial fulfilment of the requirements
for the degree of Master of Science

at

Dalhousie University
Halifax, Nova Scotia
August 2014

TABLE OF CONTENTS

LIST OF TABLES

LIST OF FIGURES

ABSTRACT

Food industry scientists need to predict multicomponent solid fat compositions because fat solid solutions define food texture and physical properties.

Experiments were conducted with two multicomponent fats of known composition to determine solid fraction (via NMR), phase fraction, polymorphic form (via XRD) and thermal melting profile (via DSC). A database including melting temperature and enthalpy was digitized. Wesdorp's methodology, implemented in MATLAB, was used to estimate the equilibrium mole fractions of each phase. The program estimates melting temperatures and enthalpies absent from the database, and estimates interaction parameters for a 2-suffix Margules model. These parameters were used to find the composition at equilibrium for each phase. The estimated overall melting enthalpy of the mixtures was compared to the value obtained by DSC.

The predicted temperature values using Wesdorp's coefficients were unsatisfactory; hence an alternative approach was developed. The estimated overall melting enthalpies agreed well with the experimental enthalpies.

LIST OF ABBREVIATIONS AND SYMBOLS USED

A_f	The integrated intensity of phase f, n.d
d	The lamellar spacing of crystal planes (nm)
DSC	Differential scanning calorimetry
FA	Fatty acid
g_E	The excess Gibbs energy (J)
h_0	Enthalpy contribution of the head and end group (J/mol)
k_i	The temperature constant (thermal factor) of component i, n.d
K_f	The proportional factor of phase f, n.d
n_c	The carbon numbers of TAG
n_D	The number of Elaidic chains
n_{DD}	The number of Elaidic - Elaidic pairs
n_J	The number of Linoleic chains.
n_{JJ}	The number of Linoleic - Linoleic pairs
n_{JN}	The number of Linoleic - Linolenic pairs
n_N	The number of Linolenic chains
n_{NN}	The number of Linolenic - Linolenic pairs
n_O	The number of Oleic chains
n_{OJ}	The number of Oleic- Linoleic pairs
n_{ON}	The number of Oleic- Linolenic pairs
n_{OO}	The number of Oleic- Oleic pairs
R	Universal gas constant, 8.314 J/(mol·K)
RBD394	Refined, bleached and deodorized fat, includes 30 TAGs
RBD470	Refined, bleached and deodorized fat, includes 22 TAGs

s_0	Entropy contribution of the head and end group (J/(mol·K))
SFC	Solid fat content (%)
S_f	Mass fraction of phase f, n.d
SXRD	Small-angle x-ray diffraction
T	The temperature of the material (K)
T_{fi}	The melting temperature of a solid TAG i in a particular polymorphic form (K)
v_{non}	The volume of the non-overlapping parts of TAGs (nm^3)
v_o	The volume of the overlapping parts of TAGs (nm^3)
WXRD	Wide-angle x-ray diffraction
x_{if}	The mole fraction in terms of component i in phase *f*
y_i	The mole fraction in terms of component i in liquid phase
XRD	X-ray diffraction
z_i	The overall mass of component i
Δc_{Pi}	Heat capacity difference between the liquid and the solid of component i (J/(mol·K))
ΔH_{fi}	The heat of fusion of the TAG polymorph of component I (J/mol)
ΔH	Enthalpy change at constant temperature and pressure (J/mol)
ΔS	Entropy change at constant temperature and pressure (J/(mol·K))
γ_i^p	The activity coefficient of component i in phase p
μ_i^p	Chemical potential of component i in phase p (J/mol)
ε	The degree of isomorphism, n.d
θ	The scattering angle (°)
λ	The wavelength of x-ray (nm)
φ_{ij}	The interaction parameter between components i and j

Fatty acids in order of carbon number and saturation:

U	Butyric	4:0
K	Caproic	6:0
R	Caprylic	8:0
C	Capric	10:0
L	Lauric	12:0
M	Myristic	14:0
P	Palmitic	16:0
S	Stearic	18:0
A	Arachidic	20:0
B	Behenic	22:0
G	Lignoceric	24:0
F	Ceric	26:0
T	Palmitoleic	16:1
O	Oleic	18:1
J	Linoleic	18:2
N	Linolenic	18:3
D	Elaidic	18:1 trans
E	Erucic	22:1ω9
H	Arachidonic	20:4(ω-6)

ACKNOWLEDGMENTS

I would like to gratefully acknowledge my supervisor Dr. Gianfranco Mazzanti who offered his encouragement, guidance, inspiration, enthusiasm and patience to help me finish this project. Deepest gratitude is also due to my co-supervisor Dr. Alejandro G. Marangoni, who offered his guidance and assistance to this work, and other members of the supervisory committee Dr. Stephen Kuzak and Dr. Jan Haelssig, for their review of my Thesis. I also want to thank my group colleagues: Omar Al-Qatami, Amro Al-Khudiar, Pavan Karthik Batchu, Mohit Kalaria, Pranav Arora, Liangle Lin, Xiyan Deng, Yujing Wang, your very insightful discussions and support made this work possible and enjoyable. To Dr. Wesdorp for his previous work.

My deepest gratitude and acknowledgement to my parents, who bore me, raised me, supported me, taught me, and loved me. Words cannot express how much I thank to you and love you.

Thanks to Edmund Co, for his work on SFC measurements.

I also would like to thank all my friends, no matter where you are, your support and love is always with me.

Chapter 1. INTRODUCTION

Solid solutions, also wrongly called mixed crystals (Breitschuh & Windhab, 1998), are very common in material science and food science (Hollingsworth, 2002). However, multicomponent crystals are far less common. Due to the large variety of triglyceride molecules that are, nonetheless, similar, fats do commonly form multicomponent crystals. The behavior of fat crystallization depends on the composition of fats, due to the different molecular interactions, and upon crystallization conditions, chiefly temperature and shear history. The prediction of fat crystallization behavior is very important in the food industry. For instance, changing the fat composition and cooling rate will alter the texture and mouth feel of the food.

Fat consists mostly of triacylglcerols (TAGs) and minor amounts of other lipids. TAGs exhibit polymorphism in the solid phase. There are three main polymorphs: α, β', β. Previous research by Wesdorp (1990, published in 2013) was done to formulate a predictive model for melting range, solid phase composition and crystallization behavior of fats in equilibrium. He compiled a comprehensive database of thermal properties, and developed the bases for liquid – multiple solid phase equilibria in fat. Los and Flöter (1999), based on Wesdorp's work, created a kinetic-equilibrium model to describe the crystallization process in binary mixtures of fats away from equilibrium. Furthermore,

Los, van Enckevort and Vlieg (2002) extended the model for multicomponent fat systems.

In this thesis, part of Wesdorp's method for multicomponent systems was tested. The study focuses on two parts of the method; one is used to estimate the thermodynamic properties of TAGs for which there are no experimental data, and the other is used the to predict the crystallization behavior in equilibrium from thermodynamic properties. Two commercial samples were provided by a company that is interested in their thermodynamic properties. Those two samples contain different number and kinds of TAGs; however, they produce similar solid fat content (SFC) curves developed following the AOCS method **(**AOCS Cd 16b-93 revised in 2000; Direct Method**)**. In the food industry, SFC is an essential value during creates fat formulation. Therefore, for economic and health concerns, it is important to study why different TAGs blends can produce similar SFC curves in the food industry. For instance, some cheap fats may be used to replace expensive fats, or add high concentration of healthy fats (such as EPA, DHA) and remove trans-fats to improve the food quality, without changing the processing conditions and performance of the final products.

In this thesis, four key parts of Wesdorp's broad liquid-multiple solid research were extracted and interpreted. Wesdorp's experimental enthalpy and melting point data of

pure TAGs were extracted and digitized into a database. The enthalpy and melting temperature of three polymorphs of the pure TAGs in the samples were either found in the database or estimated using Wesdorp's method. Another part of Wesdorp's method was interpreted and used to estimate the interaction parameters and activity coefficients. The thermodynamic properties were applied to the calculation of the composition in each phase and of the overall melting enthalpy, following a method developed from Wesdorp's work. The method's accuracy was verified by comparing overall crystallization enthalpy with the experimental crystallization data.

Mathematical modeling is a common and efficient method to describe physical phenomena and to predict the molecular behavior of materials. MATLAB was chosen for this work, because it is a numerical computing environment and high level programming language, widely used to implement theoretical developments. Using MATLAB it was possible to complete some very complex mathematic calculations (matrices, non-linear systems of equations, etc,). Within the MATLAB environment it is possible to develop stand-alone user-friendly software. The current work is a core precursor for those applications.

1.1. Objectives

It is important to predict the crystallization behavior of multiple fat systems in food industry applications. However, both equilibrium and kinetic models are time consuming to understand for plant managers and engineers. The main objective of this research is to extract, interpret and implement Wesdorp's thermodynamic work, so that it can be incorporated in future user-friendly software. In order to achieve this, the following specific objectives were defined:

1) Digitize a database that includes the physical properties of pure TAGs such as melting temperature and enthalpy of crystallization of different polymorphs.
2) Include predictive tools for thermodynamic properties when not available.
3) Create MATLAB code to estimate the interaction parameters.
4) Calculate the mass fraction of each component in each phase.
5) Extend the model to solve the problem of same polymorph in different phases.
6) Verify the accuracy of Wesdorp's model using overall melting enthalpy.

Chapter 2. LITERATURE REVIEW

2.1. Lipids and fats

Lipids are "fatty acids and their derivatives, and substances related biosynthetically or functionally to these compounds" (Christie, 2003). Lipids are classified into two broad categories: simple lipids, which contain only two types of compounds, one of which is usually a fatty acid (e.g., triglycerides, wax); and complex lipids, which contain three or more types of compounds (e.g., phospholipids) (Christie, 2003). Fats are subgroups of lipids, and the main source of lipids and fats are vegetable and animal oils. Lipids and fats have a wide application in the food, cosmetics and pharmaceuticals industries (Sato, 2001) .

2.2. Triglycerides (TAGs)

Triacylglycerols are the main constituents of natural fats and oils (Szydłowska-Czerniak, Karlovits, Lach, & Szłyk, 2005). They consist of three fatty acids esterified to the three alcohol groups of a glycerol, and the locations of the fatty acids are referred to as sn-1, sn-2, sn-3. According to the number of fatty acids esterified, lipids are classified as monoacyglycerols, diacyglycerols and triacylglycerols (Marangoni et al., 2012). Due to the difference of the fatty acids, TAGs can also be classified as saturated and unsaturated.

The saturated TAGs do not contain double bonds and they are more abundant in animal fats; the unsaturated TAGs are usually extracted from plants. The typical structure of TAG is shown in Figure 2- 1. Natural lipids usually are a mixture of a wide range of TAGs. Milk fat, for instance, contains more than 200 molecular species (Marangoni & Lencki, 1998).

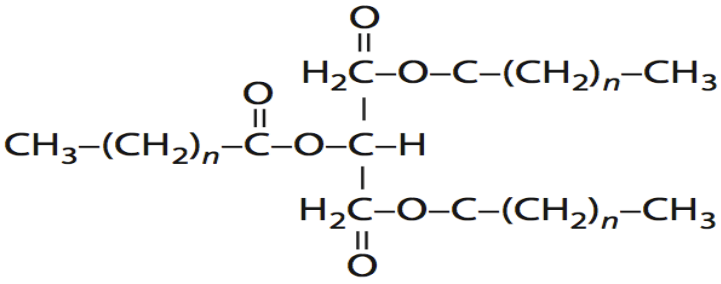

Figure 2- 1. The structure of a typical saturated triacylglycerol molecule (Marangoni & Wesdorp, 2013)

2.3. Fat crystallization

Fat crystallization has two main applications in the food industry; one is to process fat crystal containing products, such as chocolates and margarine; the other one is to separate specific fats and liquid materials from natural resources (Sato, 2001; Ueno, Ristic, Higaki, & Sato, 2003). Fat crystallization is a process in which fat molecules rearrange themselves to form a solid lattice crystal from a supersaturated liquid or solution. Supersaturation is a state of a solution with a concentration that is larger than the solubility concentration, and supercooling is the process of lowering the temperature

below the melting point; both of them are driving forces for crystallization (Liang, Shi, & Hartel, 2003). At low supercooling, the driving force of crystallization is small, so the crystallization process time increases, and vice versa (Breitschuh & Windhab, 1998).

Fat crystallization is a kinetic process in which the lipid melt must be significantly supercooled in order to start crystallization. Liquid metastable phase is a state in which lipids are supercooled but not crystallized and it is related to the induction time for onset of nucleation (Liang et al., 2003). The speed of fat crystallization is primarily determined by the rate of nucleation. During nucleation, the molecules of the melted fats will arrange themselves to form stable clusters that eventually form crystal lattice structures (Garti & Sato, 2001; Marangoni et al., 2012). Rapid cooling of the liquid fat normally causes the formation of less organized (more loosely packed) crystals due to the lack of time for molecules to rearrange themselves. On the other hand, slower cooling tends to form more ordered (more tightly packed) crystals (Karray, Lopez, Lesieur, & Ollivon, 2005). In the metastable state, the crystallization can occur due to the presence of foreign nuclei, this phenomenon is known as heterogeneous nucleation, and the foreign nucleus serves as a 'catalyst' in the crystallization process (Winkler & Singer, 1972). TAG crystals are made by the stacking of molecular layers, the thickness of which depends on the length and unsaturation of the fatty acid chains and their angle of tilt with respect to the basal planes formed by the methyl end groups of the TAGs (Lopez, Lesieur, Keller, & Ollivon, 2000).

Acevedo and Marangoni (2010) summarized the different levels of structure of a bulk fat, including its nanostructure, in the illustration reproduced in Figure 2- 2.

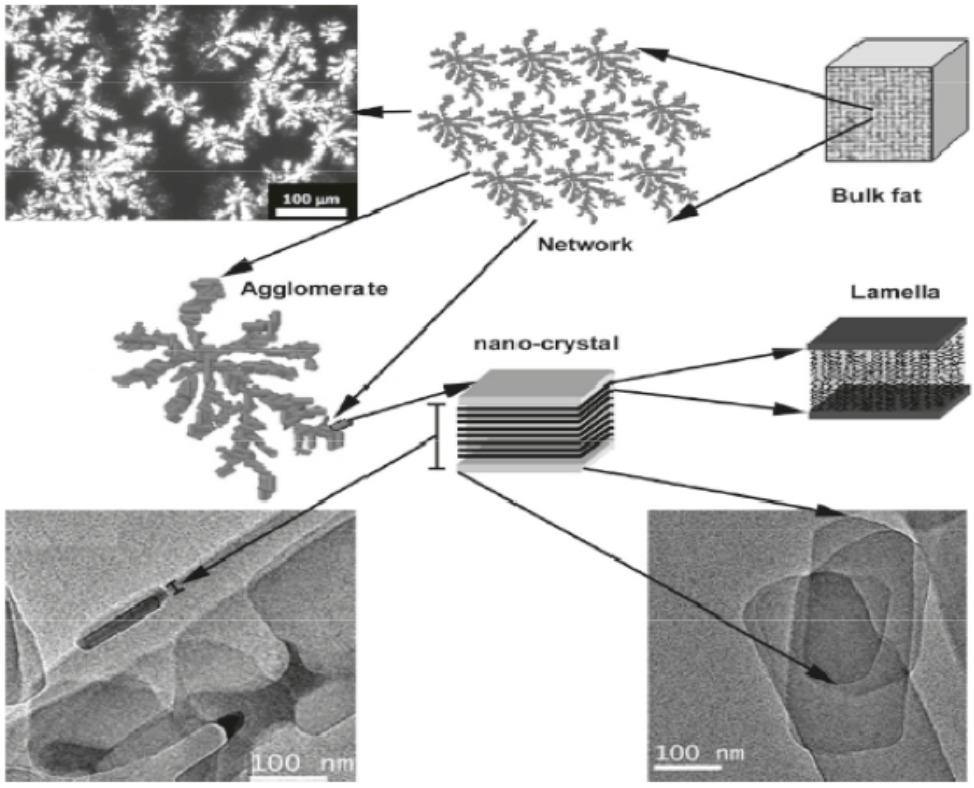

Figure 2- 2. Schematic representation of the different levels of structure in a bulk fat (Acevedo & Marangoni, 2010). (Permission has been obtained by ACS).

Both thermodynamic and kinetic information need to be considered in order to gain a full understanding of fat crystallization behavior, and it is useful to be able to classify behaviors according to whether they are controlled by thermodynamics, kinetics or both. Thermodynamic studies start with finding the polymorphic form, and then determine the stability and miscibility of TAGs in a mixed crystal system. Kinetic studies allow us to explain the timescale problems (Himawan, Starov, & Stapley, 2006). This study focuses

on predicting composition of each phase based on the thermodynamics of the fats crystallization.

2.4. Polymorphism

Polymorphism is the arrangement of the molecules within a crystal lattice in a number of different ways of packing (Lopez, Lavigne, Lesieur, Bourgaux, & Ollivon, 2001). The different chain packing sub-cells in TAGs are classified into three main types of crystalline modification: α, β', β forms. Their corresponding sub-cell structures are the hexagonal (H) for α, triclinic (T //) for β and orthorhombic perpendicular (O ⊥) for β ' (Piska, Zárubová, Loužecký, Karami, & Filip, 2006; Sato, 2001). The three acyl chains of TAG can pack themselves in either a double or triple chain length structure (see Figure 2-3a) and this stack arranges itself side by side to form a crystal plane, known as crystalline lamella. TAGs with three similar acyl chains are usually formed into a double chain length structure, while TAGs with large difference in acyl chains, such as chain length and chemical structure, tend to form a triple chain length structure (Sato, 1999). The sub-cell structures of the different polymorphs are easy to understand if observed from the top of the crystal plane (Figure 2- 3b) (Himawan et al., 2006).

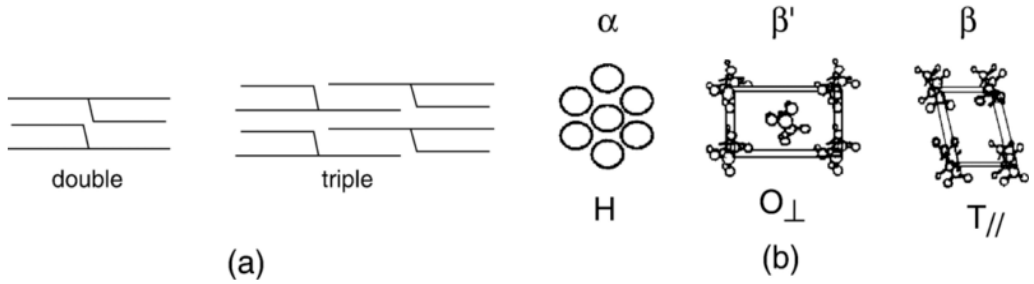

Figure 2- 3(a). Chain-length packing structure in TAG. (b). The polymorph sub-cell structure (Himawan et al., 2006). (Permission has been granted by Elsevier).

The α-form has the lowest density, melting point and enthalpy, and it is the least stable polymorph, while the β-form has the highest density, melting point and enthalpy, and is the most stable polymorph; the stability and the values of the same three physical properties of the β' polymorph are between α and β-form (Lopez, Lavigne, Lesieur, Bourgaux, et al., 2001; Piska et al., 2006).

TAG molecules tend to form the most suitable and stable sub-cell and arrange to accomplish the most efficient close-packing (Marangoni & Wesdorp, 2013). The α and β' polymorphic forms are metastable phase. Therefore, the polymorphic transitions happen from less stable polymorphic forms to more stable polymorphic forms (Ostwald's step rule); the crystallization process is from α to β. The recrystallization of a more stable phase after melting of a less stable phase can reduce the total activation energy of polymorphic transition if the liquid retains some organization (Sato, 1993). Figure 2- 4 shows that the polymorphic transition within the solid phase occurs from α to β' and β or

α to β, and all the polymorphic forms can be directly crystallized from a hypothetical liquid crystal structure (Himawan et al., 2006; Sato, 1993).

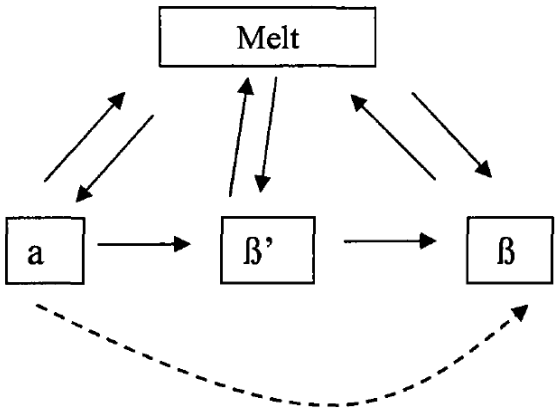

Figure 2- 4. Polymorphic transition pathway in fat (Marangoni & Wesdorp, 2013)

2.5. Techniques used in fat crystallization studies

Basic methods for studying the crystallization of fats include both thermal and optical analytical methods. Differential scanning calorimetry (DSC), x-ray diffraction (XRD), nuclear magnetic resonance (NMR), neutron diffraction, infrared absorption spectroscopy and polarized light microscopy (PLM) are typical techniques used to study the crystallization and polymorphism of TAGs and their mixtures over the past several decades (Sato, 2001). In this research, DSC experiments were performed to measure the isothermal crystallization and subsequent melting heat flow as a function of temperature and calculate the overall melting enthalpy for each holding temperature. Both small-angle and wide-angle XRD experiments were conducted in our in-house x-ray system to

determine the number of phases and type of phases. The solid fat content (SFC) of the samples was measured by using NMR and was provided by Dr. Alejandro G. Marangoni.

2.5.1. Differential Scanning Calorimetry (DSC)

DSC is a widely used technique to study the thermal properties of materials and investigate the transition between crystal forms during a melting or cooling process (Lopez et al., 2002; Szydlowska-Czerniak, Karlovits, Lach, & Szlyk, 2005; Vereecken, Graef, Smith, Wouters, & Dewettinck, 2010). It is a useful tool to study both the thermodynamics and the kinetics of the crystallization process. For thermodynamic studies, DSC can produce the melting and crystallization temperature profiles, heat capacities, phase diagrams and the heat transition information during heating or cooling of the samples. Moreover, it can sometimes identify the polymorphic form by a subsequent melting of the crystallized fats. DSC is able to provide accurate and reproducible support data for kinetic studies (MacNaughtan, Farhat, Himawan, Starov, & Stapley, 2006). DSC combines three strategies to measure thermal properties: it controls temperature directly; it uses a small sample size to limit the influence of foreign nuclei on crystallization; and it measures free from mechanical effects (Foubert, Dewettinck, & Vanrolleghem, 2003).

2.5.1.1. The principle of DSC

DSC estimates the difference between the amounts of heat required to change the temperature of the sample and of the reference pan. This is done by accurately measuring the voltage difference between two thermocouples: one is placed under the sample pan, and the other is under the reference empty pan. The results of the DSC experiment are the difference of heat flow between the sample and reference pans as a function of time and temperature. During the experiment, the sample and reference pans are maintained at nearly the same temperature, but the heat flow into the pans is different. More (or less) heat flow into the sample means there is an endothermic (or exothermic) process. With the DSC heat flow curves, the crystallization, polymorphic transition, and melting of the polymorphs can be observed (Verdonck, Schaap, & Thomas, 1999).

2.5.2. X-ray Diffraction (XRD)

XRD is a widely used method to identify the molecular structure of fat crystals and to detect phase transition phenomena of TAG polymorphic forms (Szydlowska-Czerniak et al., 2005). The first x-ray experiments on edible fats to gain a better understanding of fat crystal polymorphic behavior under different process conditions were done by Kellens & Ollivon, after that many XRD experiments of fats have been done (Cisneros, Mazzanti, Campos, & Marangoni, 2006; Loisel, Keller, Lecq, Bourgaux, & Ollivon, 1998; Lopez et al., 2002; Lopez, Lesieur, Bourgaux, Keller, & Ollivon, 2001; Mazzanti, Marangoni, &

Idziak, 2009; Szydlowska-Czerniak et al., 2005).

2.5.2.1. The principle of XRD

When a beam of x-rays falls on a sample, the x-rays are scattered by the crystals in the sample due to the interactions with electrons. These scattered beams produce a diffracted beam due to interference. The x-rays coming out of the sample produce constructive interference at specific angles, depending on the structure of the crystals. Different polymorphic forms produce interference at different angles of the diffracted beam, and the detected position and strength of these beams is called the diffraction pattern. Therefore, by measuring the diffraction patterns, the polymorphic form of the sample can be determined (Mazzanti, Marangoni, & Idziak, 2005). For a given set of lattice planes, Bragg's law (Bragg, 1913) describes the relation between wavelength λ, an inter-plane distance d and the scattering angle θ (see Figure 2- 5 and Eq.1).

$$\lambda = 2d \sin\theta \qquad \text{Eq.1}$$

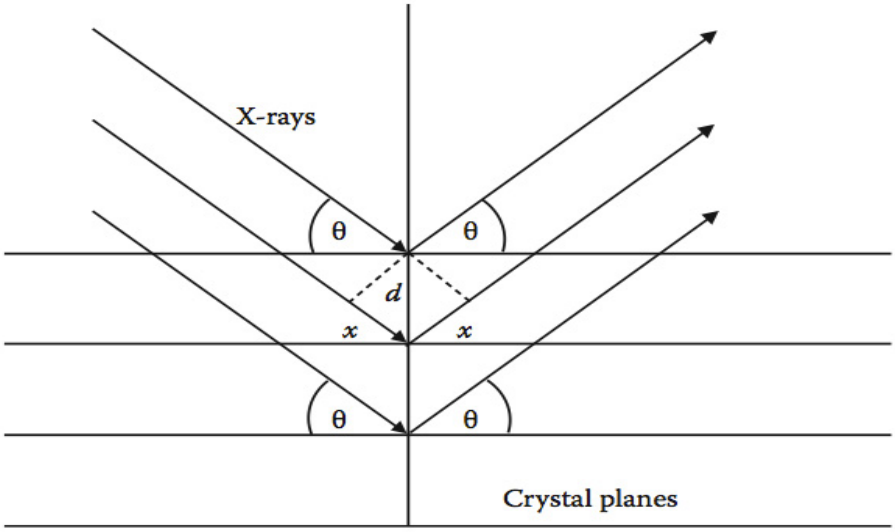

Figure 2- 5. Geometry of the reflection of x-rays from crystal planes used in the derivation of Bragg's law (Marangoni & Wesdorp, 2013)

The experiments to detect the scattering angle in the range $0^{\circ} < \theta < 5^{\circ}$ are small-angle diffraction (SXRD) experiments and the d-spacings correspond to TAG longitudinal stacking (long spacing). The range of scattering angles for wide-angle diffraction experiments (WXRD) is $8.5^{\circ} < \theta < 13^{\circ}$, which can detect the cross-sectional packing of the aliphatic chains (short spacing). WXRD is widely used for identifying the various crystalline subcells (Lopez, Lavigne, Lesieur, Keller, & Ollivon, 2001; Lopez et al., 2002; Lopez, Karray, Lesieur, & Ollivon, 2005).

Polymorphism results from the different possibilities of lateral packing of the fatty acid chains and from the longitudinal stacking of molecules in lamellae, which can be easily identified by WXRD and SXRD respectively (Lopez, Lavigne, Lesieur, Bourgaux, et al.,

2001; Lopez et al., 2000). In WXRD patterns, the α-form is characterized by one strong wide- angle peak in the XRD pattern near 0.42 nm. The β′-form is characterized by two strong wide-angle peaks at 0.37–0.40 nm and at 0.42–0.43 nm. The β-form is characterized by a strong wide-angle peak near 0.46 nm and a number of other peaks around 0.36–0.39 nm (Himawan et al., 2006).

2.5.2.2. Proportionality factor calculation

The area under the XRD peak is called integrated intensity and it is proportional to the crystallinity of the sample (Cisneros et al., 2006). A proportionality factor K_f is used to describe the proportion between the SFC of each solid phase and the area under the SXRD peak. Because each SXRD peak comes from a different phase, the proportionality factor between area and mass may not be the same (see Figure 2- 6). Hence the area fraction of a peak does not necessarily correspond to the mass fraction of phase that produced it. The factor can be estimated using the SXRD integrated intensity and SFC in Eq.2, (Cisneros et al., 2006; Mazzanti, Li, Marangoni, & Idziak, 2011). The size of the capillary tube containing the sample might affect the integrated intensity and value of the proportionality factor. Therefore, in this thesis two different groups of proportionality factors for each sample were calculated, because there were two capillaries for each sample.

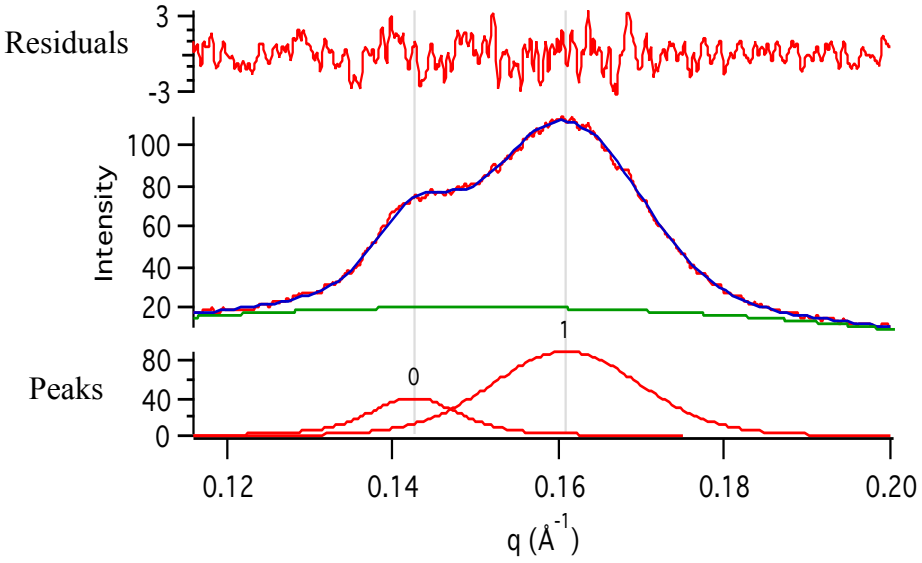

Figure 2- 6. Example of SXRD peak areas

$$SFC = \sum K_f \cdot A_f \qquad \text{Eq.2}$$

With the proportionality factor of each phase and SFC, the mass fraction of each phase at different temperatures can be calculated.

$$Mass\ fraction\ S_f = \frac{A_f \cdot K_f}{SFC} \qquad \text{Eq.3}$$

f represents each different phase, A_f is the integrated intensity of phase *f*.

2.5.2.3. Previous work using DSC and XRD

In order to study the effect of the cooling rate on the hardness of a fat crystal network, DSC was used to monitor the melting process, and XRD was used to determine the

polymorphic forms of the sample (Campos, Narine, & Marangoni, 2002). Cisneros et al. (2006) used XRD to study the polymorphic transformation in mixtures of high- and low-melting fractions of milk fat, and found that the polymorphic transition to β′-form was delayed in the absence of liquid fat. Sato & Ueno (2011) used synchrotron radiation microbeam XRD to study polymorphic structures, kinetic and microscopic properties of fat crystals in colloidal dispersion states. Another study using DSC (MacNaughtan et al., 2006) looked at the isothermal crystallization and subsequent melting of tripalmitin-tristearin mixtures covering all the composition range. They found that forming a more stable polymorph required a higher crystallization driving force for nucleation to occur. However, DSC may not provide a clear identification of polymorphic form, especially for the multicomponent systems where each component has a different melting point (MacNaughtan et al., 2006); therefore, the DSC and XRD experiments are usually conducted for the same sample in order to determine an accurate polymorphic form. In recent years, combined DSC and XRD have found wide application in fat crystallization research, and this technique allows users to relate the structural change to the thermal transition of crystallization behavior.

Lopez et al. (2000) used a new technique to perform XRD and DSC simultaneously to detect unstable species of cream. Lopez et al. (2002) used the same coupled instruments to study the crystal formation during the slow cooling of natural milk fat globules of

cream and found that the progressive transformations of the crystalline varieties correlated with endotherms and exotherms recorded by DSC. By coupling DSC and XRD, Michalski, Ollivon, Briard, Leconte, & Lopez, (2004) found that the size of the native milk fat globules did not have a large influence on crystalline structure. Using DSC and XRD, the crystallization behavior of crude palm oil was studied and the results revealed that the β' and β polymorphs coexist during slow cooling and there were four or five phases coexisting depending on the temperature (Chong et al., 2007). Karray et al., (2005) also used the coupling of DSC and XRD to study the thermal and structural behavior of dromedary milk fats.

DSC and XRD also have a wide application in modeling fat crystallization behavior. The melting profile and heat of fusion was measured by DSC and compared with calculated results for modeling the solubility of high-melting fats in low-melting fats (Zhou & Hartel, 2006).

2.6. Fat crystallization models

Some studies have tried to develop models to describe both thermodynamics and kinetics of the fat crystallization process (Kloek, Van Vliet, & Walstera, 2005; Lopez et al., 2001; Marangoni & Wesdorp, 2013; Rousset, Rappaz, & Minner, 1998). These models are

proposed to estimate the equilibrium compositions of each phase, the crystallization onset times, SFC, and other crystallization thermal and kinetic properties. The main objective of this research is to test Wesdorp's thermodynamic model; therefore, the following parts are an introduction of Wesdorp's model and brief summary of previous modeling research.

2.6.1. Wesdorp's model

Wesdorp developed his thermodynamic model in his PhD thesis in 1990. This thesis was published with many publishing errors as a chapter in a book edited by Marangoni (2005), *Fat Crystal Networks*. An improved version was published in the book edited by Marangoni & Wesdorp (2013) *Structure and Properties of Fat Crystal Networks*. There are many facets of Wesdorp's research, however, only the four parts of his work that related to this project were extracted and interpreted. In this thesis Wesdorp's experimental data of enthalpy and melting point of pure TAGs were digitized into a database for further application. For TAGs without available experimental thermodynamic information, Wesdorp developed a method to estimate the enthalpy and melting point of pure TAGs. He then used Margules's theory from liquid-vapor equilibrium (Margules, 1895) to estimate the excess energy of mixing. The binary interaction parameter in the Margules equation was estimated by using the degree of isomorphism value, following the method developed by Kitaigorodsky (1973, 1984)

(Himawan et al., 2006; Marangoni & Wesdorp, 2013). Then Wesdorp selected a collection of methods to perform the flash calculations necessary to estimate the composition of several phases in equilibrium. For this thesis we extracted the options and methods that were found to work. It must be noted that the complexity of Wesdorp's manuscript required considerable selection and interpretation of its content. Furthermore, due to the publishing errors and the specific application, some parts of the method had to be corrected and improved, as described in the methodology part Chapter 3.

2.6.1.1. Estimates of enthalpy and melting point

The methods to estimate enthalpy and melting point was extracted and interpreted from Wesdorp et al's work (Wesdorp et al., 2013, page 277-286). It should be noted that some symbols were changed in the equation for clarity. For instance, in Eq.9, Wesdorp used A and B to represent the constants of the Taylor series expansion. However, in this thesis, A_{sat} and B_{sat} were used to make it easier to understand the relation between Eq.9, Eq.18 and Eq. 19.

Wesdorp's plotted the enthalpy (or entropy) as a function of the carbon numbers of fatty acids, and he found that the enthalpy (or entropy) followed an experimental linear relation with the carbon numbers of fatty acids (Eq.4 and Eq.5). Therefore, enthalpy and melting temperature of a TAG could be estimated as the result of contributions of hydrocarbon

chains (slope) and the end and head groups (intercept). The head group corresponds to the glycerol group of a TAG, and the end group corresponds to the last methyl group of fatty acid.

For monoacid saturated TAGs with even carbon numbers

$$\Delta H = h \cdot n_c + h_0 \quad (J/mol) \qquad \text{Eq.4}$$

$$\Delta S = s \cdot n_c + s_0 \quad (J/(mol \cdot K)) \qquad \text{Eq.5}$$

Since G= H - T·S, and for a system is in equilibrium state G=0, therefore,

$$T_{fi} = \frac{\Delta H}{\Delta S} = \frac{h \cdot n_c + h_0}{s \cdot n_c + s_0} \qquad \text{Eq.6}$$

Using Taylor series expansion:

$$T_{fi} \approx \frac{h}{s}\left[1 + \left(\frac{h_0}{h} - \frac{s_0}{s}\right)\frac{1}{n_c} - \frac{s_0}{s}\left(\frac{h_0}{h} - \frac{s_0}{s}\right)\frac{1}{{n_c}^2}\right] \qquad \text{Eq.7}$$

$$T_{fi} = T_\infty\left(1 + \frac{A}{n_c} - \frac{AB}{{n_c}^2}\right) \qquad \text{Eq.8}$$

$$T_\infty = \frac{h}{s} \quad A_{sat} = \left(\frac{h_0}{h} - \frac{s_0}{s}\right) \; B_{sat} = \frac{s_0}{s} \qquad \text{Eq.9}$$

Where,

n_c is the carbon number of the fatty acids in the TAG.

h, s are slope of the linear function between enthalpy (entropy) and carbon numbers. The units for h are J/mol, and the units for s are J/(mol·K).

h_0, s_0 are the contributions of the head and end group. For h_0 J/mol, and for s_0 J/(mol·K).

T_∞ is the melting temperature if fatty acid has infinite carbon numbers, (K).

A_{sat} and B_{sat} are constant to simplify the Taylor series expansion for saturated TAG.

For saturated TAGs that are not monoacid, Wesdorp used X and Y to determine whether the TAG shares the same end group.

Here,

$$X = n_c \text{ of } 2^{nd} \text{ FA} - n_c \text{ of } 1^{st} \text{ FA} \quad \text{Eq.10}$$

$$Y = n_c \text{ of } 3^{rd} \text{ FA} - n_c \text{ of } 1^{st} \text{ FA} \quad \text{Eq.11}$$

The first fatty acid is chosen as the one that has the shortest chain length in the TAG.

For saturated TAGs,

$$\Delta H_{sat} = hn_c + h_0 + h_{xy}f_{xy}$$

$$\Delta S_{sat} = sn_c + s_0 + s_{xy}f_{xy} \quad \text{Eq.12}$$

$$f_{xy} = 2 - exp\left[-\left(\frac{X - X_0}{k}\right)^2\right] - exp\left[-\left(\frac{Y}{k}\right)^2\right] \quad \text{Eq.13}$$

For an asymmetric TAG, if it is β polymorph, ΔS needs to add an extra term to give better prediction of entropy. In this case,

$$\Delta S = sn_c + s_0 + s_{xy}f_{xy} + Rln(2) \quad \text{Eq.14}$$

In order to calculate the melting point of saturated TAGs, firstly the enthalpy and entropy are calculated by using Eq.12 and Eq.13 (or Eq.14), and then using Eq.6 to calculate the melting point.

In Eq.10 to Eq.14,

f_{xy} is the effect on the thermodynamic properties of the difference in chain length, n.d.

k is the scaling factor of chain length difference, n.d.

X_0 is the reference factor of chain length difference, n.d.

h_{xy}, s_{xy}, are the enthalpy and entropy produced by the effect of the thermodynamic properties of the difference in chain length, units are J/mol and J/(mol·K) respectively.

h, s, h_0, s_0, h_{xy}, s_{xy}, k and X_0 are found from experimental values by Wesdorp and shown in Table 2- 1.

For unsaturated TAGs, an additional unsaturated term is needed. Therefore,

$$\Delta H = hn_c + h_0 + h_{xy}f_{xy} + h_{unsat} \quad \text{Eq.15}$$

$$\Delta S = sn_c + s_0 + s_{xy}f_{xy} + s_{unsat} \quad \text{Eq.16}$$

An approach for unsaturated TAGs uses the most common unsaturated fatty acids as contributors.

$$\Delta \mathrm{H_{unsat}} = \Delta \mathrm{H_{sat}} + \mathrm{h_O n_O} + \mathrm{h_D n_D} + \mathrm{h_J n_J}$$
$$\mathrm{h}_{unsat} = \mathrm{h_O n_O} + \mathrm{h_D n_D} + \mathrm{h_J n_J} \quad \text{Eq.17}$$

Where,

h_{unsat} and s_{unsat} are enthalpy and entropy produced by the effect on of the unsaturated part of the fatty acid chain, units are J/mol and J/(mol·K) respectively.

n_O is the number of oleic chains, n_D is the number of elaidic chains, n_J is the number of linoleic chains.

As for saturated TAGs, the melting point can be calculated using Eq.6. However, it is

difficult to calculate the term of s_{unsat}. Therefore, Wesdorp suggested an alternative method to calculate the melting point of the unsaturated TAGs, and in this thesis, this alternative method was used.

Firstly, the enthalpy of unsaturated TAGs was calculated by using Eq.17, and then the melting point was estimated using Eq.8. The constants of the Taylor series expansion of unsaturated TAGs were calculated using Eq.18 and Eq. 19.

$$A = A_{sat} + A_O n_O + A_D n_D + A_J n_J + A_N n_N + A_{OO} n_{OO} + A_{DD} n_{DD} + A_{JJ} n_{JJ} + A_{NN} n_{NN} + A_{OJ} n_{OJ} + A_{ON} n_{ON} + A_{JN} n_{JN} \quad \text{Eq.18}$$

$$B = B_{sat} + B_O n_O + B_N n_N + B_J n_J \quad \text{Eq. 19}$$

n_N is the number of linolenic chains, n_{oo} is the number of oleic- oleic pairs, same for the others.

A and B are constant to simplify the Taylor series expansion for unsaturated TAG.

The values of the parameters mentioned above are found from experimental values by Wesdorp and shown in Table 2- 1.

Table 2- 1. Parameters to estimate of enthalpy and melting temperature of pure TAGs (Wesdorp et al., 2013, page 268)

	α	β'	β		α	β'	β
h_0	-31.95	-35.86	-17.16	A_O	3.46	2.2	2.93
h	2.7	3.86	3.89	A_D	1.38	1.34	1.68
s_0	-19.09	-39.59	31.04	A_J	3.35	2.75	4.69
s	6.79	10.13	9.83	A_N	4.2	2.2	5.2
h_{xy}	-13.28	-19.35	-22.29	A_{OO}	0.11	-0.27	-0.89
s_{xy}	-36.7	-52.51	-64.58	A_{DD}	0.01	-0.04	-0.4
k	4.39	1.99	2.88	A_{JJ}	3.68	-0.55	-1.21
X_0	1.25	2.46	0.77	A_{NN}	1	-1.51	-1.38
T_∞	397	381	395	A_{OJ}	-0.53	1	-0.71
h_o	-31.7	-28.3	-30.2	A_{ON}	-0.83	-0.76	-0.69
h_e	-11.7	-15.9	-15.9	A_{JN}	3	-1.12	-0.73
h_J	-37.7	-37.7	-37.7	B_O	0	-4.3	-3.7
A_{sat}	-9.02	-5.38	-7.57	B_J	5.4	-7.8	-1.5
B_{sat}	-2.81	-3.91	3.16	B_N	2.6	-13.7	-1.8

2.6.1.2. Liquid- multiple solid equilibrium model

If a system is in thermodynamic equilibrium condition, it should satisfy the following three conditions (Wesdorp et al., 2013, page 251-253):

1) The chemical potential of each component i in each phase must be equal to that in any other phase:

$$\mu_i^{solid} = \mu_i^{liquid} \quad \text{Eq.20}$$

Eq.20 can be applied to solid–liquid equilibrium as:

$$\mu_i^{0,S} + RT \cdot \ln\gamma_i^S x_i = \mu_i^{0,L} + RT \cdot \ln\gamma_i^L y_i \quad \text{Eq.21}$$

$$\ln\left(\frac{\gamma_i^S x_i}{\gamma_i^L y_i}\right) = \frac{1}{RT}\left(\mu_i^{0,L} - \mu_i^{0,S}\right) \quad \text{Eq.22}$$

Assuming it is a three stage thermodynamic process where a liquid sample at T was heated to melting point, crystallized and cooled to the solid at T, the total change in chemical potential is

$$\mu_i^{0,L} - \mu_i^{0,S} = \frac{\partial \Delta G}{\partial x_i} = \Delta H_{fi}\left(1 - \frac{T}{T_{fi}}\right) - \Delta c_{Pi}(T_{fi} - T) + \Delta c_{Pi}\ln\left(\frac{T_{fi}}{T}\right)$$

$$\ln\left(\frac{\gamma_i^S x_i}{\gamma_i^L y_i}\right) = \frac{\Delta H_{fi}}{R}\left(\frac{1}{T} - \frac{1}{T_{fi}}\right) - \frac{\Delta c_{Pi}}{R}\left(\frac{T_{fi} - T}{T}\right) + \frac{\Delta c_{Pi}}{R}\ln\left(\frac{T_{fi}}{T}\right) \quad \text{Eq.23}$$

Where:

T_{fi} is the melting temperature of a solid TAG i in a particular polymorphic form (K).

ΔH_{fi} is the heat of fusion of the TAG i in a particular polymorphic form (J/mol).

Δc_{Pi} is the difference in the heat capacities between the liquid and the solid (J/(mol·K)).

γ_i^S is the activity coefficient of the solid TAG i in a particular polymorphic form.

x_i is the mole fraction of component i in the solid.

y_i is mole fraction of component i in the liquid.

Since to $\Delta c_p \approx 0.2$ kJ/(mol·K) and the term $(T_{fi} - T)$ is rarely bigger than 70 K and usually between 0 and 20 K, the Δc_p terms are comparatively small and can be disregarded. Therefore, with Δc_p neglected, Eq.23 reduces to Eq.24.

$$\ln\left(\frac{\gamma_i^S x_i}{\gamma_i^L y_i}\right) = \frac{\Delta H_{fi}}{R}\left(\frac{1}{T} - \frac{1}{T_{fi}}\right) \quad \text{Eq.24}$$

Since enthalpy change and volume change of the ideal mixing are zero, the interaction between molecules are equivalent. The universal functional group activity coefficient (UNIFAC) method assumed that the activity coefficient of each component in the mixture is a function of the individual contribution of the components' function group. Moreover, Wesdorp found that there was no significant deviation from ideal miscibility when TAGs do not differ too much in molecular size (Wesdorp et al., 2013). Therefore, ideal mixing is assumed for the liquid phase; hence the activity coefficient in the liquid state γ_i^L is equal to 1. Moreover, this thesis simplified the relationship between the liquid mole fraction and solid mole fraction by introducing the thermal factor k_i (Eq.26). This factor is related to the ability of crystallization, and TAGs with large k_i are easy to crystallize. In this thesis, in order to show the clear relationship between solid and liquid mole fraction, Eq.24 was thus changed to Eq.25.

$$\frac{y_i}{\gamma_i^S x_i} = \exp\left[-\frac{\Delta H_{fi}}{R}\left(\frac{1}{T} - \frac{1}{T_{fi}}\right)\right] \quad \text{Eq.25}$$

$$k_i = \exp\left[-\frac{\Delta H_{fi}}{R}\left(\frac{1}{T} - \frac{1}{T_{fi}}\right)\right] \quad \text{Eq.26}$$

$$y_i = k_i \cdot \gamma_i^S \cdot x_i \quad \text{Eq.27}$$

Where,

k_i is thermal factor of component i, n.d.

2) The mole balance: the sum of the amount of each compound i in each phase *f*, present in fraction Φ_f must be equal to the overall amount of i, z_i:

$$\sum_{f=1}^{P} x_i \Phi_f = z_i \qquad \text{Eq.28}$$

p is the number of phases.

(For convenience, in our calculation, S_f was used to represent phase fraction Φ_f. This mole balance is easy to convert to mass balance by simply dividing by the molecular weight of that component MW_i).

3) The stoichiometric condition: the sum of the mole fractions of the components in each phase must be equal to 1:

$$\sum_{i=1}^{n} x_i = 1 \qquad \text{Eq.29}$$

n is the number of components.

2.6.1.3. Estimates of the activity coefficient

Wesdorp developed a method to estimate the activity coefficients (Wesdorp et al., 2013, page 308-310) and it was interpreted in the following paragraphs.

The activity coefficient of the α polymorph is often assumed to be 1 because it is a very simple crystalline form that in which a large degree of liquid-like disorder exists; however, for β' and β, the activity coefficient usually differs from 1, and can only be

described by non-linear equations (such as Margules). Activity coefficient equations depend exponentially on the compositions of the phases, but the compositions are what this study is trying to find. Therefore, in this thesis it is necessary to solve the system of non-linear equations to estimate the activity coefficients of β' and β.

The Gibbs energy in one phase is given by Eq.30. The excess Gibbs energy was used to explain the interaction between TAG components

$$g = \sum_{i=1}^{n} x_i \mu_i = g_{ideal} + g_E = g_{ideal} + RT \sum_{i=1}^{n} x_i \ln(\gamma_i) \qquad \text{Eq.30}$$

$$RT\ln(\gamma_i) = \frac{\partial G_E}{\partial x_i} = \mu_E$$

The excess Gibbs energy of a pure phase is equal to 0. For a multicomponent phase the excess Gibbs energy equation can be calculated, for instance, with the Margules equation:

$$g_E = \sum_{i=1}^{n} x_i \sum_{j=i+1}^{n} A_{ij} x_j \qquad \text{Eq.31}$$

For a binary system:

$$g_E = \left(A_{ij} x_i + A_{ji} x_j\right) x_i x_j \qquad \text{Eq.32}$$

$$RTln(\gamma_i) = \frac{\partial g_E}{\partial x_i} = \left(x_j\right)^2 R\overline{T_{ij}} \left[\frac{A_{ij}}{R\overline{T_{ij}}} + 2\left(\frac{A_{ji}}{R\overline{T_{ij}}} - \frac{A_{ij}}{R\overline{T_{ij}}}\right) x_i\right] \qquad \text{Eq.33}$$

For a multicomponent system, assuming only binary interactions:

$$g_E = \sum_{i=1}^{n} \sum_{j=i+1}^{n} \frac{A_{ij} x_j + A_{ji} x_i}{x_i + x_j} x_i x_j \qquad \text{Eq.34}$$

$$RT\ln(\gamma_i) = \frac{\partial g_E}{\partial x_i} = \sum_{j \neq 1}^{n} \frac{x_i}{\left(x_i + x_j\right)^2} \left[A_{ji}\left({x_i}^2 + 2x_i x_j\right) + A_{ij} {x_j}^2\right] \qquad \text{Eq.35}$$

$$\gamma_i = exp\left\{\frac{1}{T}\sum_{j\neq i}^{n}\frac{\overline{T_{ij}}x_j}{(x_i+x_j)^2}\left[\varphi_{ji}\left({x_i}^2+2x_ix_j\right)+\varphi_{ij}{x_j}^2\right]\right\} \quad \text{Eq.36}$$

$$\text{Interaction parameter:}\varphi_{ij} = \frac{A_{ij}}{R\overline{T_{ij}}} \quad \text{Eq.37}$$

$$\text{Average melting temperature: } \overline{T_{ij}} = \frac{T_{fi}+T_{fj}}{2} \quad \text{Eq.38}$$

Eq.32- Eq.37 are the 3-suffix Margules equation, if A_{ij}=A_{ji}, then Eq.32- Eq.37 becomes a 2-suffix Margules equation.

In order to calculate the interaction parameters and activity coefficients, Wesdorp et al. (2013) assumed that solid solubility is solely determined by geometrical factors, and he used the Kitaigorodsky method (1973, 1984) of 'degree of isomorphism ε' to describe the coefficient of geometrical similarity between two TAGs. The degree of isomorphism ε is defined as the maximum possible overlap between the molecules of the components. The two components will only mix in the solid state when their degree of isomorphism is larger than 0.85.

$$\varepsilon = 1 - \frac{\mathrm{v_{non}}}{\mathrm{v_O}} \quad \text{Eq.39}$$

v_{non} is the volume of the non-overlapping parts of TAGs, (nm^3), which is the sum of the absolute differences in carbon number of each of three chains.

v_o is the volume of the overlapping parts of TAGs, (nm^3), which is the sum of the carbon numbers of the smallest chain on each glycerol position.

The binary interaction parameters can be estimated from the values of the degree of isomorphism. Wesdorp indicated that that 2-suffix Margules equation could provide sufficient accuracy to describe the mixing behavior in multiple-solid phase. Therefore, In this thesis, the 2-suffix Margules equation was used to calculate activity coefficients and Eq.36 was simplified to Eq.40.

$$\gamma_i = exp\left(\frac{1}{T}\sum_{j\neq i}^{n}\overline{T_{ij}}x_j\varphi_{ji}\right) \quad \text{Eq.40}$$

Within β' polymorphism, the 2-suffix Margules binary interaction parameter was calculated as:

$$\varepsilon > 0.93, \varphi_{12} = \varphi_{21} = 0; \quad \text{Eq.41}$$

$$\varepsilon < 0.93, \varphi_{12} = \varphi_{21} = -19.5\varepsilon + 18.2;$$

For β'-2 polymorphism, $\varepsilon < 0.93, \varphi_{12} = \varphi_{21} = -21.7\varepsilon + 18.7;$ Eq.42

Within β polymorphism, the 2-suffix Margules binary interaction parameter was estimated as:

$$\varepsilon > 0.98, \varphi_{12} = \varphi_{21} = 0; \quad \text{Eq.43}$$

$$\varepsilon < 0.98, \varphi_{12} = \varphi_{21} = -35.8\varepsilon + 35.9;$$

For both β' and β, if $\varphi_{12} = \varphi_{21} > 8, then\ \varphi_{12} = \varphi_{21} = 8$ Eq.44

Due to the special case that the α-form is in different phases, this research developed a method to identify those two phases. Normally, the interaction parameter of α-form is 0,

but if two α-forms are present at the same time, one of the α-forms must have interaction parameters different from 0. Since there was no better option, in this thesis, they were estimated using Eq.45. It is the β' equation multiplied by 0.5.

For α-2 polymorphism, $\varepsilon < 0.93, \varphi_{12} = \varphi_{21} = 0.5(-19.5\varepsilon + 18.2);$ Eq.45

2.6.2. Other thermodynamic and kinetic modeling studies

Los & Flöter (1999) used Wesdorp's model as a basis for produce a kinetic phase diagram of a binary system. Los, van Enckevort, Vlieg, & Flöter, (2002a) extended the binary kinetic model to a multicomponent system, and obtained a good prediction of SFC. Los, van Enckevort, et al., (2002b) compared the results of the compositional kinetic phase separation, which was calculated by the kinetic model developed by them with the results of the standard equilibrium method. They found that phase separation during crystal growth is reduced and at the low temperature limit, the phase separation vanished and a homogeneous solid phase formed. The modeling of crystallization onset times and phase transition of liquid, α, and β' phases under shear was developed by Mazzanti et al., (2005). Foubert et al., (2003) compared several kinetic models: the Avrami model, the modified Avrami model, the Gompertz model, and the model developed by themselves that describe isothermal crystallization. They found that the most popular Avrami model has a better fit than the Gompertz model, and their model is the best fit for the sample they tested. Maximo, Costa, & Meirelles, (2013) compared the equilibrium model with

the experimental data of binary fatty alcohols system. The activity coefficients in the model were calculated by using the 2- and 3-suffix Margules equation, and the original and modified Dortmund model and all the calculations were performed using MATLAB. A good prediction of liquidus line was found.

Chapter 3. MATERIALS AND METHODOLOGY

3.1. Research plan

The purpose of this research is to check Wesdorp's method to predict the melting range and solid phase composition of fats from their overall composition. At the beginning of the study, a database was digitized, which included the enthalpy and melting temperature of 209 kinds of TAGs. Then a simple situation was assumed and used to test the model. In this ideal case, there is only one solid phase in equilibrium with liquid. Assuming that only α polymorph and liquid were in the system, by fitting the different parameters to the SFC data, a reasonable enthalpy and melting temperature can be estimated by using Wesdorp's model.

However, the real case is often that there is more than one solid phase in the system. Therefore, it is necessary find out the solid phase composition at different temperatures. In Wesdorp's work, he proposed flash calculation to estimate the number of phases and phase fractions. A problem with flash calculations in these monotropic materials is that the β phase has always a lower Gibbs energy than α or β' phase. From this point of view, the "best" solution at a given temperature could often be a combination of beta phases and liquid. In vapor-liquid equilibrium this problem does not exist because the liquid has no polymorphic forms. The TAG materials form rather stable combinations of phases that

include sometimes the three polymorphs. For this study, the results of XRD experiments gave that phase information.

SXRD experiments tell us the number of the solid phases, and combined with WXRD experiments, one can find out the number of polymorphs and the type of the polymorphs, as well as the mass fraction of each solid phase. Combining the experimental results with Wesdorp's theory, a MATLAB program was created to estimate the mole fraction of each component in each phase, and calculate the overall melting enthalpy, which was then compared with DSC measurements. Figure 3- 1 shows the steps of this research.

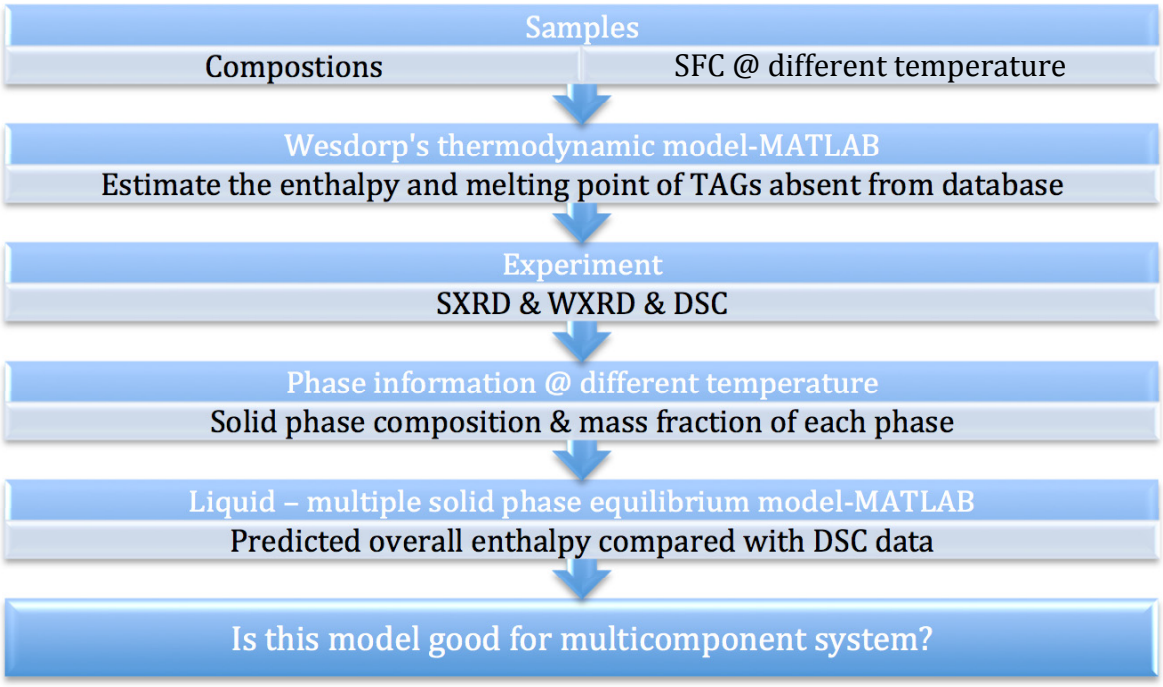

Figure 3- 1. The overall procedure of the research

3.2. Materials

Two commercial samples were studied in this research. They are equivalent to refined, bleached and deodorized (RBD) palm oil products, and are called “RBD470” and “RBD 394”. Dr. Alejandro G. Marangoni (Nov, 2012) had studied their compositions using HPLC and examined their SFC at different temperatures (see Table 3- 3 and Figure 3- 2). There are 22 different TAGs in RBD470, and 30 in RBD394. Since 11 are common to both samples, there are 41 TAGs in total. Only 6 of them have all the experimental information of enthalpies and melting points for three polymorphic forms. There are 18 temperatures for single polymorphs of a few others and 17 TAGs lack all information.

For convenience, single letter codes were assigned to the fatty acids, as listed in Table 3-1. The composition of the two samples is listed in Table 3- 2.

Table 3- 1. Characters used to represent individual fatty acids

Letter	Name	nc	s	u
U	Butyric	4	0	0
K	Caproic	6	0	0
R	Caprylic	8	0	0
C	Capric	10	0	0
L	Lauric	12	0	0
M	Myristic	14	0	0
P	Palmitic	16	0	0
S	Stearic	18	0	0
A	Arachidic	20	0	0
B	Behenic	22	0	0
G	Lignoceric	24	0	0
F	Ceric	26	0	0
T	Palmitoleic	16	1	1
O	Oleic	18	1	1
J	Linoleic	18	1	2
N	Linolenic	18	1	3
D	Elaidic	18	1	1
E	Erucic	22	1	1
H	Arachidonic	20	1	4

Table 3- 2. The compositions of RBD470 and RBD394 (provided by Dr. Marangoni)

No.	RBD394	Mass fraction (%)	RBD470	Mass fraction (%)
1	MML	10.14	POP	36.21
2	MOP	9.69	PJP	13.16
3	POP	9.32	POO	8.85
4	LMP	9.23	MOP	8.59
5	MMP	8.19	POS	7.47
6	COP	5.90	POJ	4.09
7	PPM	5.65	MPJ	3.39
8	LLM	5.52	PPP	2.90
9	MOM	4.80	MPP	2.80
10	CLM	3.63	PJS	2.28
11	PJP	3.58	MOO	1.49
12	MJP	3.49	JOO	1.21
13	COM	3.22	OOS	1.18
14	CCM	2.50	MPT	1.13
15	POS	2.32	MOJ	1.04
16	CJP	2.28	SOS	0.93
17	PPP	2.08	OOO	0.85
18	MJM	1.84	PJJ	0.76
19	CJM	1.13	PPS	0.60
20	POO	0.87	JOS	0.49
21	COC	0.85	JSS	0.33
22	PJS	0.83	JOJ	0.25
23	MOO	0.56		
24	ROP	0.49		
25	PPS	0.45		
26	CCL	0.33		
27	COO	0.31		
28	POJ	0.29		
29	SOS	0.25		
30	CCC	0.24		

Table 3- 3. SFC (%) data of the two samples (provided by Dr. Marangoni)

Temperature (°C)		5	10	15	20	25	30	35	40
Sample	RBD470	79.3	75.0	62.7	44.0	26.7	14.8	4.2	0.1
	RBD394	83.3	78.6	66.9	44.8	28.8	9.3	3.2	0.0

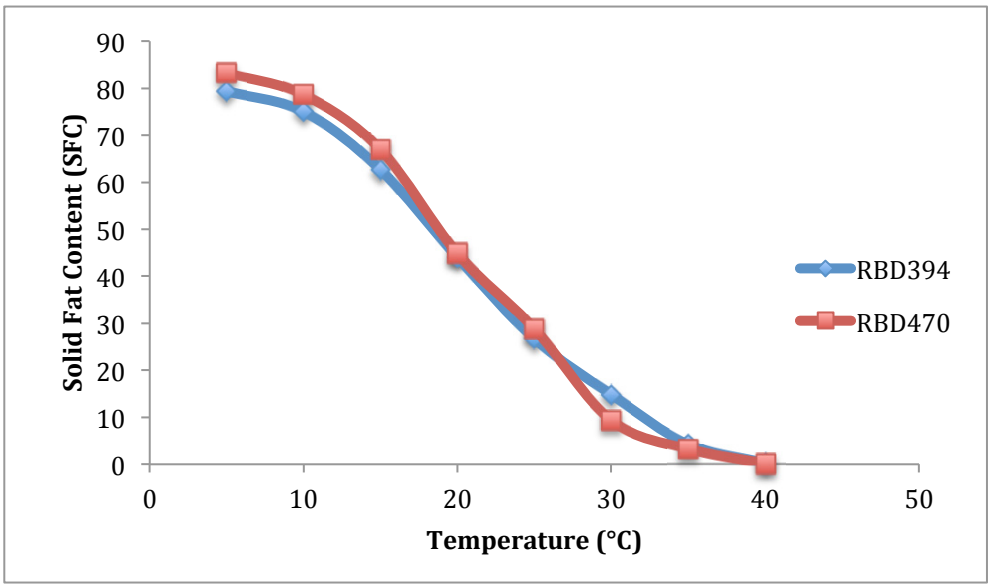

Figure 3- 2. SFC diagram of RBD470 and RBD394

3.3. Instruments and methods

3.3.1. Differential Scanning Calorimetry (DSC)

A TA Instruments heat-flux differential scanning calorimeter (TA Instrument DSC Q100 V9.4 Build 287, Module DSC Standard Cell FC connected to a Windows-based computer system, New Castle, DE, US) was used to perform all thermal experiments. The DSC is equipped with a refrigerated cooling system (RCS) with an optional Modulated DSC

MDSC®. Two gas cylinders were connected to the sample cell, closed by an auto-lid: one for nitrogen and the other for air. Figure 3- 3 shows the setup of the DSC.

The instrument was calibrated by running the TA calibration protocols. (Appendix C1)

Figure 3- 3. TA Instruments heat flux DSC Q100 equipped with modulated® DSC connected to a refrigerated cooling system, RCS (Al-Qatami, 2011)

3.3.1.1. Sample preparation

The samples were melted at 100 °C using a hot plate (Cole-Parmer, USA) for ten minutes to ensure that the samples were totally melted and mixed keep their original composition. An empty hermetic aluminum pan and lid was selected and weighted as reference pan;

other pans and lids were selected within the range of the reference pan weight ± 0.05 mg. The weighing measurements were carried out using a microbalance (Cahn Instruments, C-33 Microbalance Model Number 13633-013, US) with a precision ≤ 0.001 mg. All the pans and lids were then immersed in acetone to clean, and left to dry in the air. Approximately 5-10 mg of melted sample was transferred to the pan by using disposable capillary tubes with a wire plunger (Drummond Scientific Company, Wiretrol® II, US, 5 µL and l0 µL) and sealed with a lid by a TA instruments blue encapsulating press (Al-Qatami, 2011).

3.3.1.2. Procedure

In order to attain a steady experimental environment, after turning on the DSC and TA Instrument program, a cyclic run was performed, which was heating and cooling to the highest and the lowest temperature of the system three to six times without putting any pan into the DSC cell. The sample and reference pans were then loaded into the cell and the sample information (sample name, sample weight, saved file name, etc.) was put into the program. All the samples were initially heated to 100 °C for 10 minutes, cooled to 0 °C with a cooling rate of 20 °C /min, and held at that temperature for 60 minutes. They were then heated to the holding temperature (5, 10, 15, 20, 25, 30 °C) at a rate of 20 °C /min, and kept isothermal for 90 minutes. This isothermal time was set to make sure the sample had stopped changing. After keeping the samples isothermal for 90 minutes, it

was observed that there was no change of heat flow. It was concluded the sample was not crystallizing any further. After that, all samples were melted with a heating rate of 5 °C /min to 100 °C. Figure 3- 4 gives the temperature profile of DSC experiments.

Two pans were prepared for each sample and each pan was measured twice for each holding temperature.

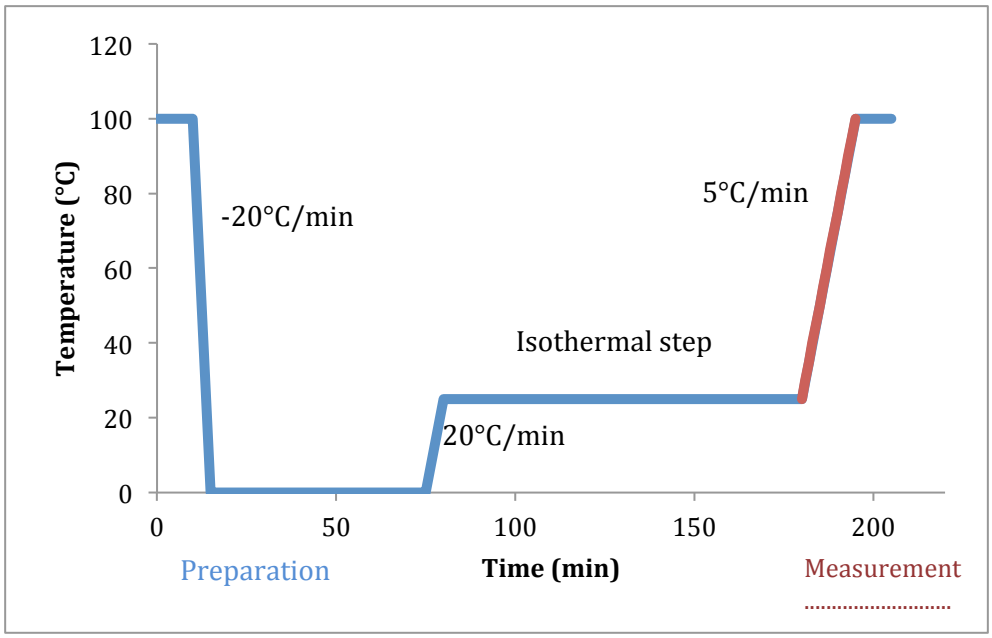

Figure 3- 4. Temperature profile of DSC experiments

3.3.1.3. Analyzing the DSC Data

The third heating part was the analytical part of the research (see Figure 3- 4 red line part). The heat flow data of the melting corresponded to the phases present at the end of the second isothermal period, which was applied at different temperatures. This part was used to calculate the overall melting enthalpy of the material prepared at each temperature.

Combined with SXRD and WXRD, a clear picture of the phase numbers and types at a specific temperature was sought.

The overall melting enthalpy of a partially solid material in this work is defined as the amount of energy needed to melt the solid phases at a specific temperature to total liquid. This definition is commonly used in the fat processing industry and research, and should not be confused with the melting enthalpy of a pure substance. In order to calculate the overall melting enthalpy from DSC data, the following analysis needs to be done.

Due to the slight difference of the pan position on the platform for each experimental run, the heat flows of the liquid part of different experimental runs were not equal (see Figure 3-5a). Therefore, normalization of the liquid part (50-90 °C) was necessary. This study assumed that the corrected heat flow was a linear transformation of the measured heat flow. The slope and intercept of the linear equation were calculated using Excel solver by minimizing the error between a reference measured heat flow and the linear transformation of each one of the other heat flows. This was done for data from each isothermal treatment. The heat absorbed by the sample could be converted to energy/temperature by dividing it by the heating rate, which was constant at 5 °C/min (0.0833 °C/s). A running integral of this normalized heat flow was done as a function of temperature. Literature (Morad, Idrees, & Hasan, 1995) and research in our group

indicates that most liquid TAGs, pure or mixed, have a specific heat that depends linearly on the temperature. The integral with respect to temperature was thus expected to yield a quadratic line. This was in fact observed, and therefore the quadratic equation of the liquid part (50-90 °C) of the integrated heat flow was calculated and extended to the lower temperatures. The melting enthalpy was calculated as the difference between liquid integrated heat flow and initial integrated heat flow.

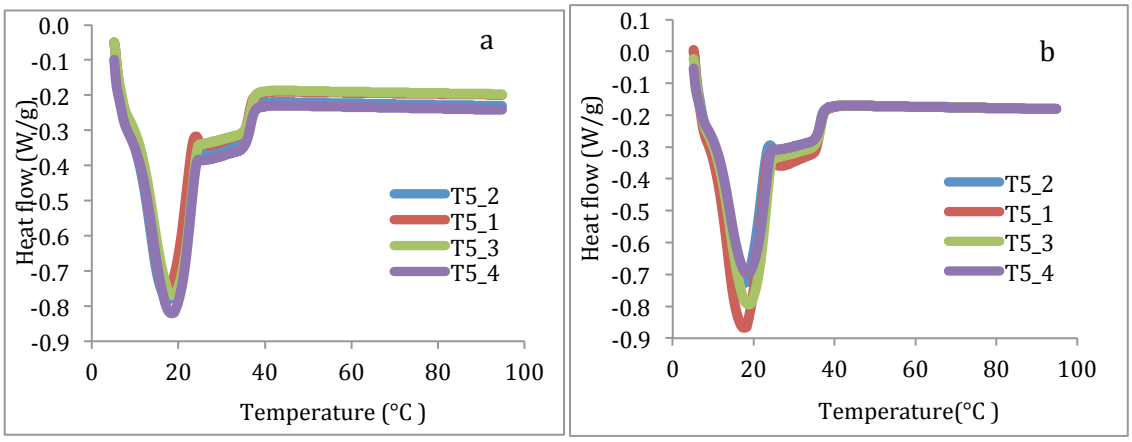

Figure 3-5. Example of heat flow as a function of temperature for replicates from the same temperature. a. Before normalization. b. After normalization.

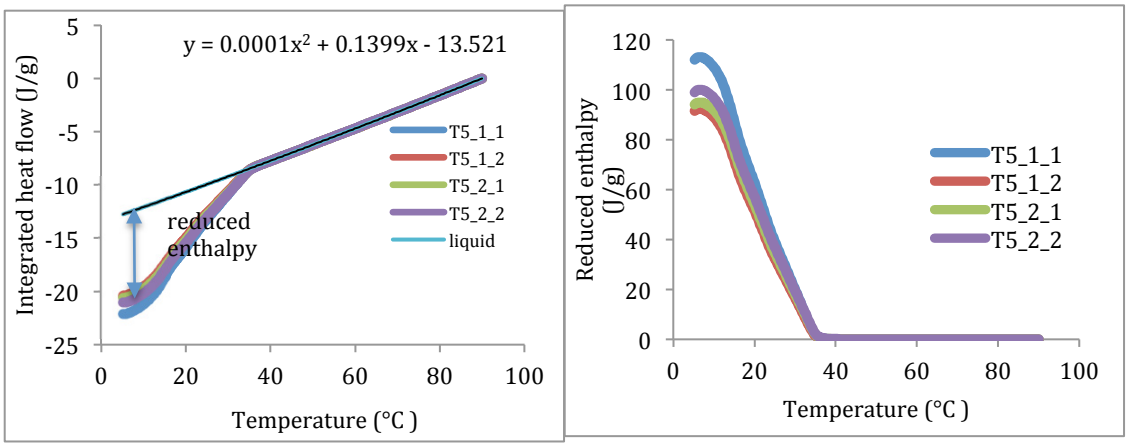

Figure 3- 6. Integrated heat flow as function of temperature: example of reduced enthalpy difference calculation.

3.3.2. X-ray Diffraction (XRD)

Both SXRD and WXRD experiments were performed with our in-house XRD instrument to detect crystallization processes at different isothermal temperatures.

3.3.2.1. In house XRD

The in-house small-angle XRD experimental set up is shown in Figure 3- 7 and Figure 3-8. The x-ray generator uses a Commercial GeniX x-ray source (Xenocs Corporation, Sassenage, France), which produces 0.7093 Å wavelength Mo K_α radiation. After being focused by a mirror, the x-ray is collimated by two sets of scatterless slits aligned on a small diameter fly-path, and is then projected on to the sample. The beam size at the sample is approximately 0.4 x 0.5 mm. Another fly-path with a large diameter is installed between the sample holder and the detector. The inside of the two fly-paths are under

vacuum, which is produced by a vacuum pump. By removing the large fly-path between the detector and the sample holder, the in-house small-angle XRD experimental set up can be changed to the wide-angle experimental set up.

The detector in our in-house x-ray experimental set up is XRI-UNO/Si 2D x-ray detector (XRAY-IMATEK, Barcelona, Spain). The active area of this detector is 14 mm × 14 mm and it is built as a single chip array of silicon sensors. The pixel size (p_s) is 0.055 mm × 0.055 mm. All the images were collected to a computer by 'XRI-UNO' software, which controls the detector camera.

There is an enclosure around the whole system to isolate the surroundings and minimize the danger of x-ray exposure.

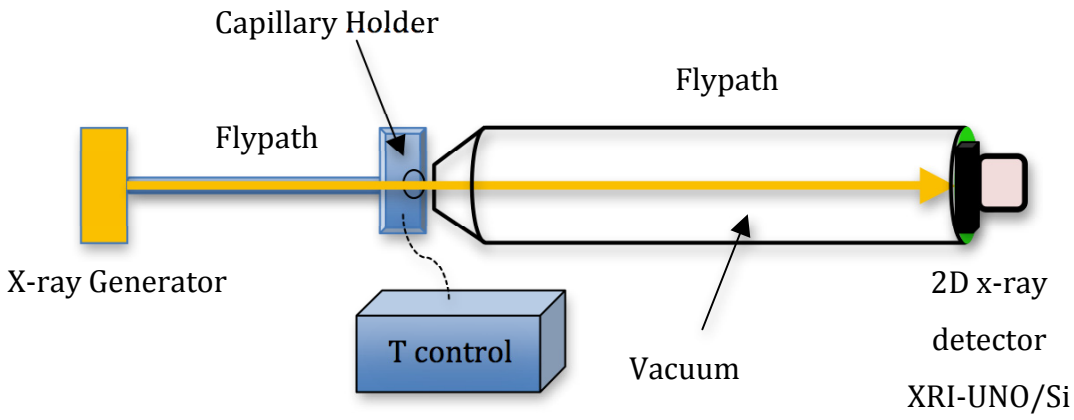

Figure 3- 7. In-house XRD set up

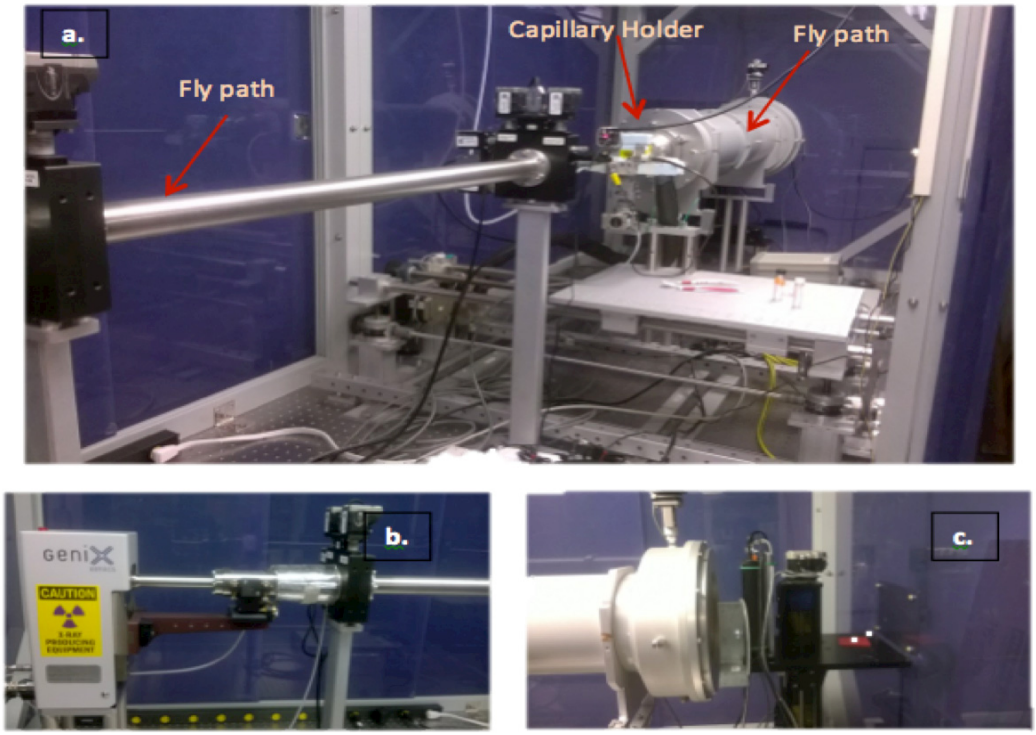

Figure 3- 8. In-house experimental setup for XRD experiments. a. The position of the capillary holder and fly paths. b. X-ray generator. c. 2D detector (Photos by Pavan K. Batchu)

3.3.2.2. Centering the diffraction patterns

Before putting a sample capillary into the capillary holder, the detector was moved to center position (both x-axis, y-axis were 0, which corresponded to pixel position (128,128)), a short exposure (10 s) was taken and a beam spot was captured. By using ImageJ program, the beam spot was located in our 256×256 pixel imageJ image. This pixel location had been converted to the pixel location in the IgorPro program. Then the

detector was moved, usually to -22.02 mm (or other position) horizontally. So the final center location should take this -22.02/0.055 pixel into account. The XY coordinates in pixels for the center for SXRD of RBD470 was (-281.1, 128) and RBD394 was (-317.5, 128). For WXRD of both samples was (-261.40, 127.08). The center locations were used to calculate the distance from the sample holder to the detector. This calibration allows the proper calculation of the scattering vector q.

3.3.2.3. Detector distance calibration

The distance from the sample to the detector was 1366.9 mm for small angle XRD measurements and 130.36 mm for wide angle ones. The short distance was calibrated using Al_2O_3 that has known d-spacings, and the long distance was calibrated using silver behenate. By using the ImageJ plug-in program XR2D (developed by Mazzanti and Idziak), a radial plot of Al_2O_3 was obtained, which gave the pixel location (c_{px}) of each diffraction pattern. The angular location difference between each diffraction pattern would keep constant, no matter what the detector distance was.

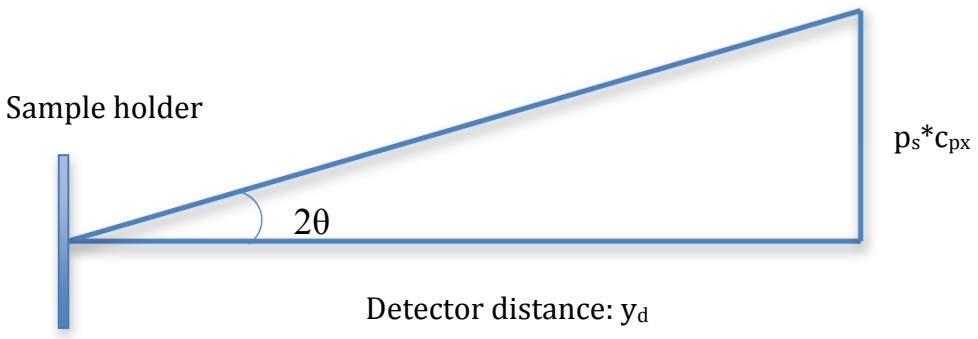

Figure 3- 9. Explanation of distance calibration.

Bragg's law Equation:

$$\lambda = 2d \sin\theta \quad \text{Eq.46}$$

$$\theta = \sin^{-1}(\lambda/2d) \quad \text{Eq.47}$$

$$y_d = p_s \cdot c_{px} / \tan(2\theta) \quad \text{Eq.48}$$

First, a measured y_d value and known Al_2O_3 d-spacings were used to calculate the $p_s \cdot c_{px}$ values of each pattern and took the difference between each patterns of calculated $p_s \cdot c_{px}$ values, and similarly experimental $p_s \cdot c_{px}$ values. Excel solver was used to minimize the difference between calculated and experimental values by changing the y_d value and the cpx value. The final y_d value was the calibrated distance, and c_{px} was the refined centre point.

3.3.2.4. Sample preparation

The samples were melted at 100 °C using a hot plate (Cole-Parmer, USA) for ten minutes. Using preheated disposable capillary tubes with a wire plunger (Drummond Scientific Company, Wiretrol® II, Cat. Number 5-000-2010, 5 µL and l0 µL), approximately 20-30 µL of sample were transferred to the x-ray capillary (Charles Supper Co., 1.5 mm diameter, 10 µm wall) and sealed by fire. Two capillaries were prepared for each sample.

3.3.2.5. Procedure

Due to the low intensity of the x-rays, a long exposure time was necessary to acquire good resolution images and make sure the system reached equilibrium. The smaller SFC required a longer exposure time; therefore, the minimum exposure time was calculated according to the SFC at each holding temperature. This study required quantitative SXRD data to calculate the phase fractions, so it needed a longer exposure time than WXRD. The temperature profile shown in Figure 3- 10 and Table 3- 4 gives the isothermal time of the XRD experiments. Each capillary was used in three runs for both SXRD and WXRD experiments.

A LabView program developed by Dr. Gianfranco Mazzanti and Dr. Stefan Idziak, and upgraded by Pavan K. Batchu, controlled the temperature of the capillary cell. The GUI in this program allows the user to input a temperature profile, Figure 3- 11. For convenience, instead of taking a single image for such a long exposure time, an image is taken every 75 seconds. This way partial images are saved and an interruption in the experiment does not lose all the previous acquisition.

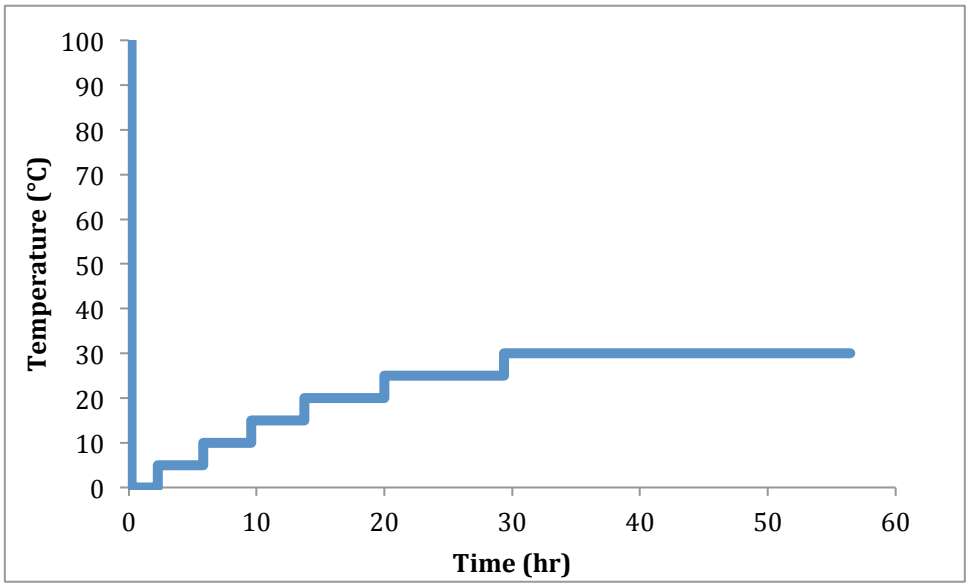

Figure 3- 10. Temperature- time profile of XRD experiments

Table 3- 4. Isothermal time (min) of XRD experiments

Temperature (°C)	RBD470		RBD394	
	SXRD	WXRD	SXRD	WXRD
100	13	13	13	13
0	125	63	125	63
5	213	50	225	50
10	225	56	238	56
15	250	56	275	63
20	375	75	388	75
25	563	100	588	113
30	1625	263	1050	200

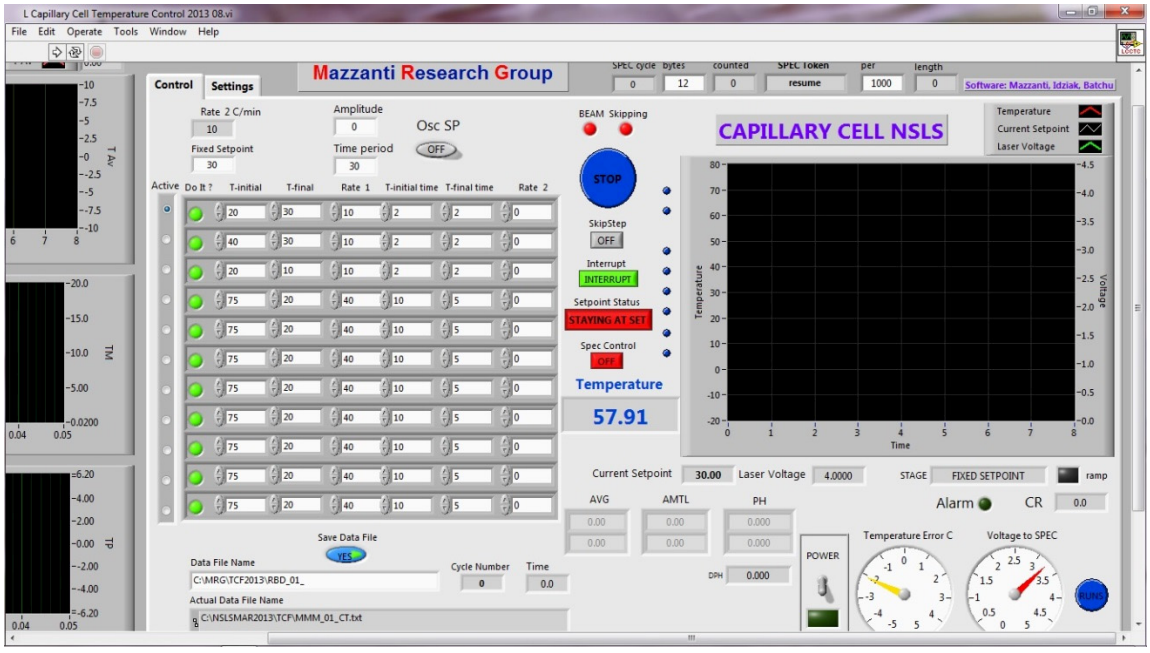

Figure 3- 11. A GUI interface of the capillary cell temperature control program (Provided by Pavan K. Batchu)

3.3.2.6. Analyzing the XRD Data (Appendix C2)

All the images of SXRD and WXRD were analyzed by using ImageJ and Igor Pro software. By using ImageJ, images were normalized and radial plots were created. All the peak fittings were done by using Igor Pro. The mass fraction of each phase was calculated by finding proportionality factors that satisfied the SFC values (Cisneros et al. 2006), using Excel.

3.3.3. MATLAB programming

The first step of the MATLAB (2014b) programs was an estimation of the enthalpy and

melting temperature for TAGs that do not have experimental data. The second, independent step was the estimate of the interaction parameters. With those values the program proceeded to estimate the values for compositions and activity coefficients, while the mass balance of the system was strictly obeyed, even if the theoretical equilibrium constraints were not all satisfied. The mass balance of the different phases is explained in Table 3- 5. Wesdorp mentioned a method to create mass balance constraints (Wesdorp et al., 2013, page 265), but the method was not clearly explained. Therefore, this research created a new constraint matrix based on the concept he mentioned in the book (Wesdorp et al., 2013).

Table 3- 5. Mass balance calculation matrix

Phase / TAG	Solid 1	Solid 2	Solid f	(Liquid)	
1	m_{11}	m_{12}	m_{1f}	m_{1L}	z_1
2	m_{21}	m_{22}	m_{2f}	m_{2L}	z_2
.					
i	m_{i1}	m_{i2}	m_{if}	m_{iL}	z_i
.					
n	m_{n1}	m_{n2}	m_{nf}	m_{nL}	z_n
Total	$\widehat{S_1}$	$\widehat{S_2}$	$\widehat{S_f}$	$\widehat{S_L}$	1

Where,

z_i is overall mass of TAG i.

$\widehat{S_f}$ is the solid mass fraction of phase *f*.

n is the number of TAGs.

$$m_{if} = \widehat{x_{if}} \times \widehat{S_f} \quad \text{Eq.49}$$

($\widehat{x_{if}}$ is mass fraction of component i in phase *f*)

$$\text{For phase j: } \sum_{i=1}^{n} m_{if} = \widehat{S_f}. \quad \text{Eq.50}$$

$$\text{For component i: } \sum_{f=1}^{p} m_{if} = z_i. \quad \text{Eq.51}$$

It is the same as Eq.28, but on a mass base

$$\sum z_i = 1 \quad \text{Eq.52}$$

p is the number of phases.

A matrix was created that included all the variables of the mass balance. Within the boundary, the variation of the estimated mass of each component in the solid phase was changed by the 'fmincon' function to minimize the error from the equilibrium, defined by Eq.66. The 'fmincon' program is used to find the set of values of the variables that produce the minimum of a constrained nonlinear multivariable target function (MathWorks, 2014, para.1). The variation of each component in the liquid phase is equal to -1 multiplied by the sum of the variation for that component in solid, so the sum of variation of all the phases is equal to 0. The mass fraction of each component in each phase was calculated and converted to mole fraction. This study used Wesdorp's liquid – multiple solid phase equilibrium model and the mole fraction of β' was chosen as the reference with which to calculate the mole fraction of the other phases. The error was

defined as the difference between the mole fractions calculated by mass balance and those calculated from the equilibrium model. This error was minimized to find the composition of each phase. With the composition of each component in each phase, the melting enthalpy was calculated and compared with DSC data. Figure 3- 12 summarizes the procedure of MATLAB calculations. The calculation details are shown below.

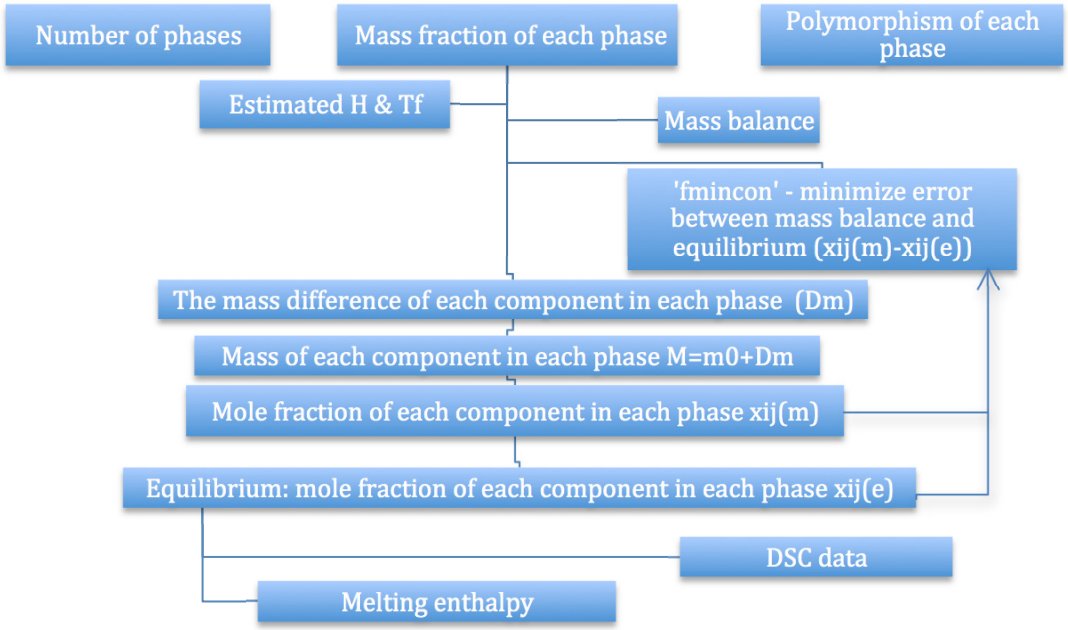

Figure 3- 12. The procedure of the MATLAB calculation

Parts of this logic are described in Wesdorp et al. (2013) in separate sections, or are suggested rather than clearly stated. The following program logic was selected, extracted, organized and, when necessary, interpreted from the original work. Methods such as the one described by Eq.54b and Eq.59 were extracted and interpreted from Wesdorp's work (2013). However, some modification turned out to be necessary in order to perform

correct calculations, according to what was interpreted as Wesdorp's intent. The implementation, setup and detailed programming are additional work done for this thesis within the framework of known mass fraction and polymorphism of phases.

The program logic is shown below:

1) Estimate enthalpy (H) and melting point (T) [from database or calculation]

2) Create the vector Dn as the mass variation of each component in sequentially each solid phase with,

$$\mathrm{Dn}=\begin{Bmatrix} 0 \\ \vdots \\ 0_{p*n} \end{Bmatrix} \quad \text{Eq.53}$$

3) Create four matrices (A, b, Aeq, beq). They restrict Dn's boundary:

$$A \times Dn \leq b \quad \text{Eq.54a}$$

$$Aeq \times Dn = beq \quad \text{Eq.54b}$$

$$-z_i \widehat{S_r} \leq Dn \leq z_i(1-\widehat{S_r}) \quad \text{Eq.54c}$$

$\widehat{S_r}$ is the mass fracion of a solid phase

$$A = \begin{Bmatrix} 1 & & 1 & & 1 & & \\ & \ddots & \cdots & \ddots & \cdots & \ddots & \\ & 1_{n1} & & 1_{nf} & & 1_{n(p-1)} & \end{Bmatrix} \quad \text{Eq.55}$$

$$b = \begin{Bmatrix} z_1 \widehat{S_L} \\ \vdots \\ z_n \widehat{S_L} \end{Bmatrix} \quad \text{Eq.56}$$

$$Aeq = \begin{Bmatrix} 1 & \dots & 1_{n1}0 & \dots & 0_{nf}0 & \dots & 0_{n(p-1)} \\ 0 & \dots & 0_{n1}1 & \dots & 1_{nf}0 & \dots & 0_{n(p-1)} \\ 0 & \dots & 0_{n1}0 & \dots & 0_{nf}1 & \dots & 1_{n(p-1)} \end{Bmatrix} \quad \text{Eq.57}$$

$$beq = \begin{Bmatrix} 0 \\ \vdots \\ 0_{p-1} \end{Bmatrix} \quad \text{Eq.58}$$

4) Create a matrix Z to calculate the mass variation of the liquid phase, which is equal to -1 multiplied by the sum of Dn

$$Z = \begin{Bmatrix} -1 & & -1 & & -1 & & \\ & \ddots & \dots & \ddots & \dots & \ddots & \\ & -1_{n1} & & -1_{nf} & & -1_{n(p-1)} & \\ & & & IM & & & \end{Bmatrix} \quad \text{Eq.59}$$

IM is an identity matrix of dimension $(p-1)$ by n.

$Dn2 = Z \times Dn = \begin{Bmatrix} -sum(Dn) \\ Dn \end{Bmatrix}$, Which is a matrix of dimensions p·n by 1. Eq.60

Dn2 is the mass variation of each component in each phase, and the first n variables are the mass variation of each component in the liquid phase.

5) Calculate initial mass (m_{if}) of each component in each phase, and create a matrix (Dm) of dimensions n by p, each column of this matrix corresponds to the mass variation of each component in each phase

$$m_{if} = z_i \times \widehat{S_f} \quad \text{Eq.61}$$

6) Calculate corrected mass:

$$m_{cif} = m_{if} + Dm \quad \text{Eq.62}$$

7) Calculate mass fraction ($\widehat{x_{if}}$) of each component in each phase

$$\widehat{x_{if}} = m_{cif}/\widehat{S_f} \quad \text{Eq.63}$$

8) Convert mass fraction ($\widehat{x_{if}}$) to mole fraction (x_{if}) of each component in each phase; choose one solid phase as reference phase, mole fraction is x_{ir}

$$x_{if} = \frac{(\widehat{x_i}/MW_i)}{\sum_i^n (\widehat{x_i}/MW_i)} \quad \text{Eq.64}$$

9) Use Eq.39 - Eq.44 to calculate the interaction parameters (φ_{ijf})

10) Use Eq.36, φ_{ijf} and x_{if} to calculate activity coefficients (γ_{if})

11) With the activity coefficients (γ_{if}) calculate the mole fractions of each solid phase x_{if} and the liquid phase y_i under equilibrium by using Eq.27 to calculate x_{ife}.

$$\text{Solid - Solid: } x_{ife} = \frac{x_{ir}\gamma_{ir}k_{ir}}{\gamma_{if}\cdot k_{ij}} \text{ or Solid –Liquid: } x_{ife} = \frac{y_i}{\gamma_{if}\cdot k_{ij}} \quad \text{Eq.65}$$

12) Use the mole fraction calculated by mass balance minus the mole fraction calculated by equilibrium, to calculate the error between the two methods.

$$SSE = \sum_i^n (x_{if} - x_{ife})^2 \quad \text{Eq.66}$$

13) Use the ‘fmincon’ function to minimize this error, and find the variation that satisfies the mass balance.

14) With the ‘fmincon’ result, step 4 to 6 are repeated, to calculate the mass fraction that satisfied the constraints.

15) Convert the final mass fraction to mole fraction, and calculate A_{ij} using Eq.37 and Eq.38.

16) Use Eq.31, ignoring the entropy term, to calculate the excess enthalpy of each solid phase (H_{Ef}). Then multiply by the mass fraction of each solid phase, to calculate the overall excess enthalpy (H_E). The overall excess enthalpy plus the ideal enthalpy term (H_{ideal}) is the overall enthalpy ($H_{predict}$).

17) Assume there is total 1 mole of sample. The enthalpy of each component divided by its molecular weight converts the units of the enthalpy from J/mol to J/g.

$$H_E = \sum_{f=1}^{p-1} H_{Ef} \hat{S}_f \qquad \text{Eq.67}$$

$$H_{ideal} = \sum_{i=1}^{n} \sum_{f=1}^{p-1} x_{if} H_{if} \qquad \text{Eq.68}$$

$$H_{predict} = H_E + H_{ideal} \qquad \text{Eq.69}$$

Chapter 4. RESULTS AND DISCUSSION

4.1. Differential Scanning Calorimetry (DSC)

4.1.1. Heat flow charts

Figure 4- 1 and Figure 4- 2 show the melting heat flow chart for the pans containing RBD470 and RBD394, after holding them isothermally at different temperatures. According to Figure 4- 1, there are two phases at 5, 10, 15 °C as can be seen by the presence of two melting events. As the holding temperature increased, the amount of the second phase increased. From the holding temperature of 20 °C, only the second phase existed for RBD470, and from 25 and 30 °C, another phase might be formed due to the recrystallization.

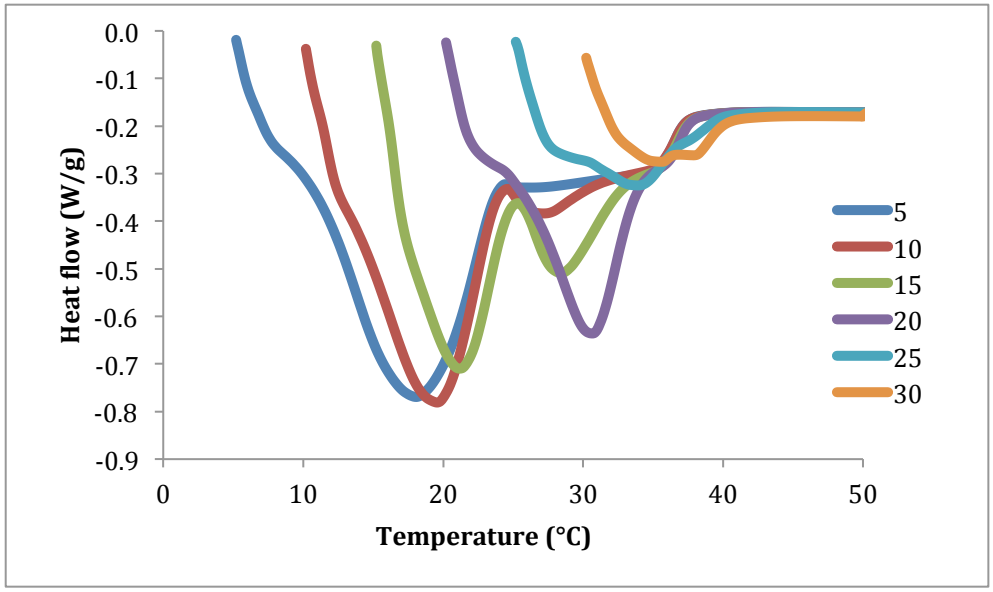

Figure 4- 1. Heat flow as a function of temperatures for melting RBD470

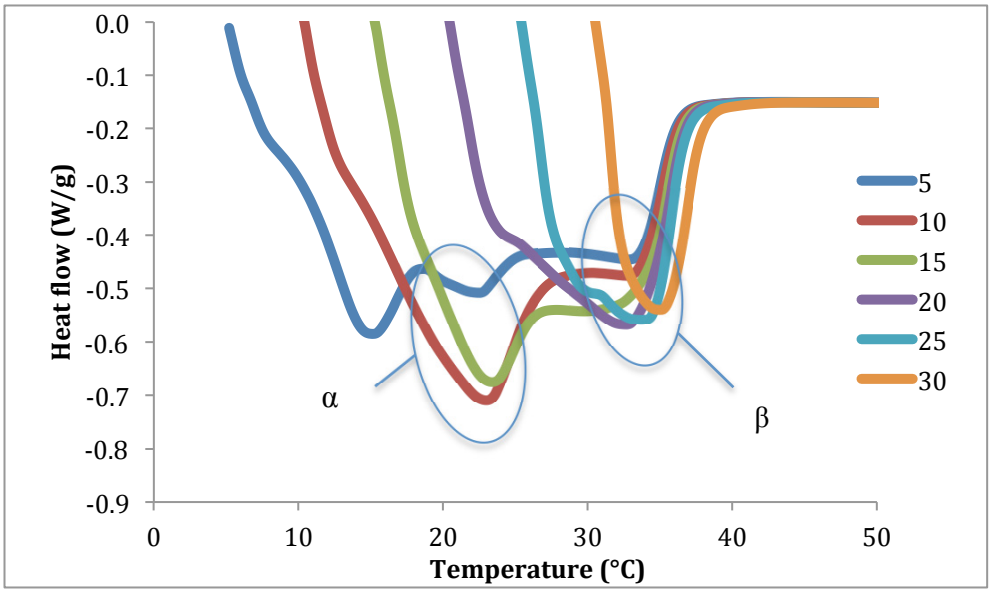

Figure 4- 2. Heat flow as a function of temperatures for melting RBD394

Figure 4- 2 shows that two different solid phases are formed after melting RBD394 held at 5 °C. For the 10 and 15 °C holding temperatures, the first phase disappeared while the second phase increased. After the second phase melted, there were constant heat flows for 5, 10 and 15 °C holding temperatures, which might be because the melting rate and recrystallization rate were same, which consumed and created the same amount of energy. Melting RBD394 held at other temperatures shows that a third phase existed in those crystals. For 30 °C, there is a big shift in the final melting part of the curve compared to other holding temperatures. This probably means that a large proportion of high melting point molecules were present in the solid phases.

4.1.2. Overall melting enthalpy of samples

According to Table 4- 1, the overall melting enthalpy decreased with temperature increase, except for RBD394 at 5 °C. This enthalpy decrease at lower temperature might be because a large amount of α polymorph existed, which has the smallest enthalpy among the three polymorph forms. The enthalpies at some temperatures have relatively large standard errors, which may be due to the different sample pans position. The melting and recrystallization process would not affect the overall melting enthalpy values. This is because the energy released by recrystallization would cancel out by the energy provided to melt; the overall energy difference in the material between the initial temperature and the final temperature would not change.

Table 4- 1. Experimental melting enthalpy of samples

Temperature (°C)	Enthalpy (J/g)	
	RBD394	RBD470
5	100.18±4.62*	94.74±5.94
10	110.46±7.52	84.83±10.69
15	88.00±4.90	71.67±6.36
20	54.61±2.17	43.26±3.99
25	39.56±3.60	15.54±0.32
30	22.95±2.61	8.68±1.63

* The range of the enthalpy is the average ± standard error.

4.2. XRD experiments

4.2.1. Small-angle diffraction experiments of RBD470

From Figure 4- 3, it is clear that two SXRD peaks exist at 0 °C, and the peak around 0.13 $Å^{-1}$ (d-spacing = 4.7 nm) disappears when the temperature increased to 10 °C. The SXRD d-spacing plot (Figure 4- 4) shows the d-spacing calculated from the positions of the four SXRD peaks observed in the experiments. It can be seen that there are two different solid phases for all temperatures except 10 and 15 °C. The phase with a d-spacing of 4.7 nm at 5 and 10 °C was identified as an α polymorph phase. Although in the WXRD diffraction pattern the characteristic α polymorph peak (d-spacing = 0.42 nm) cannot be cleanly resolved from an overlapping large peak, (Figure 4- 7), its presence is indubitable.

The phases that have SXRD d-spacing around 4.3 nm are likely β' or β polymorphs. The SXRD integrated intensity plot in Figure 4- 5 includes the results from both capillaries (_1 and _2 in the legend). The plot shows that with the decrease of the amount of α polymorph, the amount of the other phase increases. The phase that existed at 15 °C might be transformed to the other two phases; one of which is present in a large proportion (about 38%), while the other has smaller proportion (less than 5%).

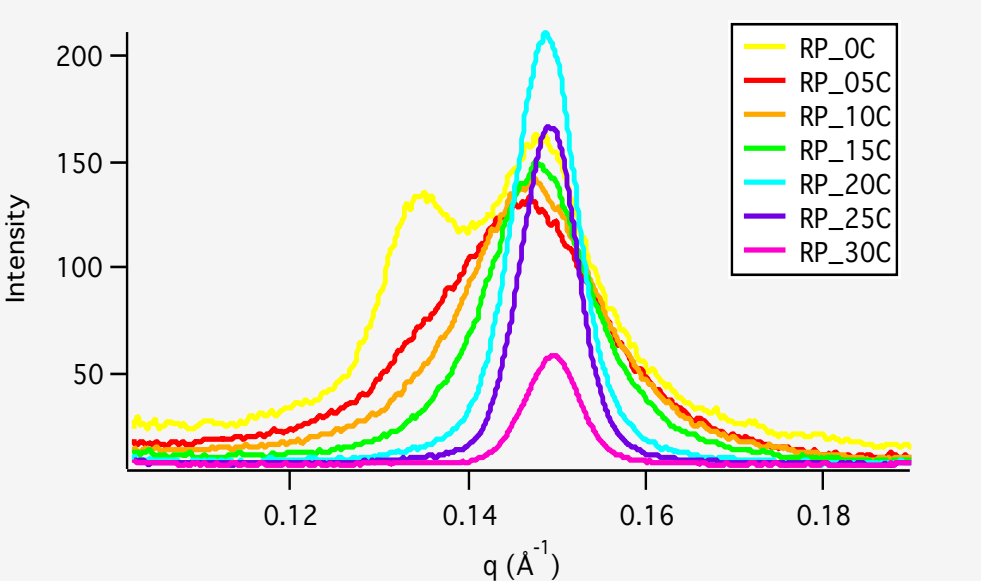

Figure 4- 3. SXRD radial plots of RBD470_01_03

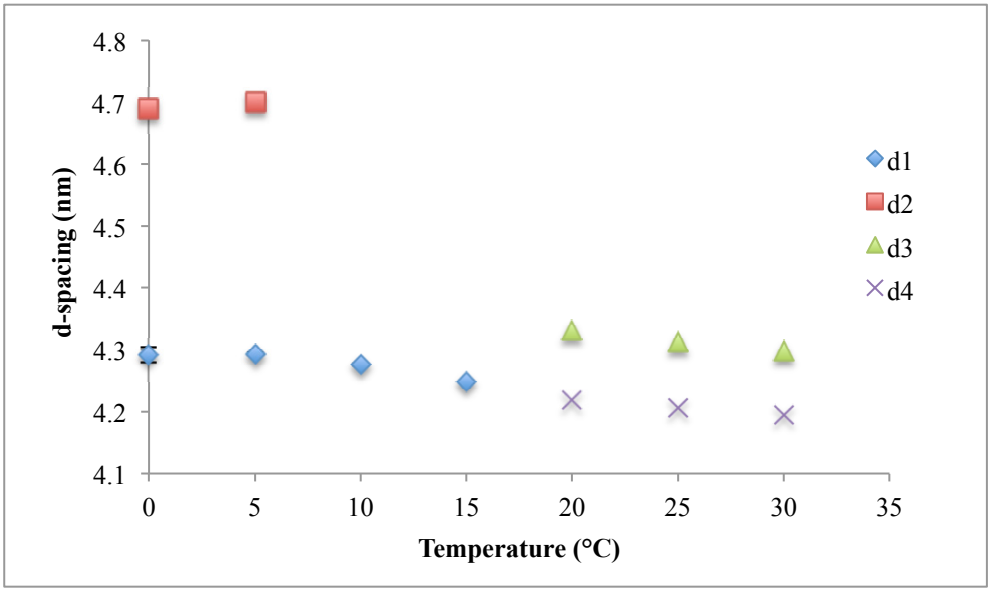

Figure 4- 4. SXRD d-spacing vs. temperature of RBD470

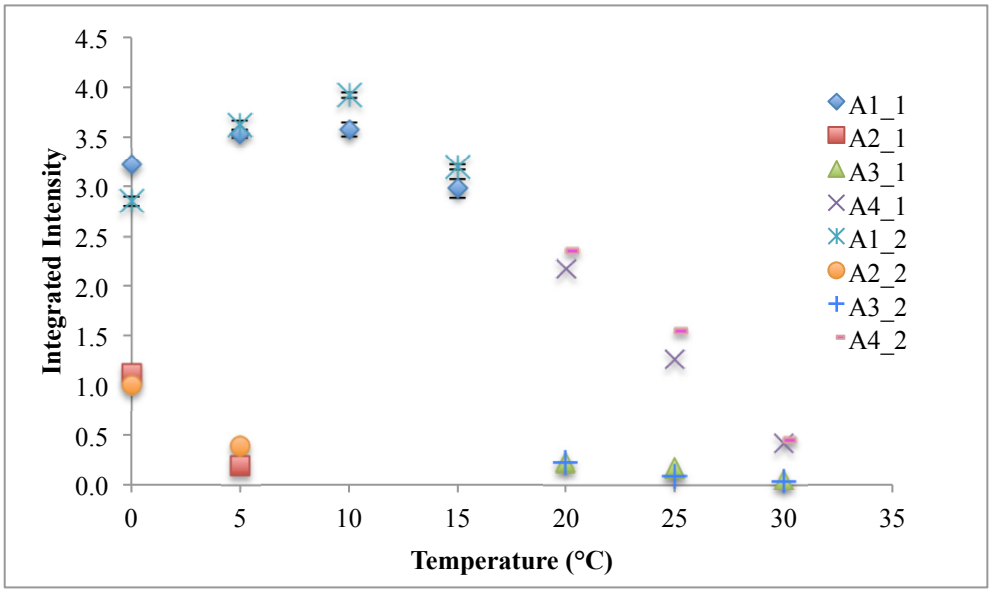

Figure 4- 5. SXRD integrated intensity vs. temperature of RBD470

4.2.2. Wide-angle diffraction experiments of RBD470

4.2.2.1. Solid part analysis

From Figure 4- 6, it is obvious that α polymorph is present at 0 and 5 °C, along with form β'. Polymorph α has a single strong peak around q = 1.48 $Å^{-1}$ (d-spacing = 0.42 nm). The intensity of the peak decreases with the temperature increase. The diffraction patterns at 20 and 25 °C, have a peak around q = 1.58 $Å^{-1}$ (d-spacing = 0.39 nm), and that indicates the presence of another polymorphic form, which is consistent with SXRD results.

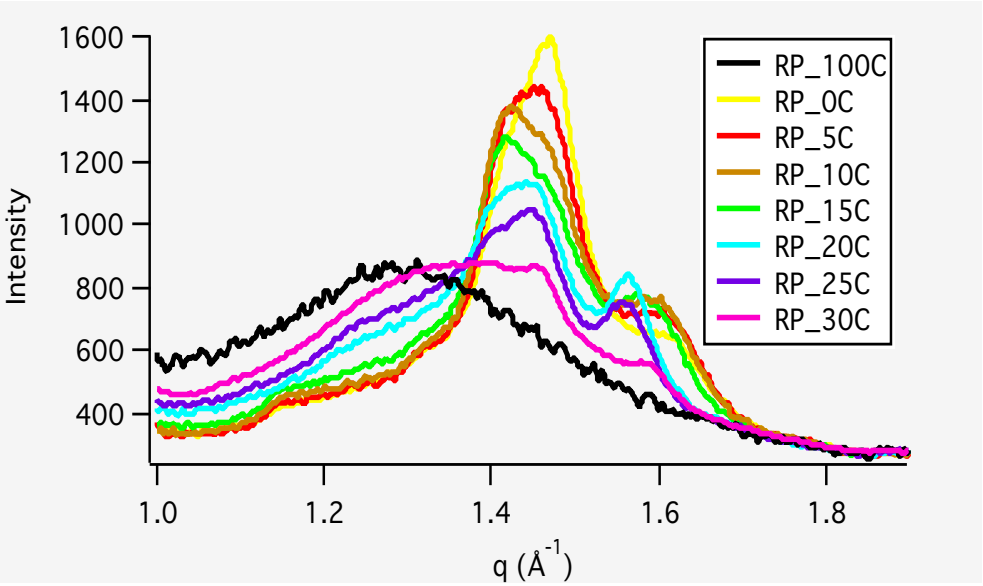

Figure 4- 6. WXRD radial plots of RBD470_01_03

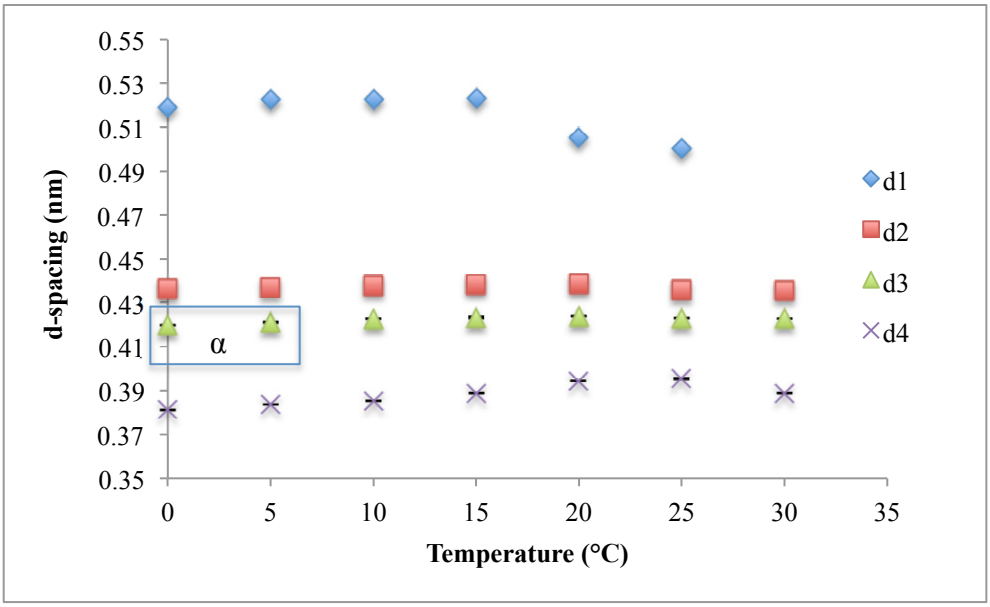

Figure 4- 7. WXRD d-spacing vs. temperature of RBD470

In the WXRD d-spacing plot (see Figure 4- 7), there are no β polymorph characteristic

peaks, so RBD470 did not form any β polymorph at those temperatures. The d-spacing 0.52 nm at 0, 5, 10, 15 °C belongs to one of the β' polymorphs showing in SXRD. The sudden increase in integrated intensity of this peak at 20 °C might be due to the new β' phase formed at 20 °C, which also showed both in the heat flow chart and the SXRD plot. At 10 and 15 °C, the peaks with d-spacing 0.42 nm are present in Figure 4- 7, so they might belong to the α polymorphic form or the β' polymorphic form. Figure 4- 5 shows that the integrated intensity of the α phase decreases from 1 to 0.3, therefore the α phase might disappear and those peaks with d-spacing 0.42 nm at 10 and 15 °C belong to the β' polymorphic form.

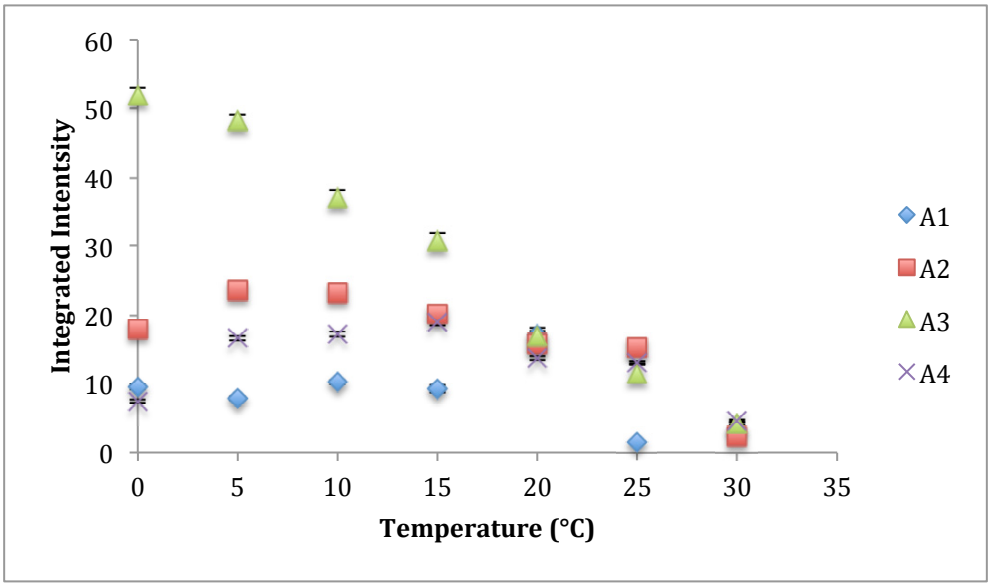

Figure 4- 8. WXRD integrated intensity vs. temperature of RBD470

4.2.3. Small-angle diffraction experiments of RBD394

The radial plots (see Figure 4- 9) show that two peaks located around q = 0.143 $Å^{-1}$ (d-spacing = 4.4 nm) and 0.162 $Å^{-1}$ (d-spacing = 3.9 nm) were present at 0 and 5 °C. The peak around 0.143 $Å^{-1}$ disappears when temperature increases. It is therefore likely that this peak belongs to the α polymorph. Since the peak around 0.162 $Å^{-1}$ increases with the temperature increase, it must correspond to the β' polymorph.

According to the SXRD d-spacing plot, except 0 °C, there were two different solid phases at each temperature. There might be two α polymorphs and one β' polymorph (d-spacing 3.8 nm) at 0 °C. Due to the high cooling rate, at first, the large molecules will crystallize and start to form large size α polymorph (phase 1, d-spacing at 4.4 nm), then as cooling continues, smaller molecules such as unsaturated TAGs form small size α polymorphs (phase 2, d-spacing at 4.25 nm). However, at 5 °C, even though DSC heat flow shows the same result, the peak was not found in SXRD, perhaps because the amount of phase 2 at 5 °C was too small. The phase with d-spacing around 3.8 nm is a β' polymorph phase as is the phase around 3.9 nm. The integrated intensity of the β' polymorph with d-spacing around 3.9 nm increases as the α polymorph decreases, and reaches the highest integrated intensity at 10 °C. Due to the decrease of total solid as the temperature increases, the integrated intensity of this β' polymorph also decreases above 10 °C.

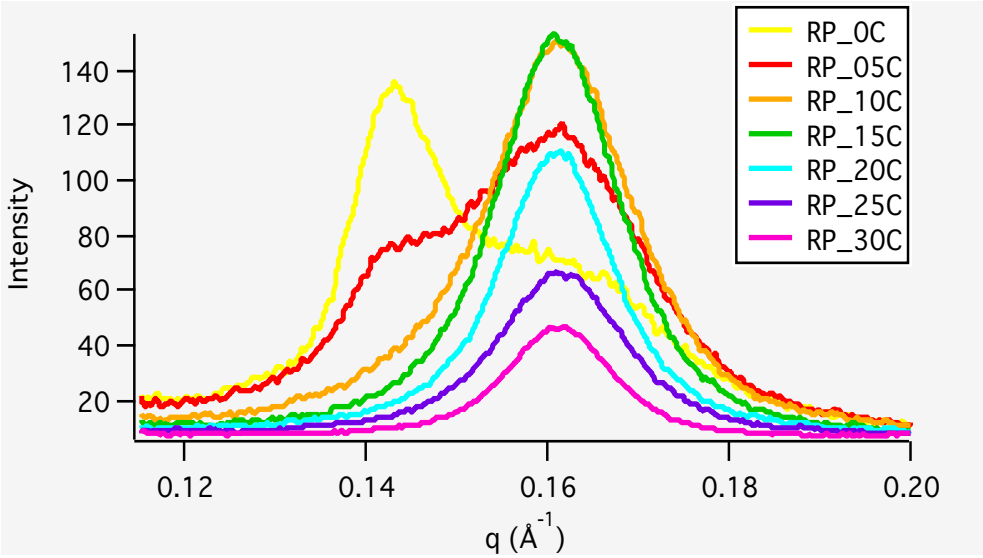

Figure 4- 9. SXRD radial plots of RBD394_01_02

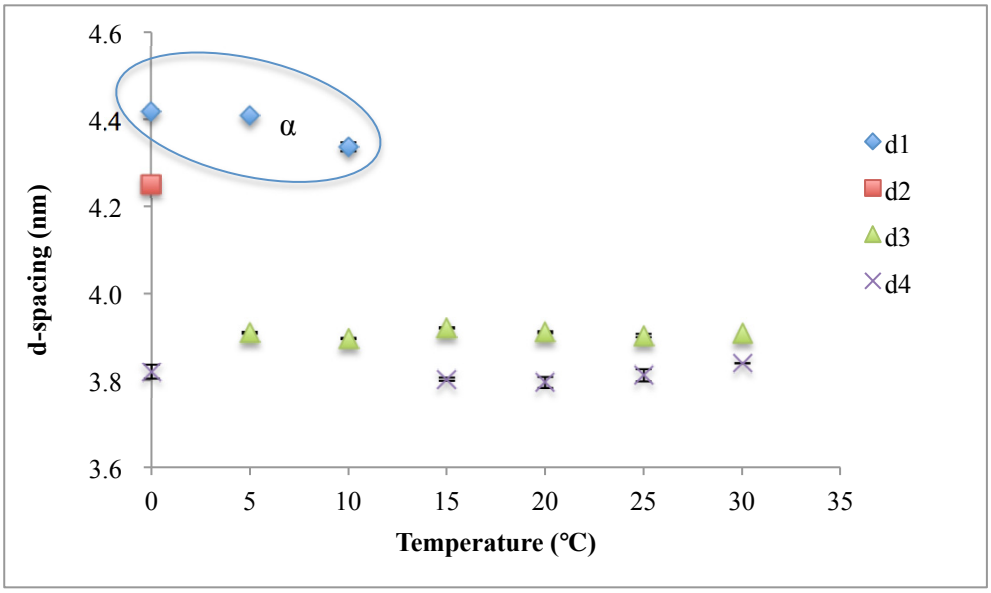

Figure 4- 10. SXRD d-spacing vs. temperature of RBD394

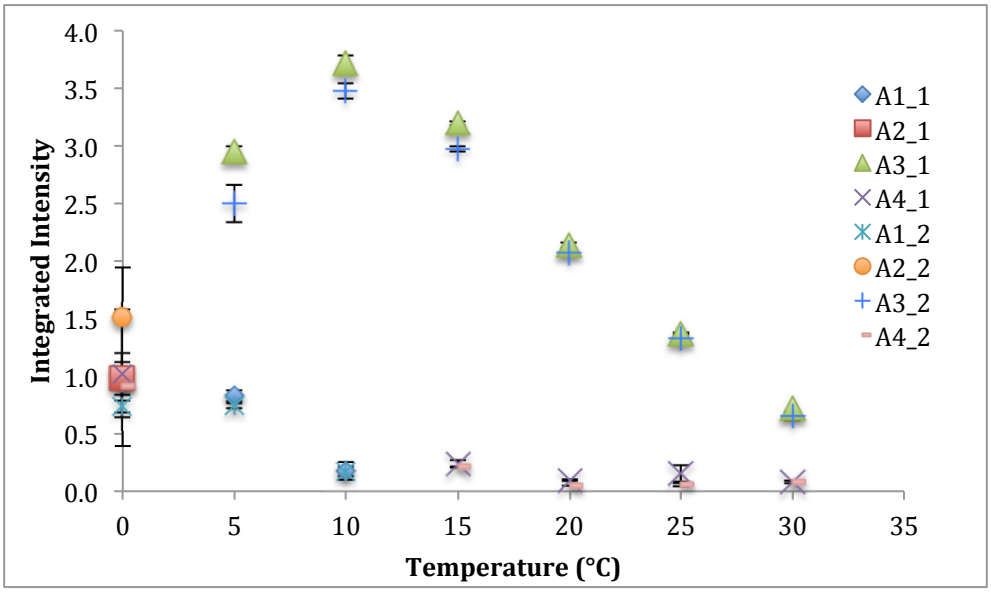

Figure 4- 11. SXRD integrated intensity vs. temperature of RBD394

4.2.4. Wide-angle diffraction experiments

4.2.4.1. Solid part analysis

From Figure 4- 12, it is clear that the phases change during the increase of temperature. There is a large amount of α and little β' polymorph present at 0 °C. With the temperature increase, the α peak at 1.55 $Å^{-1}$ (d-spacing = 0.41 nm) decreases but other peaks increase. The peaks around 1.38 (d-spacing = 0.46 nm) and 1.65 $Å^{-1}$ (d-spacing = 0.38 nm) are β polymorph; they appear at 10 °C and increase with temperature. However, the β polymorph at 10 °C is too small for SXRD to resolve (Figure 4- 14).

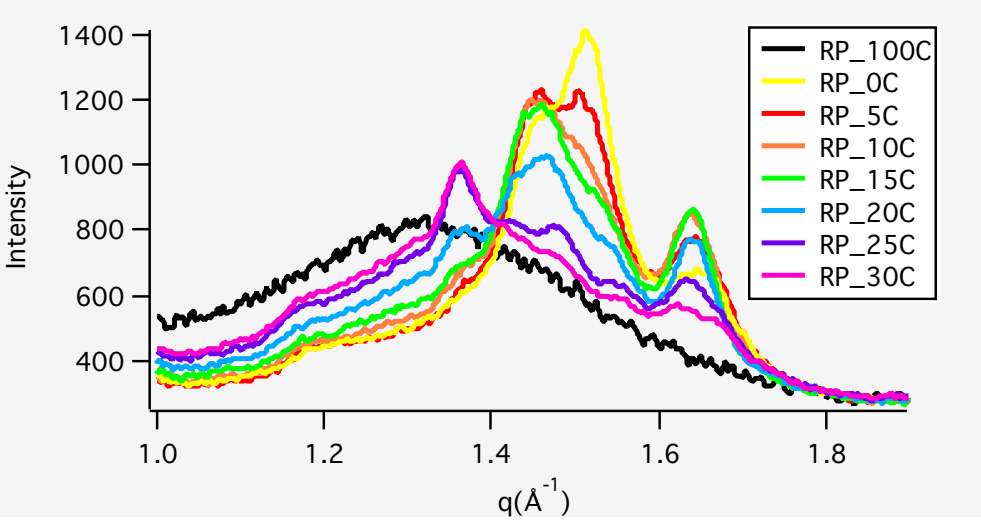

Figure 4- 12. WXRD radial plots of RBD394_01_02

According to Figure 4- 13, the d-spacing around 0.51 nm, same as RBD470, might belong to one the of β' polymorphs which is observed in the SXRD plot. There is a WXRD peak at d-spacing 0.41 nm for 0, 5, 10 °C, which indicates α polymorph. From Figure 4- 14, the α polymorph-form decreases with temperature increase; the phase indicated by the peak with d-spacing around 0.40 nm for 15, 20, 25, 30 °C might be transformed from α polymorph-form, because its integrated intensity is relatively small and it appears after the α polymorph-form had disappeared. Peaks with d-spacing 0.46 nm and 0.38 nm indicate the presence of β polymorph. Their integrated intensities slightly increase with temperature increase.

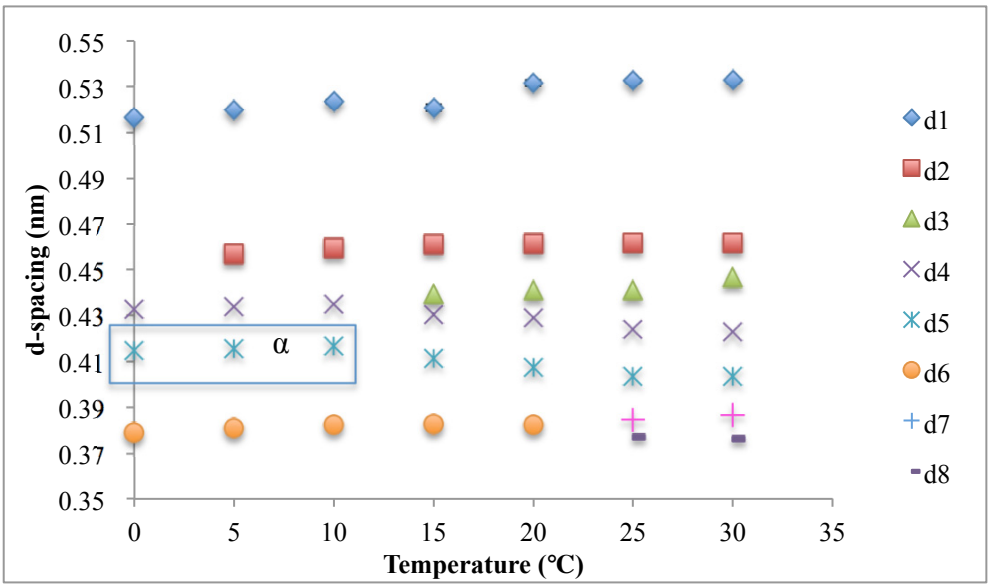

Figure 4- 13. WXRD d-spacing vs. temperature of RBD394

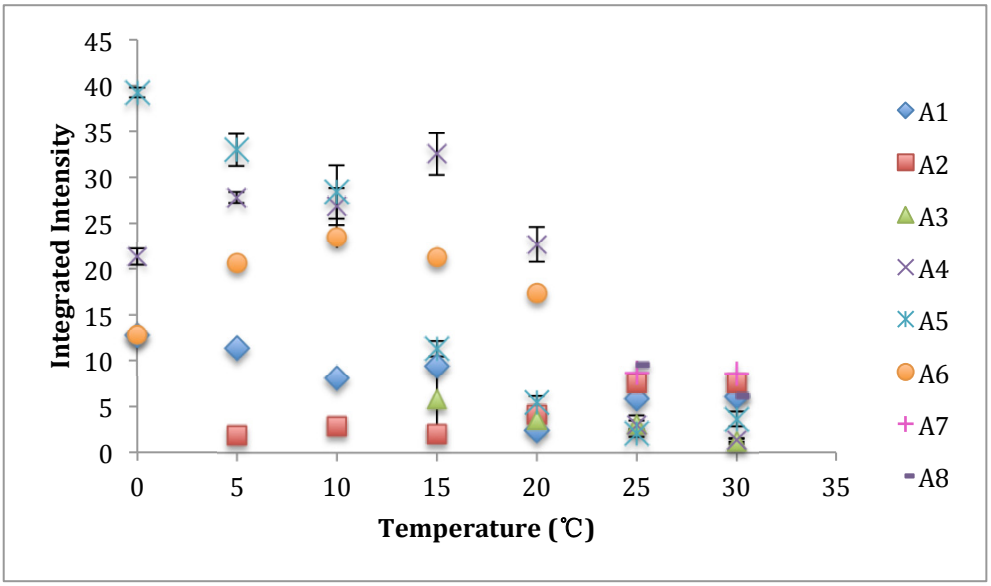

Figure 4- 14. WXRD integrated intensity vs. temperature of RBD394

4.2.5. Liquid part analysis

As shown in Figure 4- 15 and Figure 4- 16 and Figure 4- 7, the liquid d-spacing of both samples increases with temperature, and at each temperature, RBD470 and RBD394 have similar d-spacing. For RBD394, the liquid d-spacing follows the same trend of RBD470, i.e. the liquid d-spacing increases as temperature increases. The integrated intensity of RBD470 has the same general trend as d-spacing changes, except for 5 and 20 °C, where the integrated intensity decreases. The liquid integrated intensity of RBD394 does not have any qualitative trend. The area under the wide-angle liquid scattering peaks could not be used to estimate the total liquid fraction of the material. The integrated intensities at 100 °C are same for both samples. The large standard error of the liquid integrated intensity is due to the fitting error. During the fitting, peaks with similar d-spacing were easy to resolve in some experiments, but some were not, which affect the liquid integrated intensity value.

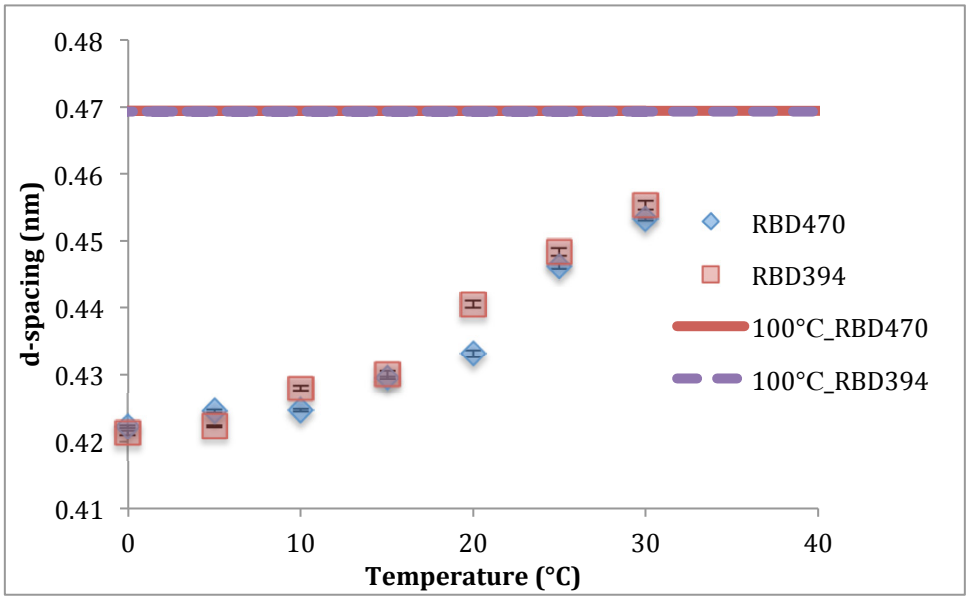

Figure 4- 15. WXRD liquid d-spacing vs. temperature

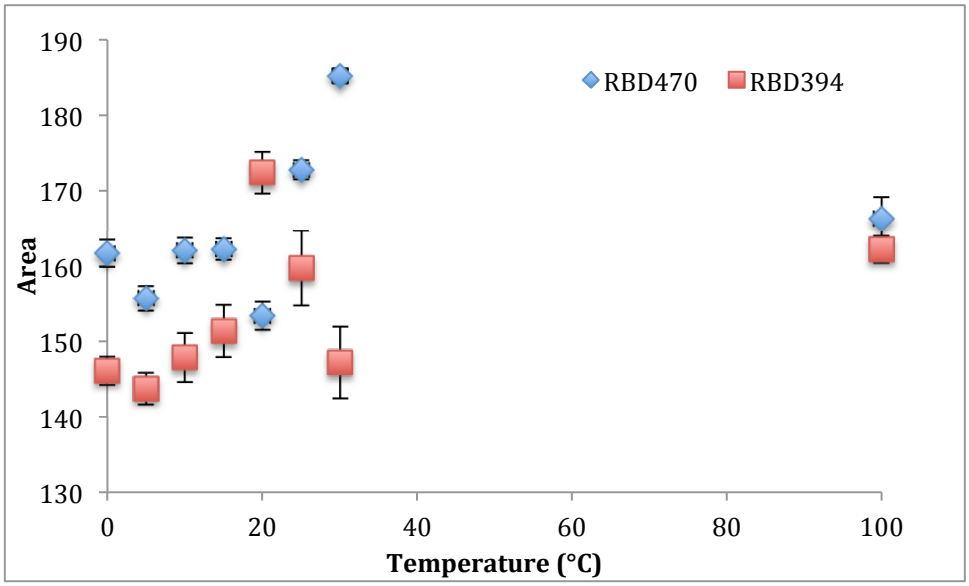

Figure 4- 16. WXRD liquid integrated intensity vs. temperature

4.2.6. Calculation of mass fraction of each phase

The proportionality factors between integrated intensity and solid fat content are calculated using Eq.2 and Excel solver, and the results are shown in Table 4- 2 and Table 4- 3. Some of the standard errors are extremely large. The phases with relative large standard errors have smaller integrated intensity compared to other phases, which causes the standard error to increase, since a small change in the amount of phase is a relative large change. Two main reasons for those changes seem probable. The first one is that the mixed fat does not form exactly the same amount of each phase every time, so there might be some difference in the proportion of each phase for different runs. The second reason is that crystal clusters might be formed in different places of the capillary. The beam, however, always went through the sample at the same spot of the capillary, which can lead to different integrated intensity of each phase for each run. To solve this problem in the future, a capillary holder with a vertical moving stage may be required. During the XRD experiments, the stage moves within the range of sample in the capillary providing an averaging effect.

Table 4- 2. Proportionality factors K_f of each phase of RBD470

Capillary	K_1	K_2	K_3	K_4
1	26.26±11.11	22.22±0.66*	20.98±26.64	16.34±3.13
2	24.18±3.13	20.39±0.16	22.45±5.11	17.47±0.55

Table 4- 3. Proportionality factors K_f of each phase of RBD394

Capillary	K_1	K_3	K_4
1	28.1±3.90*	18.96±0.05	11.13±5.53
2	39.37±7.39	19.95±0.66	17.66±7.85

* The range of the proportionality factor is the average ± standard error. K_3 and K_4 correspond to the phase 3 and 4 shown in Figure 4- 10 and Figure 4- 11.

Figure 4- 17 and Figure 4- 18 give the mass fraction of each phase of RBD470 and RBD394 respectively, which were calculated using Eq.3 and the average of proportionality factors.

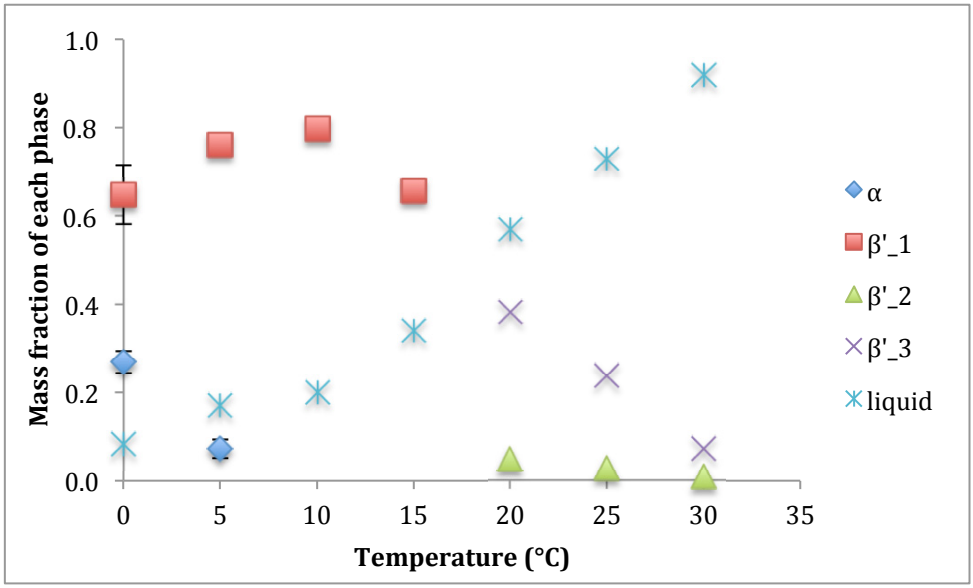

Figure 4- 17. Total mass fraction of each phase vs. temperature of RBD470

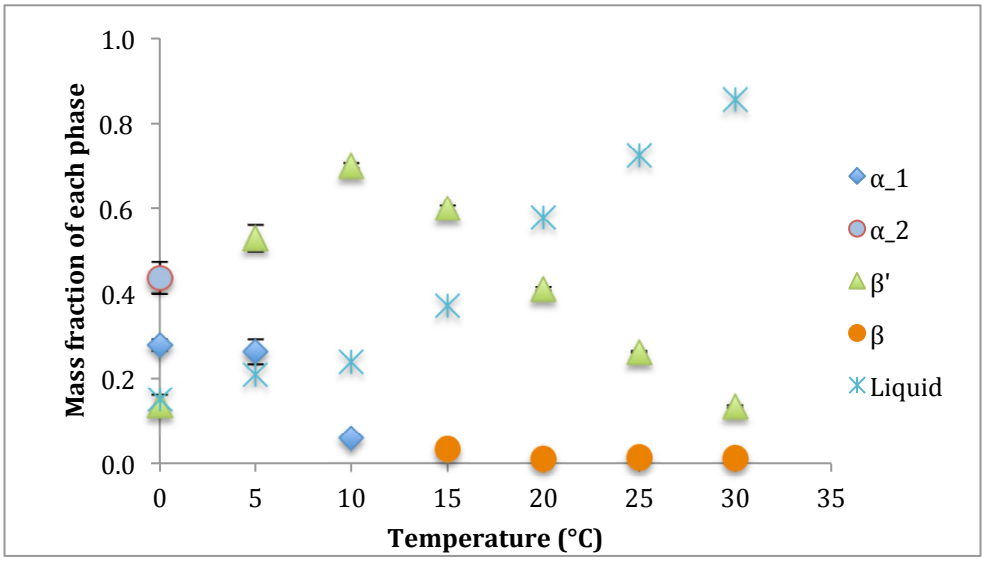

Figure 4- 18. Total mass fraction of each phase vs. temperature of RBD394

Table 4- 4. Total mass fraction of each phase of RBD470

Temperature (°C)	α	β'_1	β'_2	β'_3	Liquid
0	0.27±0.026*	0.65±0.061			0.08
5	0.07±0.021	0.76±0.023			0.17
10		0.80			0.20
15		0.66			0.34
20			0.05±0.002	0.38±0.028	0.57
25			0.03±0.008	0.24±0.032	0.73
30			0.01±0.001	0.07±0.005	0.92

Table 4- 5. Total Mass fraction of each phase of RBD394

Temperature (°C)	α_1	α_2	β'	β	Liquid
0	0.28±0.013*	0.44±0.037	0.14±0.024		0.15
5	0.26±0.029		0.53±0.030		0.21
10	0.06±0.009		0.70±0.006		0.24
15			0.60±0.007	0.03±0.006	0.37
20			0.41±0.004	0.01±0.001	0.58
25			0.26±0.003	0.01±0.004	0.72
30			0.13±0.004	0.01±0.003	0.86

* The range of the mass fraction is the average ± standard error. Phase α_2 only exists at 0°C and there is no SFC data to calculate proportionality factor, so this study assume SFC at 0°C is 85% and the average proportionality factor of phase α_2 is 37.17 ± 10.80.

For the subsequent prediction, the β'_1 and β'_3 phases observed in WXRD of RBD470 were simply assumed to be the same β' phase and use the same method to estimate the enthalpy, melting point and interaction parameters. The α_1 phase of RBD394 was assumed to be the ideal α phase, whose activity coefficient is equal to 1.

4.3. MATLAB calculation

4.3.1. Estimates of enthalpy and melting point

By using Wesdorp' s method, the enthalpy and melting point of the TAGs of two samples for three different polymorphs was estimated. When the parameters shown in Table 2- 1 were applied, the estimated melting temperatures were quite large, around 200 °C.

Therefore, simply changing the sign of the parameters in the right side of the table was tried, because the unsaturated TAGs must have a negative effect on the melting point. For elaidic, it has to have opposite effect to oleic, linoleic and linolenic.

Table 4- 6. The checked parameters for estimation of enthalpy and melting point

	α	β'	β		α	β'	β
h_0	-31.95	-35.86	-17.16	A_O	-3.46	-2.2	-2.93
h	2.7	3.86	3.89	A_D	1.38	1.34	1.68
s_0	-19.09	-39.59	31.04	A_J	-3.35	-2.5	-4.69
s	6.79	10.13	9.83	A_N	-4.2	-2.2	-5.2
h_{xy}	-13.28	-19.35	-22.29	A_{OO}	-0.11	-0.27	-0.89
s_{xy}	-36.7	-52.51	-64.58	A_{DD}	0.01	0.04	0.4
k	4.39	1.99	2.88	A_{JJ}	-3.68	-0.55	-1.21
x_0	1.25	2.46	0.77	A_{NN}	-1	-1.51	-1.38
T_∞	397	381	395	A_{OJ}	-0.53	-1	-0.71
h_o	-31.7	-28.3	-30.2	A_{ON}	-0.83	-0.76	-0.69
h_e	-11.7	-15.9	-15.9	A_{JN}	-3	-1.12	-0.73
h_J	-37.7	-37.7	-37.7	B_O	0	-4.3	-3.7
A_{sat}	-9.02	-5.38	-7.57	B_J	-5.4	-7.8	-1.5
B_{sat}	-2.81	-3.91	3.16	B_N	-2.6	-13.7	-1.8

The values shown in Table 4- 6 were used to recalculate enthalpy and melting point, and the results are shown in Table 4- 7 and Table 4- 8. The green numbers are experimental data taken from Wesdorp's paper, the black and red numbers are estimated values, and those red numbers do not satisfy the requirement that the magnitude of enthalpy and

melting point should be α < β' < β polymorph for the same TAG. By comparing the prediction value of Wesdorp's, it was found that our enthalpy values are consistent with his values; however, there are still large differences for the melting point values, which may be caused by a publishing error in the table of parameters. It is outside of the scope of this project to calculate all the parameters again; therefore, another method was developed to find reasonable melting point estimates. For PJP β'-form's enthalpy, the average of enthalpy of α and β was taken to do the correction, and the corrected value is 82.5 KJ/mol.

Table 4- 7. Molecular weight and estimated enthalpy and melting point of RBD470

NO.	TAG	MW	H (KJ/mol)			T (°C)		
			α	β'	β	α	β'	β
1	POP	838.56	70.00	104.00	140.00	16.60	33.20	37.20
2	PJP	836.56	64.97	118.43	100.00	9.55	33.79	27.10
3	POO	864.58	42.18	95.00	112.48	-5.26	16.55	18.50
4	MOP	810.54	59.15	100.10	114.88	14.64	37.44	27.00
5	POS	866.58	78.00	114.00	150.00	19.60	43.59	31.00
6	POJ	862.58	36.18	85.55	104.98	13.30	1.72	37.43
7	MPJ	808.54	52.08	91.70	109.09	4.09	30.09	68.27
8	PPP	812.54	95.80	126.50	171.30	44.70	55.70	65.90
9	MPP	784.52	89.00	128.39	140.00	36.00	52.00	55.80
10	PJS	864.58	67.88	113.85	135.18	14.55	37.16	24.50
11	MOO	836.56	27.85	72.81	81.93	-10.70	12.16	12.80
12	JOO	888.61	11.72	63.13	93.26	-2.20	-33.37	-4.36
13	OOS	892.61	49.42	100.83	130.96	-0.24	20.56	23.50
14	MPT	782.52	89.38	128.39	149.54	41.30	59.55	110.43
15	MOJ	834.56	21.85	63.41	74.43	-27.33	-3.56	33.56
16	SOS	894.61	73.00	111.00	154.00	22.90	37.00	43.00*
17	OOO	890.61	37.00	79.00	100.00	-33.70	-10.00	4.80
18	PJJ	860.58	30.18	76.15	97.48	-62.98	-4.20	21.31
19	PPS	840.56	100.00	124.00	166.30	46.40	58.70	62.60
20	JOS	890.61	43.42	91.43	123.46	-14.66	-3.50	40.98
21	JSS	892.61	75.12	119.73	153.66	19.13	40.25	35.80
22	JOJ	886.61	5.72	53.73	85.76	-96.28	-39.00	-18.15

* value is corrected from paper (Takeuchi, Ueno, Flöter, & Sato, 2002)

Table 4- 8. Molecular weight and estimated enthalpy and melting point of RBD394

NO.	TAG	MW	H (KJ/mol)			T (°C)		
			α	β'	β	α	β'	β
1	MML	700.46	73.18	105.23	126.20	26.06	46.22	46.71
2	MOP	810.54	59.15	100.10	114.88	14.64	37.44	27.00
3	POP	838.56	70.00	104.00	140.00	16.60	33.20	37.20
4	LMP	728.48	74.00	94.00	125.00	16.49	28.27	48.50
5	MMP	756.50	82.00	100.00	131.00	34.50	48.50	53.30
6	COP	754.50	34.76	67.80	80.33	4.11	30.02	78.52
7	PPM	784.52	89.38	128.39	149.54	40.11	55.83	56.58
8	LLM	672.44	67.13	83.36	116.00	19.00	37.80	42.30
9	MOM	782.52	56.24	104.68	115.63	11.70	26.40	28.00
10	CLM	644.41	57.38	83.08	100.11	8.67	36.70	35.15
11	PJP	836.56	64.97	118.43	100.00	9.55	33.79	27.10
12	MJP	808.54	53.15	90.70	107.38	4.09	30.09	68.27
13	COM	726.48	33.10	60.42	75.50	-1.96	25.70	76.17
14	CCM	616.39	51.33	61.22	94.51	3.00	31.00	34.50
15	POS	866.58	78.00	114.00	150.00	19.60	43.59	31.00
16	CJP	752.50	28.76	58.40	72.83	-8.54	21.51	62.93
17	PPP	812.54	95.80	126.50	171.30	44.70	55.70	65.90
18	MJM	780.52	50.24	95.28	108.13	-1.91	26.02	65.73
19	CJM	724.48	27.10	51.02	68.00	-15.88	16.49	59.84
20	POO	864.58	42.18	95.00	112.48	-5.26	16.55	18.50
21	COC	670.44	29.79	63.99	78.99	-16.40	15.48	-4.80
22	PJS	864.58	67.88	113.85	135.18	14.55	37.16	24.50
23	MOO	836.56	27.85	72.81	81.93	-10.70	12.16	12.80
24	ROP	726.48	29.36	60.08	72.55	-1.96	25.70	76.17
25	PPS	840.56	100.00	124.00	166.30	46.40	58.70	62.60
26	CCL	588.37	50.93	60.20	97.25	0.00	26.00	30.00
27	COO	780.52	8.46	47.22	57.91	-23.08	2.02	-0.30
28	POJ	862.58	36.18	85.55	104.98	13.30	1.72	37.43
29	SOS	894.61	73.00	111.00	154.00	22.90	37.00	43.00*
30	CCC	560.35	57.30	64.79	95.00	-11.50	16.80	31.60

* value is corrected from paper (Takeuchi et al., 2002)

Since enthalpy values are reasonable, the relation between enthalpy and entropy was sought, so that the melting temperature could then be calculated using $T_{fi}= \Delta H/\Delta S$ (Eq.6). The TAGs with experimental thermodynamic data for three polymorphs were chosen, and their entropies were calculated. After plotting experimental enthalpy vs. entropy, the figure showed that the entropy of three polymorphs followed the same trend for most of the TAGs, and a trend line was obtained by using Excel. In Figure 4- 19, COO and COC were used as examples, both of them having experimental melting point of β. The entropy vs. enthalpy of α, β', β of COO and COC were plotted on the same graph, the entropies of β of those two TAGs were recalculated by using the trend line equation. Using the experimental entropy divided by the calculated entropy produced a corrected factor. Using the trend line equation to calculate the entropy of β' and then multiplying by a correction factor, the result is a 'corrected entropy'. With this 'corrected entropy', a reasonable melting point of β' can be estimated. The corrected melting temperatures are shown in Table 4- 9.

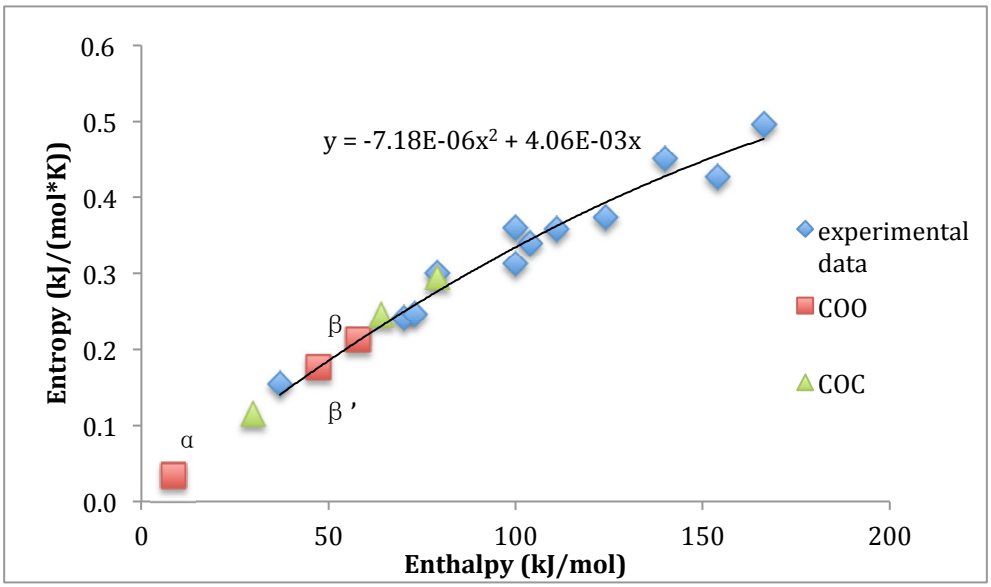

Figure 4- 19. Enthalpy vs. Entropy of TAGs with experimental data and corrected COO and COC values

Table 4- 9. The corrected melting temperatures of TAGs that do not have good prediction

TAG	α	β'	β
PJP	9.6	21.8	27.1
MOP	14.6	22.5	27.0
POS	19.6	31.6*	35.5*
POJ	13.3	27.6	37.4
PJS	4.6	17.9	24.5
JOO	-2.2	11.5	20.3
JSS	11.6	24.8	35.8
CLM	21.6	36.7	47.6
COO	-23.1	-5.7	-0.3
COC	-16.4	-12.5	-4.8

* values are corrected from paper (Arishima, Sagi, Mori, & Sato, 1991)

4.3.2. Mass fraction of component in each phase

The mass fraction of each component in each phase was plotted in order of increasing 'mass fraction difference' between two phases (solid-liquid or solid-solid). From Figure 4- 20, Figure 4- 21, MOP, PJP, POP in RBD470 have the largest difference between each phase; moreover, they tend to crystallize easily at 10 °C and melt easily at 30 °C. The different concentration of each component leads to form the different β' phases. The β'_3 phase has larger proportion than β'_2 phase. For RBD394, Figure 4- 22 and Figure 4- 23 show that the more stable phase formed when a less stable phase melted first. MML, LMP and POP have large concentration at β' phase and the temperature changes have little effect on their β' phase composition.

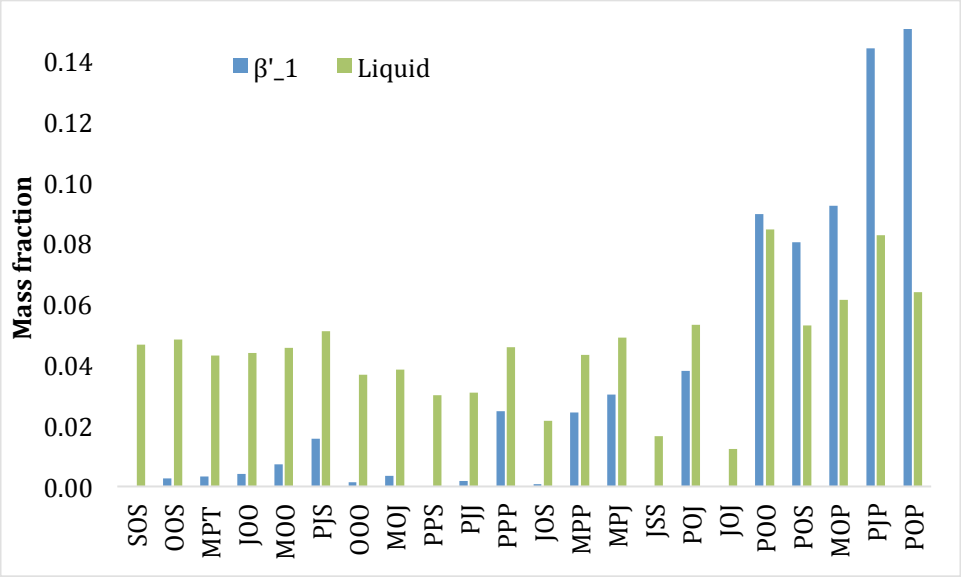

Figure 4- 20. Mass fraction of each component in each phase at 10 °C of RBD470 (POP is off scale = 0.35)

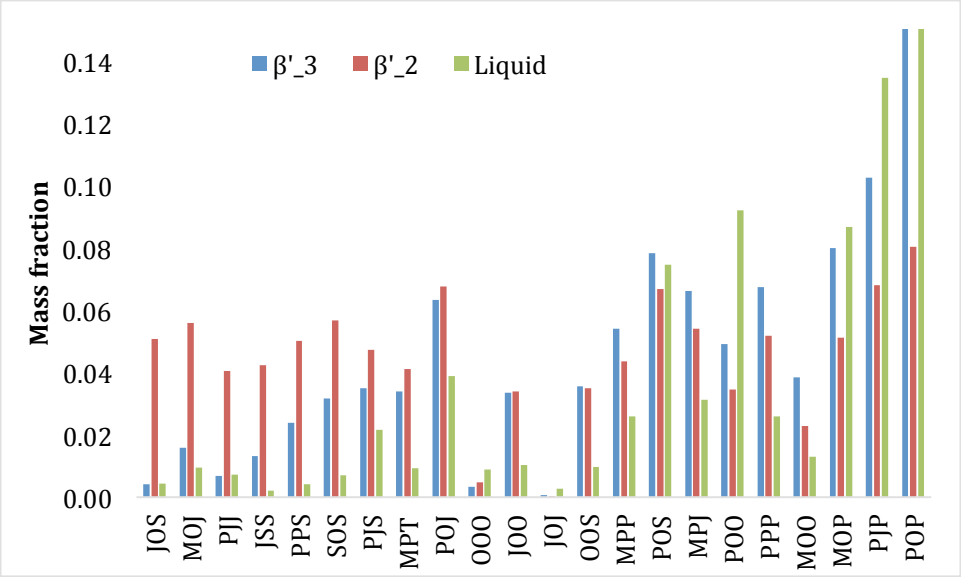

Figure 4- 21. Mass fraction of each component in each phase at 30 °C of RBD470

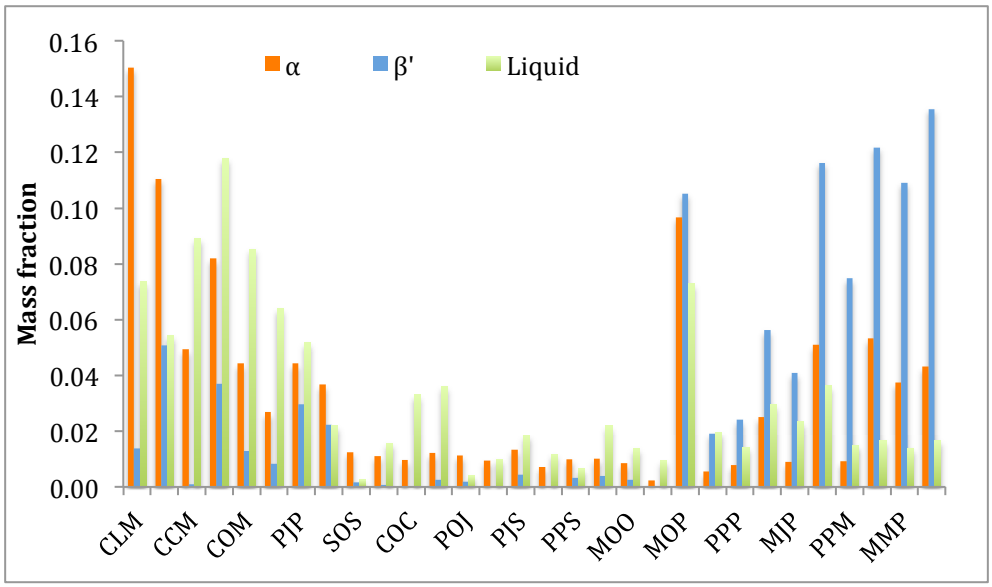

Figure 4- 22. Mass fraction of each component in each phase at 10 °C of RBD394

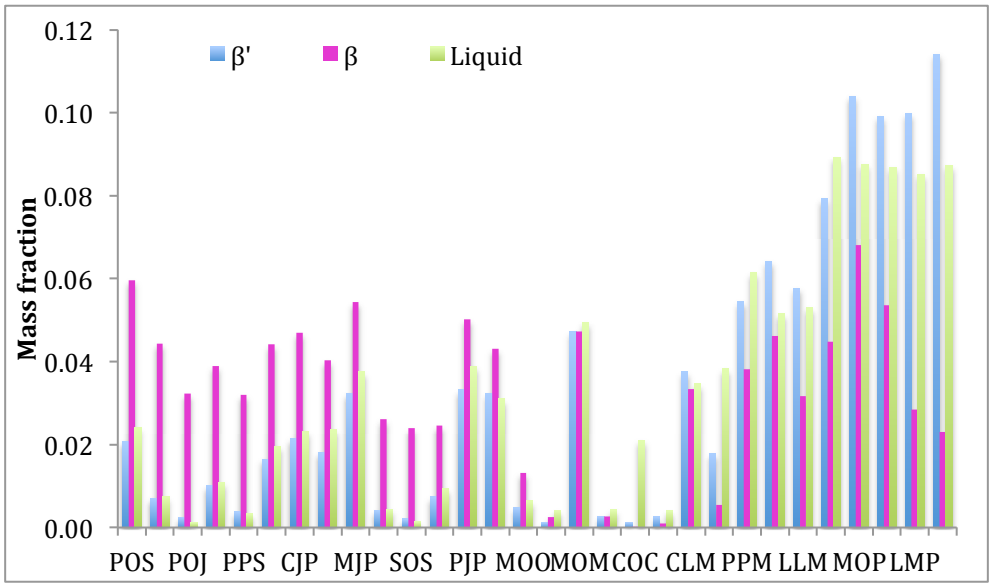

Figure 4- 23. Mass fraction of each component in each phase at 15 °C of RBD394

The fraction of each component in the solid as a function of temperature is shown in Figure 4- 24 for RBD470 and in Figure 4- 25 for RBD394. Those two figures are a general tool to check the reliability of the prediction. In order to satisfy the mass balance, if some components have a large fraction at a specific temperature, other components should have lower fraction in the solid. For instance, PJJ in RBD470 and COC in RBD394 have relative lower melting point, therefore they keep lower fraction in the solid. TAGs with large thermal factor k_i (Eq.26) are easy to crystallize and they may have a large fraction in the solid if they have a large composition in the sample. MPT and PPS have the largest thermal factor value in RBD470 and RBD 394 respectively. Moreover, similar TAGs would have similar change during the temperature change. For example, MMP, PPM, MML and LMP, all of them are saturated TAG, so they followed the same

trend as temperature changed. However, this method did not take into account the influence of the chiral molecules. TAGs with different fatty acid esterified at sn-1 and sn-3 position are chiral objects. Mizobe et al. (2013) studied the structures and binary mixing characteristics of the enantiomers of S- OPP and R- PPO. They found that there is an important relationship between subcell packing and glycerol conformation in the polymorphism of the enantiomers. Most chiral TAGs in nature are found as racemic mixtures.

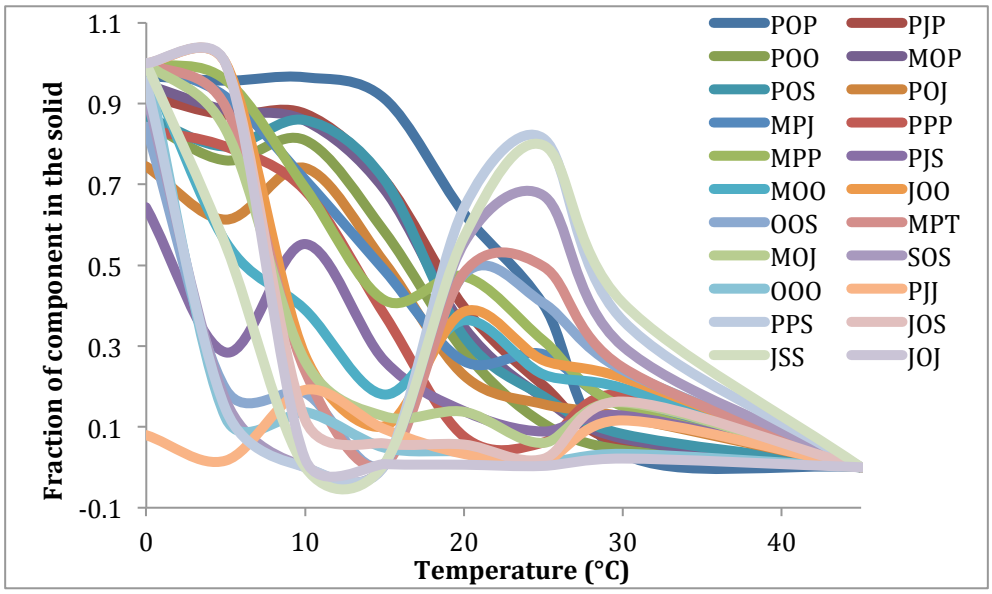

Figure 4- 24. Fraction of component in the solid vs. temperature of RBD470

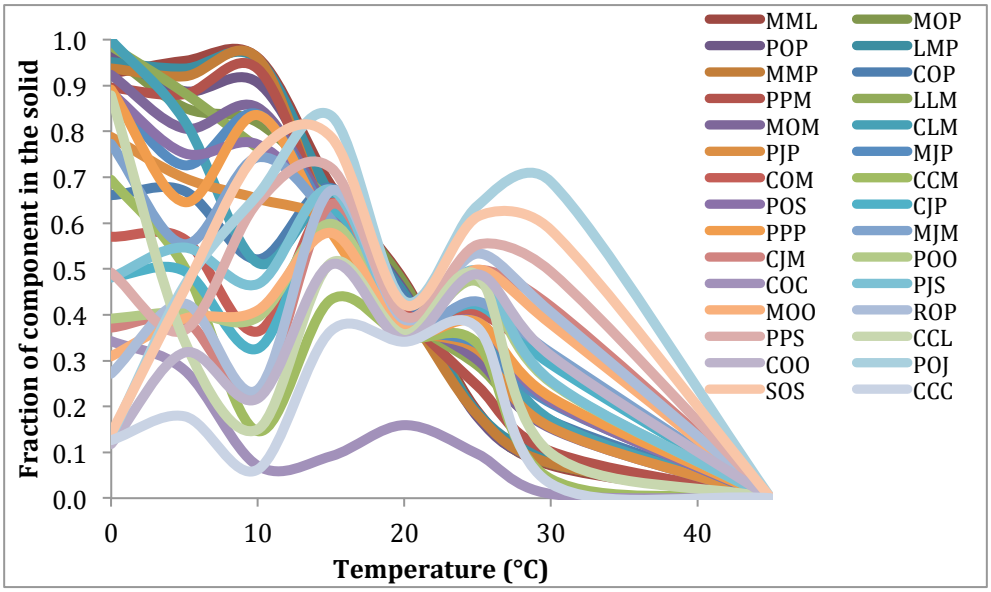

Figure 4- 25. Fraction of component in the solid vs. temperature of RBD394

Some limitations in our predictions were found by plotting the fraction of each component in the liquid vs. temperature. High melting point components in both samples, such as PPS in RBD470, PPP and PPS in RBD394 should be mostly in the solid state at lower temperature; while the lower melting point JOJ in RBD470 should mostly stay in a liquid state. However, from Figure 4- 26 and Figure 4- 27 PPS in RBD470 and PPP, PPS in RBD394 have large fractions in the liquid at lower temperatures, while JOJ in RBD 470 has a small fraction in the liquid. The reason for this problem might be the inaccuracy in estimating of the interaction parameters via the 'degree of isomorphism'. The 'degree of isomorphism' calculated by Kitaigorodsky' method is not reliable for the unsaturated TAGs, which have the same values of degree of isomorphism as the saturated TAGs. However, in reality, the saturated and unsaturated TAGs have different interaction

parameters.

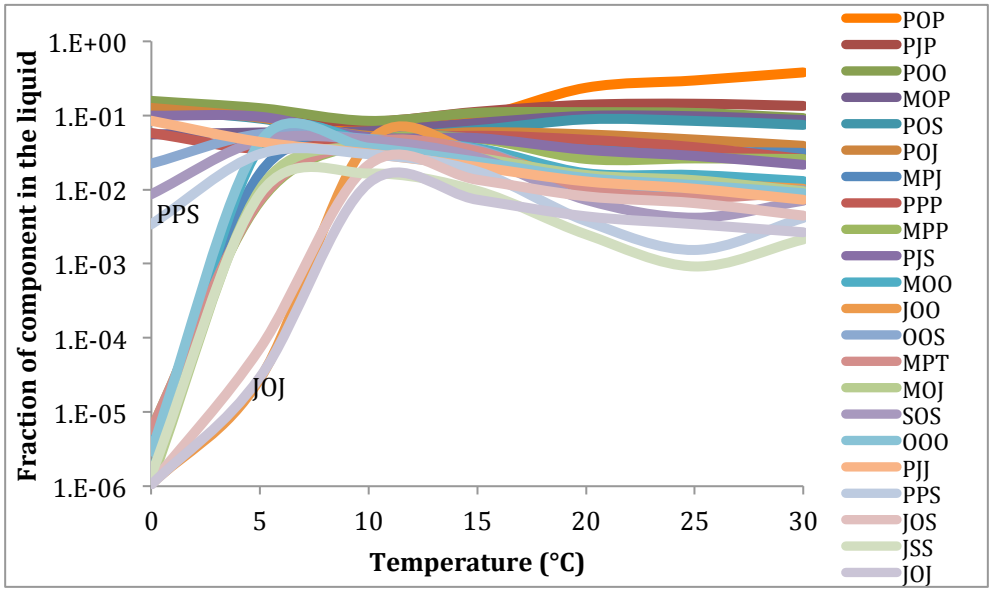

Figure 4- 26. Fraction of each component in the liquid vs. temperature of RBD470

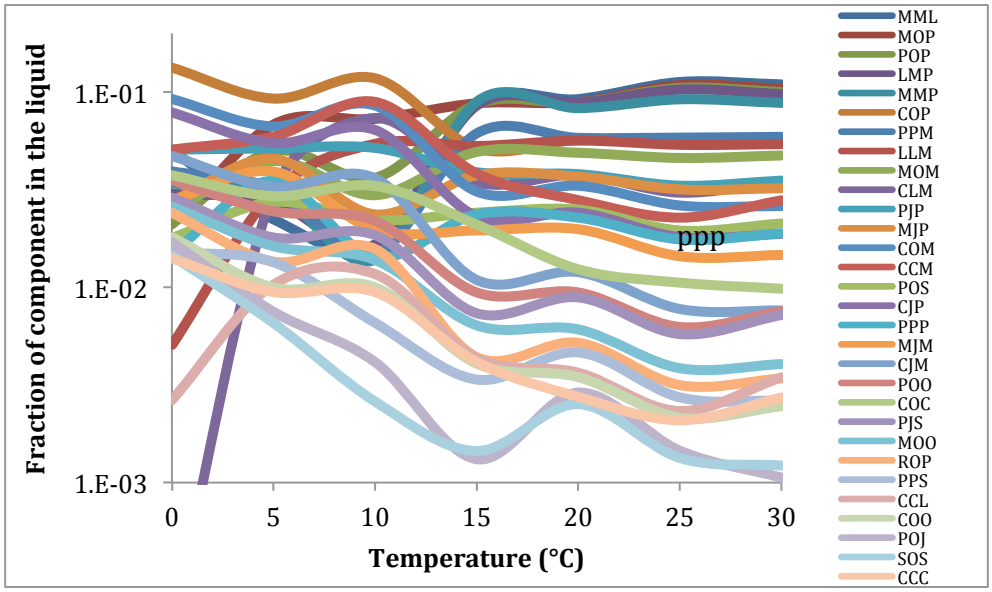

Figure 4- 27. Fraction of each component in the liquid vs. temperature of RBD39

4.3.3. Comparison of the predicted overall melting enthalpy with the DSC measured overall enthalpy

When SFC is larger than 80, for both RBD470 and RBD394, the predicted enthalpies keep around 100 J/g and 80 J/g respectively. This enthalpy trend might be due to the presence of the α-form at those SFC. The α polymorph has the lowest enthalpy compared with the other polymorphs, so the existence of the α polymorph may lower the overall melting enthalpy; even if the total SFC is larger. The mass fractions of α polymorph in RBD470 are 7% and 27% for SFC 81 % and 91%. For RBD394, they are 26% and 72% for SFC 80 % and 85%. Therefore, the decrease of enthalpy due to the increase of the α polymorph is balanced by the increase of enthalpy of the other polymorphs for RBD470; however, for RBD394, the large amount of α polymorph leads to the enthalpy decreasing from 100 J/g to 80 J/g.

When SFC is smaller than 80%, for both RBD470 and RBD394, the measured enthalpies increase with the increase of SFC and followed a linear relation with SFC. The predicted enthalpies are consistent with DSC values for both samples at lower SFC. This consistent result suggests that future studies cannot simply assume that only two different phases exist (a single solid phase for all the solid and a liquid phase) in the study of the thermodynamic properties of fat crystallization, otherwise the enthalpies will not match. However, the comparison based on the unit J/g might not provide an accurate result,

because after dividing by molecular weights of TAGs to convert enthalpy (J/mol) to enthalpy (J/g), it tends not to show large enthalpy differences between TAGs, and therefore when the concentration of each component is changed the effect is not strong (Figure 4- 30). TAGs with long chains have large molar enthalpy, so the mole based enthalpy increases with carbon number, however, mass based enthalpy keeps approximately constant as carbon number increases. Therefore, there is a limitation of DSC as a check method for a multicomponent system study.

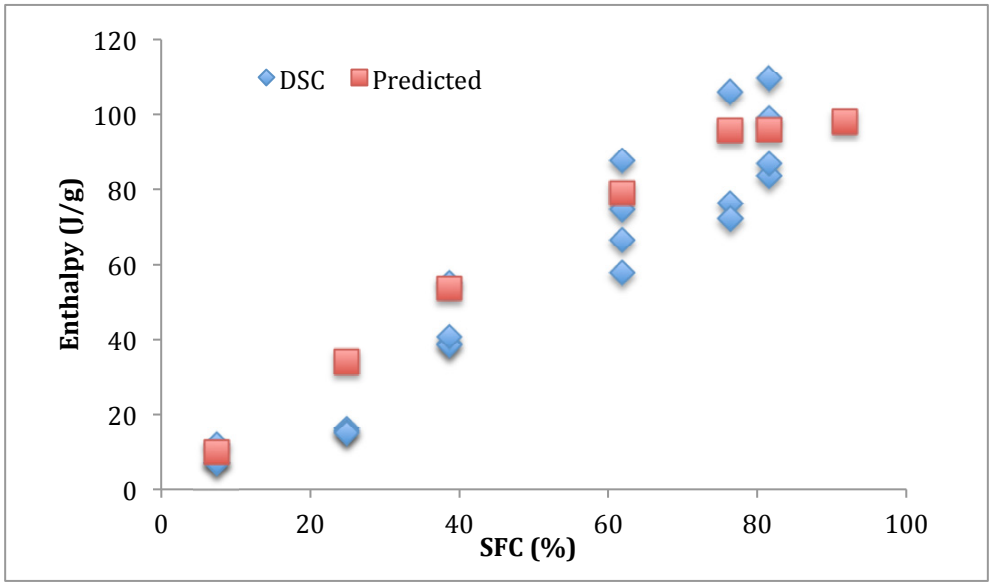

Figure 4- 28. Comparison of DSC and predicted overall enthalpy of RBD470

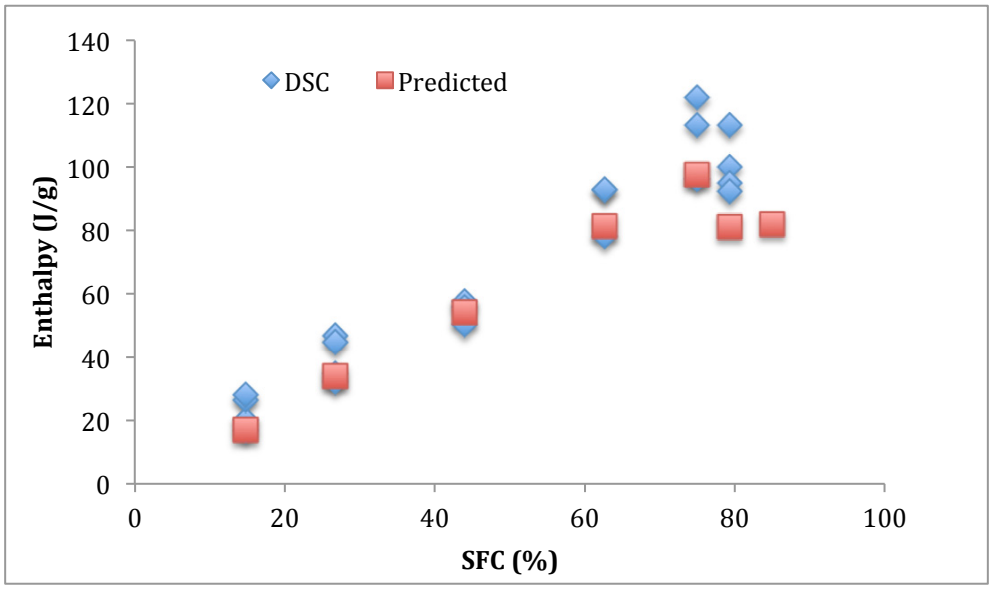

Figure 4- 29. Comparison of DSC and predicted overall enthalpy of RBD394

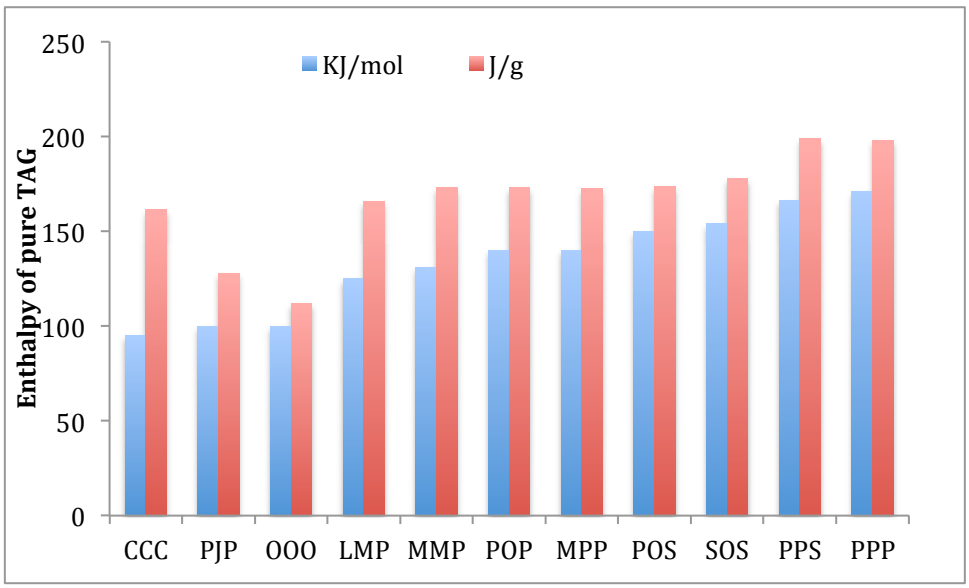

Figure 4- 30. Enthalpy of β polymorph of selected TAG with different enthalpy units

4.3.4. Residual errors

The β' phase was always present in both samples, hence it was chosen as reference phase to compute the equilibrium error. The error was defined as the difference between liquid mole fraction calculated from liquid mass fraction and liquid mole fraction calculated from equilibrium (Eq.27). As shown in Figure 4- 31, for RBD470 the errors between mass fraction and equilibrium follow the same trend.

However, for RBD394 (see Figure 4- 32), the errors separate into two regions depending on the temperatures. At high temperatures (20, 25 and 30 °C), the errors are relatively large (more than 0.1), whereas the errors of other temperatures are smaller than 0.1.

The errors shown in both Figure 4- 31 and Figure 4- 32 are not equal to 0, which means the systems based on our prediction are not in the equilibrium state. There may be several reasons for this. The first one is that both samples may have not reached equilibrium in the reality. The second reason is the possible inaccuracy of our estimates of enthalpy and melting point of pure TAGs. The last but not the least is that using the 'degree of isomorphism' to estimate interaction parameter and using 2-suffix Margules equation to calculate activity coefficients are inappropriate methods.

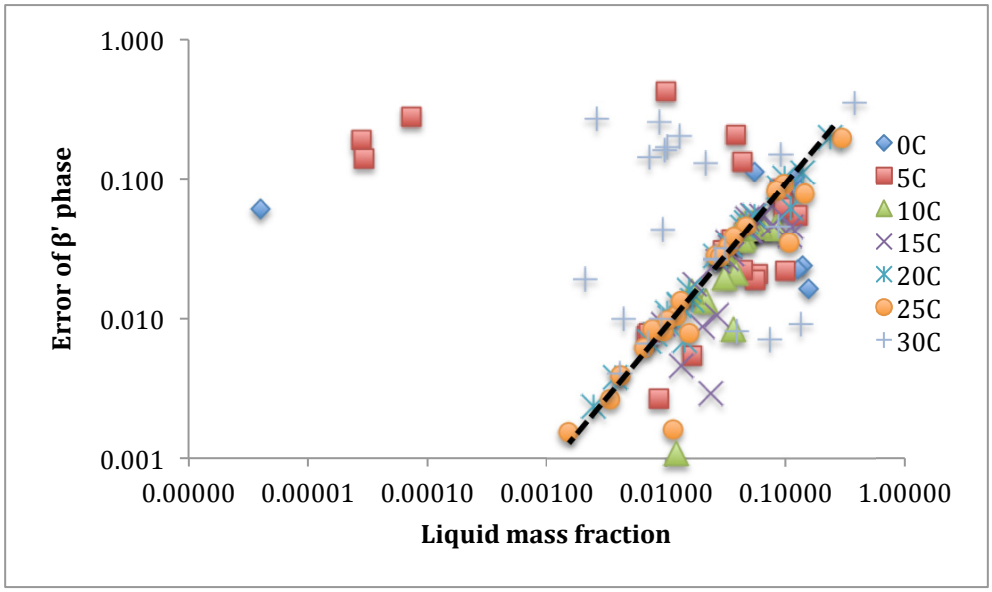

Figure 4- 31. Absolute error of β' phase as function of liquid mass fraction in a logarithmic scale for RBD470

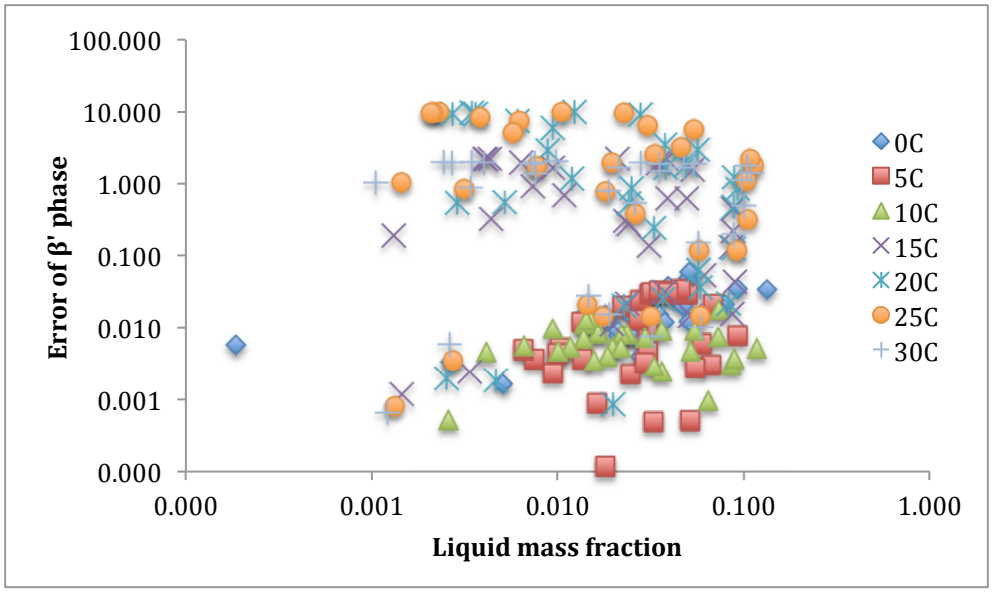

Figure 4- 32. Absolute error of β' phase as function of liquid mass fraction in a logarithmic scale for RBD394

Chapter 5. CONCLUSION AND FUTURE WORK

A database of 209 TAGs was digitized, which includes experimental enthalpy and melting temperatures of different polymorphic forms. In the future, the data from other resources and literature can be added to the database. MATLAB code was then created to estimate the enthalpy and melting temperature for TAGs that do not have experimental data. The estimated or experimental enthalpy and melting point were used in the subsequent mass balance-equilibrium MATLAB calculation. New MATLAB codes were created that used the number of phases and polymorphic information along with the equilibrium method to calculate the compositions of the phases. This code constrained the results to abide by the mass balance and the stoichiometric requirement.

This work tested Wesdorp's thermodynamic properties estimation method and solid-equilibrium model associated with 2-suffix Margules equations. This test was conducted using two commercial multicomponent samples, RBD470 and RBD394, which have 22 and 30 TAGs respectively. Instead of estimating the number of phases and phase types using Wesdorp's flash calculation method, XRD experiments provided both the phases and polymorphic information. DSC was used to help identify the polymorphic forms and to calculate the experimental melting enthalpy. MATLAB 2014b and Excel were used to perform all the calculations of the model.

The initial results of enthalpy and melting point estimation showed that Wesdorp's method provides a good prediction for enthalpy, but not for melting point. The melting point estimation had a big difference between Wesdorp's values and ours, which might be caused by the publishing error of melting point estimation parameters. Further work can be done to correct those parameters. A corrected method based on Wesdorp's method and experimental melting point was developed. Instead of finding the melting point of three polymorphs individually, this study used the trend between enthalpy and entropy and a known experimental melting point of one polymorph to produce a reasonable estimate for other polymorphs. A further study can be done to develop a new melting point estimation method. The 'degree of isomorphism' was used to estimate binary interaction parameters, and the 2-suffix Margules equation was used in solid-equilibrium model to produce activity coefficients.

The prediction results provided an overall melting enthalpy generally consistent with DSC values. However, the agreement is poorer at large SFC (80%). However, the comparison of the overall melting enthalpy by mass is not the best method to verify the compositions. Therefore, further research need be done to check the accuracy of Wesdorp's method using 2-suffix Margules equation. Moreover, improvement is clearly needed in all aspects of the method, since the equilibrium is not achieved and the errors are quite large.

For the TAGs that belong to the same polymorph but are in different phase, the estimation of the interaction parameters is based on our guess. In the future, a study relating d-spacing of different phases with interaction parameters can be done to develop a more accurate method to solve this problem.

The inconvenience of our MATLAB code is that users need to change the temperature, equations of estimation interaction parameter and the output reference phase column in the matrix manually for each run. The MATLAB code also can be improved in the future, so that users can directly receive output of all the temperatures of one sample.

REFERENCES

Acevedo, N. C., & Marangoni, A. G. (2010). Characterization of the Nanoscale in Triacylglycerol Crystal Networks. *Crystal Growth & Design*, *10*(8), 3327–3333. doi:10.1021/cg100468e

Al-Qatami, O. A. M. (2011). *Thermal study of a triglyceride mixture*. Dalhousie University.

Anom, E. Y. (2009). *Comparison of the theoretical and experimental composition of crystallizing lipid mixtures*. Dalhousie University.

Arishima, T., Sagi, N., Mori, H., & Sato, K. (1991). Polymorphism of pos. I. occurrence and polymorphic transformation. *Journal of the American Oil Chemists' Society*, *68*(10), 710–715. doi:10.1007/BF02662157

Bevington, P. R., & Keith Robinson, D. K. (1969). *Data reduction and error analysis for the physical sciences*. New York: McGraw-Hill.

Breitschuh, B., & Windhab, E. J. (1998). Parameters influencing cocrystallization and polymorphism in milk fat. *Journal of the American Oil Chemists' Society*, *75*(8), 897–904. doi:10.1007/s11746-998-0264-8

Campos, R., Narine, S., & Marangoni, A. (2002). Effect of cooling rate on the structure and mechanical properties of milk fat and lard. *Food Research International*, *35*(10), 971–981. doi:10.1016/S0963-9969(02)00159-X

Chong, C. L., Kamarudin, Z., Lesieur, P., Marangoni, A., Bourgaux, C., & Ollivon, M. (2007). Thermal and structural behaviour of crude palm oil: Crystallisation at very slow cooling rate. *European Journal of Lipid Science and Technology*, *109*(4), 410–421. doi:10.1002/ejlt.200600249

Christie, W. (2003). What is a lipid. *The AOCS Lipid Library*, 1–14. Retrieved from http: http://lipidlibrary.aocs.org/Lipids/whatlip/index.htm

Cisneros, A., Mazzanti, G., Campos, R., & Marangoni, A. G. (2006). Polymorphic Transformation in Mixtures of High- and Low-Melting Fractions of Milk Fat. *Journal of Agricultural and Food Chemistry*, *54*(16), 6030–6033. doi:10.1021/jf0600814

Foubert, I., Dewettinck, K., & Vanrolleghem, P. A. (2003). Modelling of the crystallization kinetics of fats. *Trends in Food Science & Technology*, *14*(3), 79–92. doi:10.1016/S0924-2244(02)00256-X

Himawan, C., Starov, V. M., & Stapley, A. G. F. (2006). Thermodynamic and kinetic aspects of fat crystallization. *Advances in Colloid and Interface Science*, *122*(1-3), 3–33. doi:10.1016/j.cis.2006.06.016

Hollingsworth, M. D. (2002). Crystal Engineering: from Structure to Function. *Science*, *295*(5564), 2410–2413. doi:10.1126/science.1070967

Karray, N., Lopez, C., Lesieur, P., & Ollivon, M. (2005). Original article Dromedary milk fat : thermal and structural properties 2 . Influence of cooling rate. *Lait*, *85*, 433–451. doi:10.1051/lait:2005034

Kitaigorodsky, A. I. (1973). *Molecular crystals and molecules.* New York: Academic Press.

Kitaigorodsky, A. I. (1984). *Mixed Crystals:Springer Series in Solid-State Sciences* (Vol. 33). Berlin: Springer Verlag.

Kloek, W., Van Vliet, T., & Walstra, P. (2005). Mechanical properties of fat dispersions prepared in a mechanical crystallizer. *Journal of Texture Studies*, *36*(5-6), 544–568.

Liang, B., Shi, Y., & Hartel, R. W. (2003). Phase equilibrium and crystallization behavior of mixed lipid systems. *Journal of the American Oil Chemists' Society*, *80*(4), 301–306. doi:10.1007/s11746-003-0693-1

Loisel, C., Keller, G., Lecq, G., Bourgaux, C., & Ollivon, M. (1998). Phase transitions and polymorphism of cocoa butter. *Journal of the American Oil Chemists' Society*, *75*(4), 425–439. doi:10.1007/s11746-998-0245-y

Lopez, C., Bourgaux, C., Lesieur, P., Bernadou, S., Keller, G., & Ollivon, M. (2002). Thermal and Structural Behavior of Milk Fat. *Journal of Colloid and Interface Science*, *254*(1), 64–78. doi:10.1006/jcis.2002.8548

Lopez, C., Karray, N., Lesieur, P., & Ollivon, M. (2005). Crystallisation and melting properties of dromedary milk fat globules studied by X-ray diffraction and differential scanning calorimetry. Comparison with anhydrous dromedary milk fat. *European Journal of Lipid Science and Technology*, *107*(9), 673–683. doi:10.1002/ejlt.200501179

Lopez, C., Lavigne, F., Lesieur, P., Bourgaux, C., & Ollivon, M. (2001). Thermal and structural behavior of milk fat. 1. Unstable species of anhydrous milk fat. *Journal of Dairy Science*, *84*(4), 756–66. doi:10.3168/jds.S0022-0302(01)74531-6

Lopez, C., Lavigne, F., Lesieur, P., Keller, G., & Ollivon, M. (2001). Thermal and structural behavior of anhydrous milk fat. 2. Crystalline forms obtained by slow cooling. *Journal of Dairy Science*, *84*(11), 2402–12. doi:10.3168/jds.S0022-0302(01)74689-9

Lopez, C., Lesieur, P., Bourgaux, C., Keller, G., & Ollivon, M. (2001). Thermal and Structural Behavior of Milk Fat. *Journal of Colloid and Interface Science*, *240*(1), 150–161. doi:10.1006/jcis.2001.7664

Lopez, C., Lesieur, P., Keller, G., & Ollivon, M. (2000). Thermal and Structural Behavior of Milk Fat. *Journal of Colloid and Interface Science*, *229*(1), 62–71. doi:10.1006/jcis.2000.6988

Los, J., & Flöter, E. (1999). Construction of kinetic phase diagrams. *Physical Chemistry Chemical Physics*, *1*(18), 4251–4257. doi:10.1039/A903245B

Los, J. H., Enckevort, W. J. P. Van, Vlieg, E., Gandolfo, F. G., & Flöter, E. (2002). Metastable States in Multicomponent Liquid−Solid Systems II: Kinetic Phase Separation. *The Journal of Physical Chemistry B*, *106*(29), 7331–7339. doi:10.1021/jp0257294

Los, J. H., van Enckevort, W. J. P., Vlieg, E., & Flöter, E. (2002). Metastable States in Multicomponent Liquid-Dolid Systems I: A Kinetic Crystallization Model. *The Journal of Physical Chemistry B*, *106*(48), 12651–12651. doi:10.1021/jp0223354

MacNaughtan, W., Farhat, I. A., Himawan, C., Starov, V. M., & Stapley, A. G. F. (2006). A Differential Scanning Calorimetry Study of the Crystallization. *Journal of the American Oil Chemists' Society*, *83*(1), 1–9. doi:10.1007/s11746-006-1167-1

Marangoni, A. G. (2005). *Fat crystal networks*. New York: Marcel Dekker.

Marangoni, A. G. & Wesdorp, L. H., (2013). *Structure and properties of fat crystal networks*. Boca Raton. Boca Raton, Fla.: CRC Press.

Marangoni, A. G., Acevedo, N., Maleky, F., Co, E., Peyronel, F., Mazzanti, G., … Quinn, B. (2012). Structure and functionality of edible fats. *Soft Matter*, *8*(5), 1275–1300. doi:10.1039/C1SM06234D

Marangoni, A. G., & Lencki, R. W. (1998). Ternary Phase Behavior of Milk Fat Fractions. *Journal of Agricultural and Food Chemistry*, *46*(10), 3879–3884. doi:10.1021/jf9801668

Margules, M. (1895). Über die Zusammensetzung der gesättigten Dämpfe von Misschungen. *Sitzungsberichte Der Kaiserliche Akadamie Der Wissenschaften Wien Mathematisch-Naturwissenschaftliche Klasse II*, *104*, 1243–1278.

Maximo, G. J., Costa, M. C., & Meirelles, A. J. A. (2013). Solid-liquid equilibrium of triolein with fatty alcohols. *Brazilian Journal of Chemical Engineering*, *30*(01), 33–43.

Mazzanti, G., Li, M., Marangoni, A. G., & Idziak, S. H. J. (2011). Effects of Shear Rate Variation on the Nanostructure of Crystallizing Triglycerides. *Crystal Growth & Design*, *11*(10), 4544–4550. doi:10.1021/cg200786k

Mazzanti, G., Marangoni, A. G., & Idziak, S. H. J. (2009). Synchrotron study on crystallization kinetics of milk fat under shear flow. *Food Research International*, *42*(5-6), 682–694. doi:10.1016/j.foodres.2009.02.009

Mazzanti, G., Marangoni, A., & Idziak, S. (2005). Modeling phase transitions during the crystallization of a multicomponent fat under shear. *Physical Review E*, *71*(4), 041607. doi:10.1103/PhysRevE.71.041607

Michalski, M.-C., Ollivon, M., Briard, V., Leconte, N., & Lopez, C. (2004). Native fat globules of different sizes selected from raw milk: thermal and structural behavior. *Chemistry and Physics of Lipids*, *132*(2), 247–61. doi:10.1016/j.chemphyslip.2004.08.007

Mizobe, H., Tanaka, T., Hatakeyama, N., Nagai, T., Ichioka, K., Hondoh, H., … Sato, K. (2013). Structures and Binary Mixing Characteristics of Enantiomers of 1-Oleoyl-2,3-dipalmitoyl-sn-glycerol (S-OPP) and 1,2-Dipalmitoyl-3-oleoyl-sn-glycerol (R-PPO). *Journal of the American Oil Chemists' Society*, *90*(12), 1809–1817. doi:10.1007/s11746-013-2339-4

Morad, N. A., Idrees, M., & Hasan, A. A. (1995). Specific heat capacities of pure triglycerides by heat-flux differential scanning calorimetry. *Journal of Thermal Analysis*, *45*(6), 1449–1461. doi:10.1007/BF02547438

Piska, I., Zárubová, M., Loužecký, T., Karami, H., & Filip, V. (2006). Properties and crystallization of fat blends. *Journal of Food Engineering*, *77*(3), 433–438. doi:10.1016/j.jfoodeng.2005.07.010

Rousset, P., Rappaz, M., & Minner, E. (1998). Polymorphism and solidification kinetics of the binary system POS-SOS. *Journal of the American Oil Chemists' Society*, *75*(7), 857–864. doi:10.1007/s11746-998-0237-y

Sato, K. (1993). Polymorphic transformations in crystal growth. *Journal of Physics D: Applied Physics*, *27 (B77)*. doi:10.1088/0022-3727/26/8B/011

Sato, K. (1999). Solidification and phase transformation behaviour of food fats — a review. *Lipid / Fett*, *101*(12), 467–474. doi:10.1002/(SICI)1521-4133(199912)101:12<467::AID-LIPI467>3.0.CO;2-D

Sato, K. (2001). Crystallization behaviour of fats and lipids — a review. *Chemical Engineering Science*, *56*(7), 2255–2265. doi:10.1016/S0009-2509(00)00458-9

Sato, K., & Garti, N. (2001). *Crystallization processes in fats and lipid systems*. New York: Marcel Dekker.

Sato, K., & Ueno, S. (2011). Crystallization, transformation and microstructures of polymorphic fats in colloidal dispersion states. *Current Opinion in Colloid & Interface Science*, *16*(5), 384–390. doi:http://dx.doi.org/10.1016/j.cocis.2011.06.004

Szydlowska-Czerniak, A., Karlovits, G., Lach, M., & Szlyk, E. (2005). X-ray diffraction and differential scanning calorimetry studies of β' - β transitions in fat mixtures. *Food Chemistry*, *92*(1), 133–141. doi:10.1016/j.foodchem.2004.07.010

Takeuchi, M., Ueno, S., Flöter, E., & Sato, K. (2002). Binary phase behavior of 1,3-distearoyl-2-oleoyl-sn-glycerol (SOS) and 1,3-distearoyl-2-linoleoyl-sn-glycerol (SLS). *Journal of the American Oil Chemists' Society*, *79*(7), 627–632. doi:10.1007/s11746-002-0535-1

Topin, J., Rousset, M., Antonczak, S., & Golebiowski, J. (2012). Kinetics and thermodynamics of gas diffusion in a NiFe hydrogenase. *Proteins: Structure, Function, and Bioinformatics*, *80*(3), 677–682. doi:10.1002/prot.23248

Ueno, S., Ristic, R. I., Higaki, K., & Sato, K. (2003). In Situ Studies of Ultrasound-Stimulated Fat Crystallization Using Synchrotron Radiation. *The Journal of Physical Chemistry B*, *107*(21), 4927–4935. doi:10.1021/jp027840f

Verdonck, E., Schaap, K., & Thomas, L. C. (1999). A discussion of the principles and applications of Modulated Temperature DSC (MTDSC). *International Journal of Pharmaceutics*, *192*(1), 3–20. doi:10.1016/S0378-5173(99)00267-7

Vereecken, J., Graef, V. De, Smith, K. W., Wouters, J., & Dewettinck, K. (2010). Effect of TAG composition on the crystallization behaviour of model fat blends with the same saturated fat content. *Food Research International*, *43*(8), 2057–2067. doi:10.1016/j.foodres.2010.06.008

Wesdorp, L. H., Van Meeteren, J. A., de Jong, S., Giessen, R. V. D., Overbosch, P., Grootscholten, P. A. M., et al. (2013). Liquid-Multiple solid phase equilibria in fats: theory and experiments. In Marangoni, A. G. & Wesdorp, L. H., (Ed.), *Structure and properties of fat crystal networks*. Boca Raton (pp. 241-418). Boca Raton, Fla.: CRC Press.

Winkler, E. M., & Singer, P. C. (1972). Crystallization Pressure of Salts in Stone and Concrete. *Geological Society of America Bulletin*, *83*(11), 3509–3514. doi:10.1130/0016-7606(1972)83[3509:CPOSIS]2.0.CO;2

Zhou, Y., & Hartel, R. W. (2006). Phase behavior of model lipid systems: Solubility of high-melting fats in low-melting fats. *Journal of the American Oil Chemists' Society*, *83*(6), 505–511. doi:10.1007/s11746-006-1233-8

APPENDIX A MASS FRACTION OF EACH COMPONENT IN EACH PHASE OF RBD470

Temperature (°C)	0			5		
Phase	α	β'_1	Liquid	α	β'_1	Liquid
POP	0.0380	0.5242	0.1391	0.0322	0.4527	0.0930
PJP	0.2768	0.0717	0.1279	0.1222	0.1397	0.0992
POO	0.0483	0.0969	0.1559	0.0346	0.0852	0.1254
MOP	0.1512	0.0625	0.0553	0.0920	0.0914	0.0589
POS	0.0473	0.0806	0.1195	0.0262	0.0756	0.0907
POJ	0.0463	0.0281	0.1265	0.0285	0.0303	0.0932
MPJ	0.0299	0.0397	0.0000	0.0202	0.0390	0.0167
PPP	0.0088	0.0338	0.0579	0.0047	0.0298	0.0353
MPP	0.0033	0.0417	0.0000	0.0023	0.0351	0.0069
PJS	0.0552	0.0000	0.0987	0.0317	0.0056	0.0960
MOO	0.0552	0.0000	0.0000	0.1182	0.0000	0.0388
JOO	0.0448	0.0000	0.0000	0.1727	0.0000	0.0000
OOS	0.0370	0.0000	0.0224	0.0240	0.0008	0.0560
MPT	0.0012	0.0169	0.0000	0.0008	0.0132	0.0072
MOJ	0.0385	0.0000	0.0000	0.1239	0.0000	0.0101
SOS	0.0250	0.0029	0.0087	0.0129	0.0008	0.0456
OOO	0.0315	0.0000	0.0000	0.0138	0.0001	0.0439
PJJ	0.0030	0.0000	0.0847	0.0010	0.0001	0.0440
PPS	0.0191	0.0009	0.0034	0.0085	0.0004	0.0302
JOS	0.0181	0.0000	0.0000	0.0697	0.0000	0.0001
JSS	0.0122	0.0000	0.0000	0.0244	0.0001	0.0088
JOJ	0.0093	0.0000	0.0000	0.0356	0.0000	0.0000

Temperature (°C)	10		15		20		
Phase	β'_1	Liquid	β'_1	Liquid	β'_3	β'_2	Liquid
POP	0.4367	0.0639	0.5003	0.0939	0.4910	0.8170	0.2363
PJP	0.1439	0.0824	0.1417	0.1121	0.1284	0.0676	0.1394
POO	0.0895	0.0845	0.0781	0.1086	0.0622	0.0359	0.1107
MOP	0.0921	0.0612	0.0894	0.0792	0.0783	0.0002	0.0985
POS	0.0802	0.0528	0.0805	0.0635	0.0635	0.0001	0.0887
POJ	0.0379	0.0531	0.0314	0.0594	0.0245	0.0000	0.0554
MPJ	0.0301	0.0489	0.0250	0.0512	0.0132	0.0772	0.0439
PPP	0.0248	0.0458	0.0166	0.0531	0.0058	0.0000	0.0470
MPP	0.0242	0.0432	0.0175	0.0483	0.0348	0.0001	0.0259
PJS	0.0157	0.0510	0.0091	0.0494	0.0083	0.0000	0.0344
MOO	0.0073	0.0455	0.0041	0.0359	0.0141	0.0010	0.0166
JOO	0.0042	0.0438	0.0019	0.0320	0.0123	0.0001	0.0131
OOS	0.0027	0.0482	0.0002	0.0344	0.0148	0.0001	0.0108
MPT	0.0034	0.0431	0.0001	0.0330	0.0143	0.0000	0.0103
MOJ	0.0034	0.0384	0.0020	0.0267	0.0038	0.0000	0.0157
SOS	0.0000	0.0465	0.0001	0.0272	0.0136	0.0000	0.0073
OOO	0.0015	0.0367	0.0006	0.0238	0.0008	0.0005	0.0143
PJJ	0.0018	0.0307	0.0011	0.0202	0.0007	0.0000	0.0129
PPS	0.0000	0.0300	0.0001	0.0175	0.0101	0.0000	0.0038
JOS	0.0007	0.0216	0.0004	0.0136	0.0007	0.0000	0.0081
JSS	0.0000	0.0165	0.0000	0.0096	0.0049	0.0000	0.0025
JOJ	0.0001	0.0122	0.0000	0.0073	0.0000	0.0000	0.0044

Temperature (°C)	25			30		
Phase	β'_3	β'_2	Liquid	β'_3	β'_2	Liquid
POP	0.5175	0.7173	0.2964	0.1635	0.0802	0.3803
PJP	0.1023	0.0688	0.1438	0.1025	0.0681	0.1345
POO	0.0370	0.0243	0.1081	0.0491	0.0347	0.0921
MOP	0.0600	0.0115	0.0975	0.0800	0.0512	0.0867
POS	0.0546	0.0004	0.0844	0.0783	0.0667	0.0745
POJ	0.0266	0.0002	0.0473	0.0634	0.0676	0.0389
MPJ	0.0179	0.1726	0.0335	0.0661	0.0541	0.0312
PPP	0.0074	0.0001	0.0373	0.0673	0.0519	0.0258
MPP	0.0365	0.0005	0.0263	0.0540	0.0435	0.0259
PJS	0.0084	0.0002	0.0285	0.0349	0.0473	0.0216
MOO	0.0141	0.0014	0.0157	0.0384	0.0229	0.0130
JOO	0.0133	0.0004	0.0122	0.0334	0.0339	0.0102
OOS	0.0199	0.0005	0.0096	0.0355	0.0350	0.0097
MPT	0.0234	0.0002	0.0078	0.0340	0.0412	0.0093
MOJ	0.0026	0.0002	0.0134	0.0159	0.0559	0.0095
SOS	0.0260	0.0002	0.0042	0.0316	0.0568	0.0071
OOO	0.0004	0.0003	0.0115	0.0034	0.0047	0.0089
PJJ	0.0004	0.0002	0.0103	0.0068	0.0406	0.0073
PPS	0.0203	0.0002	0.0015	0.0240	0.0502	0.0042
JOS	0.0004	0.0002	0.0066	0.0041	0.0508	0.0045
JSS	0.0109	0.0002	0.0009	0.0131	0.0423	0.0021
JOJ	0.0000	0.0000	0.0034	0.0007	0.0003	0.0027

APPENDIX B MASS FRACTION OF EACH COMPONENT IN EACH PHASE OF RBD394

Temperature (°C)	0				5		
Phase	α'_1	α_2	β'	Liquid	α	β'	Liquid
MML	0.0862	0.0948	0.2043	0.0500	0.0332	0.1663	0.0223
MOP	0.0478	0.1830	0.0001	0.0211	0.1073	0.1031	0.0682
POP	0.0641	0.1643	0.0001	0.0211	0.0567	0.1283	0.0498
LMP	0.0793	0.0826	0.2110	0.0302	0.0513	0.1381	0.0276
MMP	0.0794	0.1236	0.0040	0.0340	0.0352	0.1249	0.0311
COP	0.1233	0.0003	0.0402	0.1335	0.0964	0.0273	0.0926
PPM	0.0529	0.0762	0.0189	0.0393	0.0079	0.0900	0.0320
LLM	0.0442	0.0412	0.1712	0.0051	0.1066	0.0397	0.0305
MOM	0.0450	0.0726	0.0001	0.0246	0.0243	0.0612	0.0443
CLM	0.0322	0.0139	0.1511	0.0002	0.0926	0.0110	0.0306
PJP	0.0967	0.0028	0.0029	0.0507	0.0822	0.0069	0.0515
MJP	0.0328	0.0496	0.0001	0.0278	0.0086	0.0436	0.0455
COM	0.0520	0.0002	0.0332	0.0921	0.0486	0.0105	0.0667
CCM	0.0033	0.0001	0.1210	0.0509	0.0464	0.0010	0.0592
POS	0.0289	0.0286	0.0002	0.0179	0.0671	0.0000	0.0273
CJP	0.0376	0.0002	0.0084	0.0786	0.0307	0.0063	0.0548
PPP	0.0074	0.0378	0.0000	0.0150	0.0067	0.0221	0.0352
MJM	0.0180	0.0215	0.0001	0.0280	0.0043	0.0172	0.0392
CJM	0.0132	0.0001	0.0065	0.0471	0.0125	0.0021	0.0327
POO	0.0125	0.0003	0.0008	0.0352	0.0136	0.0000	0.0245
COC	0.0114	0.0002	0.0001	0.0374	0.0091	0.0000	0.0293
PJS	0.0138	0.0006	0.0012	0.0289	0.0175	0.0000	0.0180
MOO	0.0064	0.0003	0.0005	0.0258	0.0085	0.0000	0.0162
ROP	0.0050	0.0003	0.0004	0.0240	0.0073	0.0004	0.0135
PPS	0.0026	0.0036	0.0000	0.0151	0.0063	0.0000	0.0135
CCL	0.0000	0.0000	0.0208	0.0027	0.0042	0.0001	0.0103
COO	0.0015	0.0002	0.0001	0.0180	0.0036	0.0001	0.0100
POJ	0.0010	0.0004	0.0006	0.0170	0.0052	0.0000	0.0075
SOS	0.0007	0.0004	0.0009	0.0145	0.0044	0.0000	0.0066
CCC	0.0008	0.0001	0.0012	0.0141	0.0016	0.0000	0.0095

Temperature (°C)		10		15			20		
Phase	α	β'	Liquid	β'	β	Liquid	β'	β	Liquid
MML	0.0431	0.1355	0.0166	0.1141	0.0230	0.0872	0.1164	0.0327	0.0921
MOP	0.0967	0.1051	0.0729	0.1040	0.0681	0.0876	0.1093	0.0494	0.0889
POP	0.0509	0.1163	0.0364	0.0992	0.0536	0.0868	0.1014	0.0440	0.0883
LMP	0.0532	0.1217	0.0165	0.0999	0.0285	0.0852	0.0996	0.0338	0.0882
MMP	0.0374	0.1090	0.0139	0.0792	0.0448	0.0892	0.0818	0.0369	0.0827
COP	0.0820	0.0369	0.1177	0.0642	0.0461	0.0515	0.0621	0.0456	0.0570
PPM	0.0091	0.0748	0.0150	0.0544	0.0381	0.0614	0.0544	0.0361	0.0583
LLM	0.1105	0.0507	0.0543	0.0577	0.0316	0.0530	0.0538	0.0384	0.0564
MOM	0.0251	0.0563	0.0296	0.0472	0.0473	0.0494	0.0470	0.0421	0.0489
CLM	0.1505	0.0137	0.0737	0.0376	0.0334	0.0346	0.0341	0.0480	0.0377
PJP	0.0443	0.0296	0.0518	0.0332	0.0502	0.0389	0.0326	0.0431	0.0380
MJP	0.0089	0.0410	0.0236	0.0324	0.0543	0.0375	0.0319	0.0435	0.0369
COM	0.0443	0.0129	0.0853	0.0324	0.0431	0.0310	0.0306	0.0434	0.0331
CCM	0.0494	0.0010	0.0891	0.0178	0.0054	0.0383	0.0211	0.0181	0.0280
POS	0.0367	0.0224	0.0221	0.0208	0.0596	0.0241	0.0200	0.0481	0.0250
CJP	0.0268	0.0083	0.0640	0.0214	0.0470	0.0231	0.0204	0.0462	0.0241
PPP	0.0078	0.0242	0.0143	0.0181	0.0403	0.0236	0.0178	0.0364	0.0228
MJM	0.0055	0.0191	0.0197	0.0165	0.0441	0.0196	0.0160	0.0380	0.0199
CJM	0.0121	0.0026	0.0362	0.0101	0.0390	0.0109	0.0095	0.0421	0.0120
POO	0.0101	0.0040	0.0219	0.0074	0.0246	0.0094	0.0071	0.0300	0.0094
COC	0.0097	0.0000	0.0331	0.0013	0.0001	0.0210	0.0033	0.0003	0.0124
PJS	0.0133	0.0044	0.0185	0.0071	0.0444	0.0074	0.0068	0.0411	0.0089
MOO	0.0086	0.0025	0.0138	0.0048	0.0131	0.0064	0.0046	0.0210	0.0061
ROP	0.0111	0.0007	0.0157	0.0042	0.0261	0.0044	0.0040	0.0298	0.0052
PPS	0.0100	0.0033	0.0066	0.0038	0.0320	0.0034	0.0035	0.0323	0.0046
CCL	0.0072	0.0001	0.0117	0.0027	0.0027	0.0043	0.0027	0.0087	0.0037
COO	0.0094	0.0001	0.0100	0.0026	0.0009	0.0041	0.0025	0.0029	0.0035
POJ	0.0113	0.0018	0.0041	0.0025	0.0323	0.0013	0.0023	0.0337	0.0029
SOS	0.0125	0.0017	0.0026	0.0021	0.0239	0.0015	0.0020	0.0267	0.0025
CCC	0.0023	0.0000	0.0095	0.0013	0.0025	0.0042	0.0018	0.0075	0.0027

Temperature (°C)	25			30		
Phase	β'	β	Liquid	β'	β	Liquid
MML	0.0727	0.0310	0.1127	0.0550	0.0101	0.1095
MOP	0.0656	0.0530	0.1086	0.0508	0.0690	0.1041
POP	0.0614	0.0483	0.1051	0.0458	0.1166	0.1001
LMP	0.0649	0.0329	0.1029	0.0637	0.0135	0.0976
MMP	0.0558	0.0363	0.0918	0.0450	0.0366	0.0880
COP	0.0645	0.0425	0.0572	0.0739	0.0364	0.0570
PPM	0.0517	0.0362	0.0585	0.0414	0.0375	0.0590
LLM	0.0602	0.0317	0.0537	0.0662	0.0026	0.0541
MOM	0.0540	0.0417	0.0460	0.0541	0.0265	0.0474
CLM	0.0525	0.0400	0.0305	0.0473	0.0032	0.0351
PJP	0.0428	0.0466	0.0332	0.0378	0.0605	0.0352
MJP	0.0434	0.0471	0.0317	0.0458	0.1281	0.0322
COM	0.0485	0.0407	0.0263	0.0728	0.0295	0.0261
CCM	0.0321	0.0091	0.0227	0.0080	0.0007	0.0279
POS	0.0321	0.0552	0.0196	0.0334	0.0563	0.0212
CJP	0.0352	0.0443	0.0181	0.0486	0.0337	0.0188
PPP	0.0293	0.0380	0.0176	0.0316	0.0477	0.0189
MJM	0.0289	0.0400	0.0144	0.0401	0.0632	0.0146
CJM	0.0199	0.0411	0.0077	0.0348	0.0180	0.0076
POO	0.0148	0.0255	0.0063	0.0161	0.0099	0.0075
COC	0.0032	0.0002	0.0106	0.0006	0.0000	0.0098
PJS	0.0143	0.0416	0.0058	0.0149	0.0200	0.0072
MOO	0.0101	0.0184	0.0039	0.0158	0.0073	0.0040
ROP	0.0090	0.0300	0.0032	0.0141	0.0172	0.0034
PPS	0.0080	0.0381	0.0027	0.0135	0.0447	0.0026
CCL	0.0060	0.0044	0.0023	0.0025	0.0004	0.0035
COO	0.0057	0.0022	0.0022	0.0073	0.0003	0.0025
POJ	0.0054	0.0462	0.0015	0.0099	0.0740	0.0011
SOS	0.0047	0.0333	0.0013	0.0086	0.0362	0.0012
CCC	0.0033	0.0041	0.0021	0.0006	0.0004	0.0027

APPENDIX C DSC and X-RAY ANALYSIS

C1-DSC

TA calibration protocols use the program calibration wizard option where the T4 heat flow option and "cell resistance and capacitance (Tzero), cell constant and temperature calibration" was selected. The calibration included three steps. The Tzero calibration compensates for subtle differences in thermal capacitance and resistance between the reference and sample platforms in the DSC sensor at different temperatures. During the first step, the empty cell was heated from -60 to 250 °C at 20 °C/min. Then, two calibration sapphire discs were heated through the same temperature range. The determined sensor thermal resistance and sensor heat capacity for sample and reference were saved and used for the next DSC experiments. The cell constant is a correction factor used to adjust for subtle differences in the calorimetric (enthalpy) response of a DSC cell. Indium was used as a standard with known enthalpy. It was heated through its melting peak, and the cell constant was calculated by using measured indium enthalpy divided by theoretical value (Al-Qatami, 2011).

C2- XRD

C2.1. Normalizing images

The images opened as a stack (a series of images that share a single window) of 8-bit raw images of size 256 X 256 pixels. All images taken at the same temperature were added together to form a single image by using Z project, then converted to 32-bit, multiplied by 1000 and divided by the number of images added together, and saved as a 16-bit image to finish normalization.

C2.2. Creating radial plot

The XR2D plug-in program for ImageJ was used to reduce the XRD 2D images to 1D plots of intensity as function of scattering vector q. It allows for contrast manipulation and the definition of a region of interest (ROI). Plug-ins can filter or analyze images. Normalized images were opened as a stack of 16 bit unsigned images of size 256 X 256 pixels. The XR2D plug-in (see Figure C2- 1), developed by Stefan Idziak, Gianfranco Mazzanti, Maochen Hannah Wang and Kisun Park, was used to create the radial plots for further analysis, which were created by taking a radial average of intensity at increasing value of q on a diffraction pattern or pixel values. The radial plot provides information on the peak position, the x-ray scattering intensity and the full width at half maximum (FWHM).

The ROI boundary used for each image stack: x Left = 6.0, x Right = 249. 0, y Up = 6.0 and y Down = 249.0. Image analysis was performed using just the pixels within the specified boundary. This ROI was chosen to ensure the exclusion of noise outside the specified boundary, produced by the edges of the silicon chip. This program also has the capability of creating radial plots for a whole stack of images within ROI (see Figure C2-2). The radial plot information was saved in text image format for further analysis.

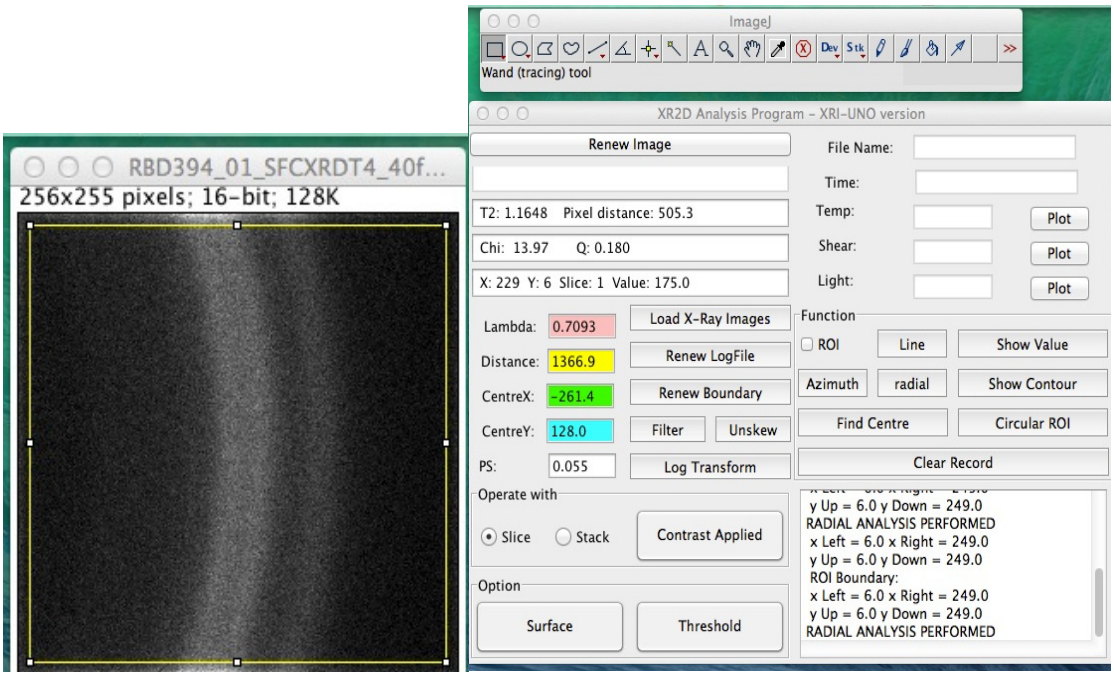

Figure C2- 1. User interface of for the XR2D plug-in for ImageJ displaying a slice of images corresponding to WXRD of RBD394 at 5°C

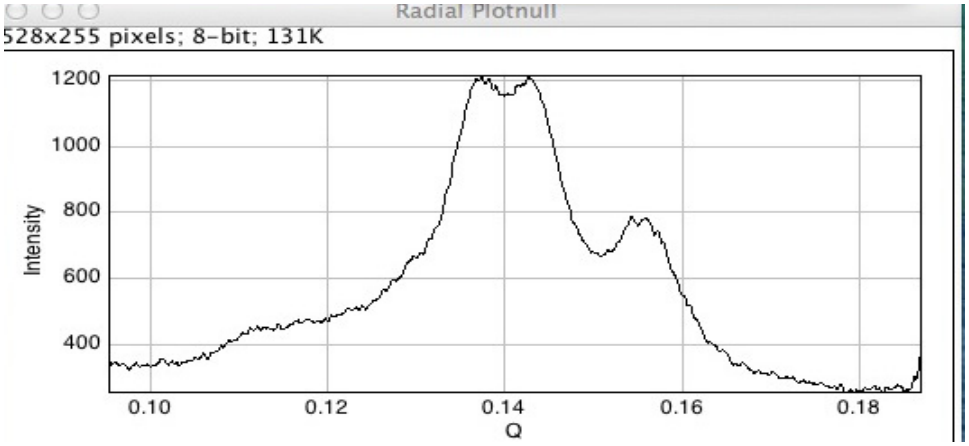

Figure C2- 2 Radial plot of WXRD of RBD394 at 5°C

C2.3. Peak fitting using Igor Pro6

Igor Pro is a statistical analysis program that allows the production of good quality scientific graphs and exports high-resolution graphics formats; it also has the capability to do curve fitting and peak fitting. In SXRD data, each resolved peak represents a polymorphic phase, for WXRD, the number and location of resolved peaks help to identify the type of polymorphic forms.

The normalized radial plot text images were uploaded to Igor pro, and radial plots for all the temperatures were made, such as Figure 4- 3. The Multi-peak Fit package was used to fit each curve. It offers constant, linear and cubic baseline functions. Those baseline functions represent the background intrinsic to the system. The baseline function coefficients can be changed freely by the program to produce a best fit or can be restricted by value. For the analysis in this Thesis, the linear baseline was selected, given the very

low background signal, and the two coefficients were allowed to freely change.

The peak fitting starts with calculation of guess values by the program, after the user selects the distribution functions for the peaks, and traces them visually. Three main distribution functions are used for XRD peak fitting: Gaussian, Lorentzian, Voigt; in this case, a Gaussian distribution was selected for all the peaks user guessed. The experimental data were fitted to a function that is the sum of the distribution functions mentioned above. The sets of parameters of both baseline function and distribution functions were found, when the sum of square of error between experimental data and the combination of these distribution functions become minimum. The program searches for the minimum using the Levenberg-Marquardt algorithm.

A general representation of Gaussian distribution function is (Bevington & Keith Robinson, 1969):

$$p_G = \frac{1}{\sigma\sqrt{2\cdot\pi}}\exp\left[-\frac{1}{2}\left(\frac{x-\mu}{\sigma}\right)^2\right]$$

Where

μ is the mean of the distribution.

σ is the standard deviation of the distribution function.

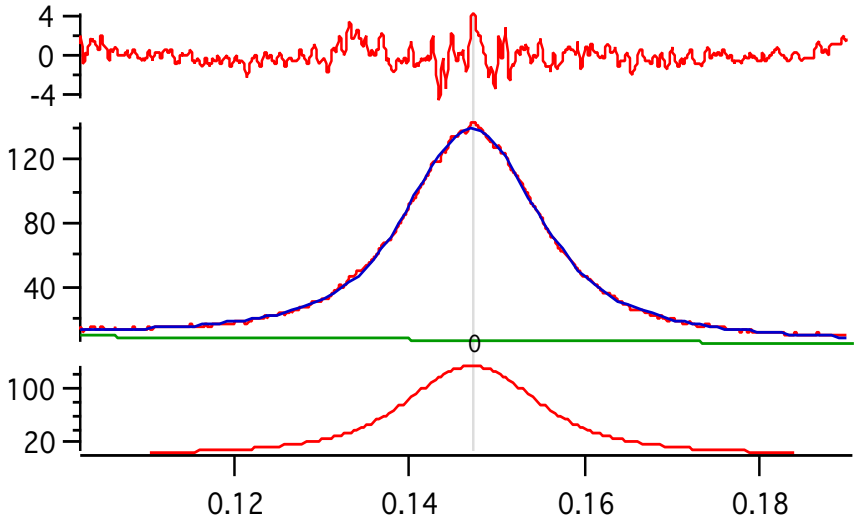

Figure C2- 3 An example of Gaussian distribution curve fitting

APPENDIX D MATLAB CODE OF ESTIMATION OF ENTHALPY AND MELTING TEMPERATURE AND MELTING ENTHALPY

1. MATLAB code for estimation of enthalpy, melting point and molecular weight

```
% Program to estimate the enthalpy, melting point and molecular weight
function [H,T,MW]=DHTF_calcu_V2(TAGMIX)
load DHTFcalcu
mwC=12.0107;
mwH=1.0079;
mwO=15.9994;
n=length(TAGMIX);
for j=1:n
    TAG=TAGMIX(j,1:3);
    for m=1:3
        FA(m)=TAG(1,m);
        id(m)=find(TAG_LIST.letter==FA(m));
        nc(m)=TAG_LIST.nc(id(m));
        sn(m)=TAG_LIST.s(id(m));
        nd(m)=TAG_LIST.u(id(m));
        nct=sum(nc);
        ndt=sum(nd);
          MW(j)=(nct+3)*mwC+6*mwO+14+(nct-3)*2-ndt*2;
    end
    ID=find(strncmp(TAG,Ref.TAG,3));
    if isempty(ID)
          for t=1:3
          [DHc, TFc]=DHTFC(TAG,t,TAG_LIST,EP);
          H(j,t)=DHc;
          T(j,t)=TFc;
          end
     else
           DH(1)=Ref.AlphaH(ID);
          TF(1)=Ref.AlphaT(ID);
          DH(2)=Ref.BetaPH(ID);
          TF(2)=Ref.BetaPT(ID);
          DH(3)=Ref.BetaH(ID);
          TF(3)=Ref.BetaT(ID);
          for t=1:3
                if isnan(DH(t))
                      [DHc, TFc]=DHTFC(TAG,t,TAG_LIST,EP);
                      H(j,t)=DHc;
                else
                      H(j,t)=DH(t);
                end
                if isnan(TF(t))
                      [DHc, TFc]=DHTFC(TAG,t,TAG_LIST,EP);
                      T(j,t)=TFc;
                else
                      T(j,t)=TF(t);
```

```
                end
            end
        end
end
end
% DH & TF model calculation
function [DHc, TFc]=DHTFC(TAG,t,TAG_LIST,EP)
Rg=8.3145;
for m=1:3
        FA(m)=TAG(1,m);
        id(m)=find(TAG_LIST.letter==FA(m));
        nc(m)=TAG_LIST.nc(id(m));
        sn(m)=TAG_LIST.s(id(m));
end
     ncc=sort([nc(1) nc(3)]);
     X=nc(2)-ncc(1);
     Y=ncc(2)-ncc(1);
     if X>6
       X=6;
     End
     if Y>6
       Y=6;
      end
           fxy(t)=2-exp(-((X-EP(8,t))/EP(7,t))^2)-exp(-(Y/EP(7,t))^2);
           DHS(t)=EP(2,t)*sum(nc)+EP(1,t)+EP(5,t)*fxy(t);
           DSS(t)=EP(4,t)*sum(nc)+EP(3,t)+EP(6,t)*fxy(t);
           if Y~=0 && t==3
           DSS(t)=EP(4,t)*sum(nc)+EP(3,t)+EP(6,t)*fxy(t)+Rg*log(2);
       %for alpha we do not need Rg*log(2) term, it fit good for beta
             end
% check TAG is saturated or unsaturated
           if sum(sn)==0
                   DH(t)=DHS(t);
                   TF(t)=DHS(t)*1000/DSS(t)-273.15;
             else
     % calculate nO J N OO JJ NN JO JN ON
         nO=length(find(TAG=='O'));
         nJ=length(find(TAG=='J'));
         nN=length(find(TAG=='N'));
         nOJ=nO*nJ;
         nON=nO*nN;
         nJN=nJ*nN;
     if nO==0
           nOO=0;
      else
           nOO=nO-1;
     end
     if nJ==0
           nJJ=0;
      else
           nJJ=nJ-1;
     end
     if nN==0
           nNN=0;
      else
           nNN=nN-1;
      end
A(t)=EP(13,t)+EP(1,t+3)*nO+EP(3,t+3)*nJ+EP(4,t+3)*nN+EP(5,t+3)*nOO+EP(7,t+3)*nJJ+EP(8,t+3)*nN
```

```
N+EP(9,t+3)*nOJ+EP(10,t+3)*nON+EP(11,t+3)*nJN;
        B(t)=EP(14,t)+EP(12,t+3)*nO+EP(13,t+3)*nJ+EP(14,t+3)*nN;
        TF(t)=EP(9,t)*(1+A(t)/sum(nc)-A(t)*B(t)/(sum(nc)^2))-273.1;
        DH(t)=DHS(t)+EP(10,t)*nO+EP(12,t)*nJ;
        end
DHc=DH(t);
TFc=TF(t);
end
```

The ‘DHTFcalcu’ file includes three matrixes: ‘EP’ is parameters shown in Table 4- 9; ‘Ref’ is a structure array that includes all the information in our database; ‘TAG_LIST’ is also a structure array that includes information in Table 3- 1. ‘t ‘ in the program respect 3 different polymorphic forms. ‘TAGMIX’ is the variable that includes all the name of TAGs in the sample.

2. MATLAB code of estimation of mass fraction of each component in each phase (total three phase)

```
% progam to use mass balance to find x satisfy all row and column then calculate enthalpy--for 3 phases
function [Dn,xhatnew,yhatnew,SSE,SE]=massbalance(TAGMIX,H,T,MW,zhat,shat)
n=length(TAGMIX);
t=2; % choose which phase need to calculate
Dn=zeros(2*n,1);
xzero=zeros(2*n,1);
xone=ones(2*n,1);
for j=1:n
     xzero(j)=-zhat(j)*shat(2);
     xone(j)=zhat(j)*(1-shat(2));
     xzero(n+j)=-zhat(j)*shat(t);
   xone(n+j)=zhat(j)*(1-shat(t));
end
b=zhat*shat(4);
A=sparse([eye(n),eye(n)]);
Aeq=sparse([ones(1,n),zeros(1,n);zeros(1,n),ones(1,n)]);
beq=zeros(2,1);
options=optimoptions('fmincon','Algorithm','interior-point','MaxFunEvals',9000,'AlwaysHonorConstrai
    nts','bounds','ScaleProblem','obj-and-constr','Display','iter');
Dn=fmincon(@error,Dn,A,b,Aeq,beq,xzero,xone,[],options);
          function [SSE]=error(Dn)
                [SSE,xhatnew,yhatnew,SE]=finalcalcu(Dn,TAGMIX,H,T,MW,zhat,shat,t);
          end
 [SSE,xhatnew,yhatnew,SE]=finalcalcu(Dn,TAGMIX,H,T,MW,zhat,shat,t);
end
% to do the final calculation using betaprime as a reference
function [SSE,xhatnew,yhatnew,SE]=finalcalcu(Dn,TAGMIX,H,T,MW,zhat,shat,t)
Rg=8.3145;
Tcc=10;
Tc=Tcc+273.15;
n=length(TAGMIX);
k=zeros(n,3);
for p=1:3
             for j=1:n
             k(j,p)=exp(-(H(j,p)*1000*((T(j,p))-Tc))/(Rg*(T(j,p))*Tc));
             end
end
I1=eye(n)*(-1);
IM=eye(2*n);     %here is 3 phase, eye((p-1)*n), need to change when phase is not 3
Z=sparse([I1,I1;IM]);
Dn2=Z*Dn;
Dm=zeros(n,4);
Dm(1:n,2)=Dn2(n+1:2*n,1);     % beta prime difference
Dm(1:n,t)=Dn2(2*n+1:3*n,1);
Dm(1:n,4)=Dn2(1:n,1);     % liquid difference
mo=zeros(n,4);
for j=1:n
      mo(j,t)=zhat(j)*shat(t);
      mo(j,2)=zhat(j)*shat(2);
      mo(j,4)=zhat(j)*shat(4);
end
mifer=mo+Dm;
xhatnew=zeros(n,3);
```

```
yhatnew=mifer(1:n,4)/shat(4);
xhatnew(1:n,t)=mifer(1:n,t)/shat(t);
xhatnew(1:n,2)=mifer(1:n,2)/shat(2);
%convert mass to mole
        for p=1:3
            [xnew_t]=masstomole(xhatnew,TAGMIX,MW,p);
            xnew(1:n,p)=xnew_t;
        end
   [ynew]=masstomole(yhatnew,TAGMIX,MW,1);
% calculate gamma and use xnew(2) to calculate y
    [gamma]=activitycoefficient(TAGMIX,xnew,T,Tcc);
        for j=1:n
            xnew2(j)=(xnew(j,t)*gamma(j,t)*k(j,t))/(gamma(j,2)*k(j,2));
            ynew2(j)=gamma(j,2)*k(j,2)*xnew(j,2);
            ynew1(j)=gamma(j,t)*k(j,t)*xnew(j,t);
        end
    % calculate SSE
    SE=zeros(n,4);
    SSE=0;
    for j=1:n
        SE(j,t)=ynew(j)-ynew2(j);
        SE(j,2)=xnew(j,2)-xnew2(j);
        SE(j,4)=ynew(j)-ynew1(j);
        SSE1=(SE(j,t)*10)^2;
        SSE2=(SE(j,2)*10)^2;
        SSEL=(SE(j,4)*10)^2;
        SSE= SSE+SSE1+SSE2+SSEL;
    end
end
% program to calculate activity coefficients
function [gamma]=activitycoefficient(TAGMIX,x,T,Tcc)
load TAG_LIST
Rg=8.3145;
Tc=Tcc+273.15;
n=length(TAGMIX);
gamma(1:n,1)=1;
for t=2:3
for j=1:n
    for l=1:n
    TAG1=TAGMIX(j,1:3);
    TAG2=TAGMIX(l,1:3);
        TF(j)=T(j,t);
        TF(l)=T(l,t);
        TFbar(j,l)=(TF(j)+TF(l))/2;
    end
end
% calculate activity coefficients
    [phi]=interactionparameter(TAGMIX,t);
    tempphi=TFbar.*phi;
    gamma(1:n,t)=exp((1/Tc)*(tempphi*x(1:n,t)));
  end
end
% program to convert mass fraction to mole fraction
function [z]=masstomole(zhat,TAGMIX,MW,t)
n=length(TAGMIX);
if zhat(1:n,t)~=0
    TM=sum(zhat(1:n,t)'./MW);
    for j=1:n
        z(j)= (zhat(j,t)'/MW(j))/TM;
```

```
        end
else
        z=zhat(1:n,t);
end
end
% program to convert mole fraction to mass fraction
function [xhat_t]=moletomass(x,TAGMIX,MW,t)
        n=length(TAGMIX);
SM = MW * x(1:n,t);
        for j=1:n
                xhat_t(j)=x(j,t)*MW(j)/SM;
        end
end
% program to calculate interaction parameters
function [phi]=interactionparameter(TAGMIX,t)
load TAG_LIST
n=length(TAGMIX);
for j=1:n
        for l=1:n
        TAG1=TAGMIX(j,1:3);
        TAG2=TAGMIX(l,1:3);
        for m=1:3
                FA1(m)=TAG1(1,m);
                id1(m)=find(TAG_LIST.letter==FA1(m));
                nc1(m)=TAG_LIST.nc(id1(m));
                FA2(m)=TAG2(1,m);
                id2(m)=find(TAG_LIST.letter==FA2(m));
                nc2(m)=TAG_LIST.nc(id2(m));
        end
        Vnon(j,l)=abs(nc1(1)-nc2(1))+abs(nc1(2)-nc2(2))+abs(nc1(3)-nc2(3));
        Vo(j,l)=min(nc1(1),nc2(1))+min(nc1(2),nc2(2))+min(nc1(1),nc2(1));
        EPS(j,l)=1-Vnon(j,l)./Vo(j,l);
        phi(j,l)=0;
        if t==2 && EPS(j,l)<0.93
                phi(j,l)=-19.5*EPS(j,l)+18.2;
        elseif t==2 && EPS(j,l)>0.93
                phi(j,l)=0;
        elseif t==3 && EPS(j,l)<0.98
                phi(j,l)= -35.8*EPS(j,l)+35.9;
        elseif t==3 && EPS(j,l)>0.98
                phi(j,l)=0;
        end
        if    phi(j,l)>8
                phi(j,l)=8;
        end
        end
end
end
```

3. MATLAB code of estimation of mass fraction of each component in each phase (total two phase)

```
% using mass balance to calculate mole fraction of two phase (one solid one liquid)
    function [Dn,xhatnew,yhatnew,SSE,SE]=mbtwophase(TAGMIX,H,T,MW,zhat,shat)
    n=length(TAGMIX);
    t=2; % choose which polymorph need to calculate
    Dn=zeros(n,1);
    xzero=zeros(n,1);
    xone=ones(n,1);
    for j=1:n
         xzero(j)=-zhat(j)*shat(t);
       xone(j)=zhat(j)*(1-shat(t));
    end
    b=zhat*shat(4);
    A=sparse(eye(n));
    Aeq=sparse(ones(1,n));
    beq=zeros(1,1);
    options=optimoptions('fmincon','Algorithm','interior-point','MaxFunEvals',9000,'AlwaysHonorConstrai
        nts','bounds','ScaleProblem','obj-and-constr','Display','iter');
    Dn=fmincon(@error,Dn,A,b,Aeq,beq,xzero,xone,[],options);
            function [SSE]=error(Dn)
                    [SSE,xhatnew,yhatnew,SE]=finalcalcu(Dn,TAGMIX,H,T,MW,zhat,shat,t);
            end
     [SSE,xhatnew,yhatnew,SE]=finalcalcu(Dn,TAGMIX,H,T,MW,zhat,shat,t);
    end
    % to do the final calculation using betaprime as a reference
    function [SSE,xhatnew,yhatnew,SE]=finalcalcu(Dn,TAGMIX,H,T,MW,zhat,shat,t)
    Rg=8.3145;
    Tcc=15;
    Tc=Tcc+273.15;
    n=length(TAGMIX);
    k=zeros(n,3);
    for p=1:3
                for j=1:n
                k(j,p)=exp(-(H(j,p)*1000*((T(j,p))-Tc))/(Rg*(T(j,p))*Tc));
                end
    end
    I1=eye(n)*(-1);
    IM=eye(n);      %here is 2 phase, eye((p-1)*n)
    Z=sparse([I1;IM]);
    Dn2=Z*Dn;
    Dm=zeros(n,4);
    Dm(1:n,t)=Dn2(n+1:2*n,1);      % beta prime difference
    %Dm(1:n,t)=Dn2(2*n+1:3*n,1);
    Dm(1:n,4)=Dn2(1:n,1);      % liquid difference
    mo=zeros(n,4);
    for j=1:n
          mo(j,t)=zhat(j)*shat(t);
          mo(j,4)=zhat(j)*shat(4);
    end
    mifer=mo+Dm;
    xhatnew=zeros(n,3);
    yhatnew=mifer(1:n,4)/shat(4);
    xhatnew(1:n,t)=mifer(1:n,t)/shat(t);
%convert mass to mole
```

```
            for p=1:3
                [xnew_t]=masstomole(xhatnew,TAGMIX,MW,p);
                xnew(1:n,p)=xnew_t;
            end
    [ynew]=masstomole(yhatnew,TAGMIX,MW,1);
% calculate gamma and use xnew(2) to calculate y
    [gamma]=activitycoefficient(TAGMIX,xnew,T,Tcc);
            for j=1:n
                ynew1(j)=gamma(j,t)*k(j,t)*xnew(j,t);
            end
    %calculate SSE
    SE=zeros(n,4);
    SSE=0;
    for j=1:n
        SE(j,4)=ynew(j)-ynew1(j);
        SSEL=(SE(j,4)*10)^2;
        SSE= SSE+SSEL;
    end
end
% program to calculate activity coefficients
function [gamma]=activitycoefficient(TAGMIX,x,T,Tcc)
load TAG_LIST
Rg=8.3145;
Tc=Tcc+273.15;
n=length(TAGMIX);
gamma(1:n,1)=1;
for t=2:3
for j=1:n
    for l=1:n
    TAG1=TAGMIX(j,1:3);    TAG2=TAGMIX(l,1:3);
        TF(j)=T(j,t);
        TF(l)=T(l,t);
        TFbar(j,l)=(TF(j)+TF(l))/2;
    end
end
% calculate activity coefficients
    [phi]=interactionparameter(TAGMIX,t);
    tempphi=TFbar.*phi;
gamma(1:n,t)=exp((1/Tc)*(tempphi*x(1:n,t)));
end
end
% program to convert mass fraction to mole fraction
function [z]=masstomole(zhat,TAGMIX,MW,t)
n=length(TAGMIX);
if zhat(1:n,t)~=0
    TM=sum(zhat(1:n,t)'./MW);
    for j=1:n
        z(j)= (zhat(j,t)'/MW(j))/TM;
    end
else
    z=zhat(1:n,t);
end
end
% program to convert mole fraction to mass fraction
function [xhat_t]=moletomass(x,TAGMIX,MW,t)
    n=length(TAGMIX); SM = MW * x(1:n,t);
    for j=1:n
        xhat_t(j)=x(j,t)*MW(j)/SM;
    end
```

```
end
function [phi]=interactionparameter(TAGMIX,t)
load TAG_LIST
n=length(TAGMIX);
for j=1:n
      for l=1:n
      TAG1=TAGMIX(j,1:3);
      TAG2=TAGMIX(l,1:3);
      for m=1:3
            FA1(m)=TAG1(1,m);
            id1(m)=find(TAG_LIST.letter==FA1(m));
            nc1(m)=TAG_LIST.nc(id1(m));
            FA2(m)=TAG2(1,m);
            id2(m)=find(TAG_LIST.letter==FA2(m));
            nc2(m)=TAG_LIST.nc(id2(m));
      end
      Vnon(j,l)=abs(nc1(1)-nc2(1))+abs(nc1(2)-nc2(2))+abs(nc1(3)-nc2(3));
      Vo(j,l)=min(nc1(1),nc2(1))+min(nc1(2),nc2(2))+min(nc1(1),nc2(1));
      EPS(j,l)=1-Vnon(j,l)./Vo(j,l);
      phi(j,l)=0;
      if t==2 && EPS(j,l)<0.93
            phi(j,l)=-19.5*EPS(j,l)+18.2;
      elseif t==2 && EPS(j,l)>0.93
            phi(j,l)=0;
      elseif t==3 && EPS(j,l)<0.98
            phi(j,l)= -35.8*EPS(j,l)+35.9;
      elseif t==3 && EPS(j,l)>0.98
            phi(j,l)=0;
      end
      if    phi(j,l)>8
            phi(j,l)=8;
      end
      end
end
end
```

4. MATLAB code of estimation of mass fraction of each component in each phase (two β' phase exist)

```
% program to calculate two beta prime and liquid
function [Dn,xhatnew,yhatnew,SSE,SE]=mbtwobetaprime(TAGMIX,H,T,MW,zhat,shat)
n=length(TAGMIX);
t=3; % choose which phase need to calculate
Dn=zeros(2*n,1);
xzero=zeros(2*n,1);
xone=ones(2*n,1);
for j=1:n
    xzero(j)=-zhat(j)*shat(2);
    xone(j)=zhat(j)*(1-shat(2));
    xzero(n+j)=-zhat(j)*shat(t);
   xone(n+j)=zhat(j)*(1-shat(t));
end
b=zhat*shat(4);
A=sparse([eye(n),eye(n)]);
Aeq=sparse([ones(1,n),zeros(1,n);zeros(1,n),ones(1,n)]);
beq=zeros(2,1);
options=optimoptions('fmincon','Algorithm','interior-point','MaxFunEvals',9000,'AlwaysHonorConstrai
    nts','bounds','ScaleProblem','obj-and-constr','Display','iter');
Dn=fmincon(@error,Dn,A,b,Aeq,beq,xzero,xone,[],options);
        function [SSE]=error(Dn
            [SSE,xhatnew,yhatnew,SE]=finalcalcu(Dn,TAGMIX,H,T,MW,zhat,shat,t);
        end
 [SSE,xhatnew,yhatnew,SE]=finalcalcu(Dn,TAGMIX,H,T,MW,zhat,shat,t);
end
% to do the final calculation using betaprime as a reference
function [SSE,xhatnew,yhatnew,SE]=finalcalcu(Dn,TAGMIX,H,T,MW,zhat,shat,t)
Rg=8.3145;
Tcc=20;
Tc=Tcc+273.15;
n=length(TAGMIX);
k=zeros(n,3);
for p=1:3
        for j=1:n
        k(j,p)=exp(-(H(j,p)*1000*((T(j,p))-Tc))/(Rg*(T(j,p))*Tc));
        end
end
I1=eye(n)*(-1);
IM=eye(2*n);    %here is 3 phase, eye((p-1)*n), need to change when phase is not 3
Z=sparse([I1,I1;IM]);
Dn2=Z*Dn;
Dm=zeros(n,4);
Dm(1:n,2)=Dn2(n+1:2*n,1);    % beta prime difference
Dm(1:n,t)=Dn2(2*n+1:3*n,1);
Dm(1:n,4)=Dn2(1:n,1);    % liquid difference
mo=zeros(n,4);
for j=1:n
    mo(j,t)=zhat(j)*shat(t);
    mo(j,2)=zhat(j)*shat(2);
    mo(j,4)=zhat(j)*shat(4);
end
mifer=mo+Dm;
```

```
xhatnew=zeros(n,3);
yhatnew=mifer(1:n,4)/shat(4);
xhatnew(1:n,t)=mifer(1:n,t)/shat(t);
xhatnew(1:n,2)=mifer(1:n,2)/shat(2);

%convert mass to mole
        for p=1:3
            [xnew_t]=masstomole(xhatnew,TAGMIX,MW,p);
            xnew(1:n,p)=xnew_t;
        end
   [ynew]=masstomole(yhatnew,TAGMIX,MW,1);
% calculate gamma and use xnew(2) to calculate y
    [gamma]=activitycoefficient(TAGMIX,xnew,T,Tcc);

        for j=1:n
            xnew2(j)=(xnew(j,t)*gamma(j,t)*k(j,t))/(gamma(j,2)*k(j,2));
            ynew2(j)=gamma(j,2)*k(j,2)*xnew(j,2);
            ynew1(j)=gamma(j,t)*k(j,t)*xnew(j,t);
        end
    %calculate SSE
    SE=zeros(n,4);
    SSE=0;
    for j=1:n
        SE(j,t)=ynew(j)-ynew2(j);
        SE(j,2)=xnew(j,2)-xnew2(j);
        SE(j,4)=ynew(j)-ynew1(j);
        SSE1=(SE(j,t)*10)^2;
        SSE2=(SE(j,2)*10)^2;
        SSEL=(SE(j,4)*10)^2;
        SSE= SSE+SSE1+SSE2+SSEL;
    end
end
% program to calculate activity coefficients
function [gamma]=activitycoefficient(TAGMIX,x,T,Tcc)
load TAG_LIST
Rg=8.3145;
Tc=Tcc+273.15;
n=length(TAGMIX);
gamma(1:n,1)=1;
for t=2:3
for j=1:n
    for l=1:n
    TAG1=TAGMIX(j,1:3);
    TAG2=TAGMIX(l,1:3);
        TF(j)=T(j,2);
        TF(l)=T(l,2);
        TFbar(j,l)=(TF(j)+TF(l))/2;
    end
end
% calculate activity coefficients
    [phi]=interactionparameter(TAGMIX,t);
    tempphi=TFbar.*phi;
gamma(1:n,t)=exp((1/Tc)*(tempphi*x(1:n,t)));
end
end
% program to convert mass fraction to mole fraction
function [z]=masstomole(zhat,TAGMIX,MW,t)
n=length(TAGMIX);
if zhat(1:n,t)~=0
```

```
        TM=sum(zhat(1:n,t)'./MW);
        for j=1:n
            z(j)= (zhat(j,t)'/MW(j))/TM;
        end
else
        z=zhat(1:n,t);
end
end
% program to convert mole fraction to mass fraction
function [xhat_t]=moletomass(x,TAGMIX,MW,t)
        n=length(TAGMIX);
      SM = MW * x(1:n,t);
        for j=1:n
            xhat_t(j)=x(j,t)*MW(j)/SM;
        end
end
function [phi]=interactionparameter(TAGMIX,t)
load TAG_LIST
n=length(TAGMIX);
for j=1:n
        for l=1:n
        TAG1=TAGMIX(j,1:3);
        TAG2=TAGMIX(l,1:3);
        for m=1:3
            FA1(m)=TAG1(1,m);
            id1(m)=find(TAG_LIST.letter==FA1(m));
            nc1(m)=TAG_LIST.nc(id1(m));
            FA2(m)=TAG2(1,m);
            id2(m)=find(TAG_LIST.letter==FA2(m));
            nc2(m)=TAG_LIST.nc(id2(m));
        end
        Vnon(j,l)=abs(nc1(1)-nc2(1))+abs(nc1(2)-nc2(2))+abs(nc1(3)-nc2(3));
        Vo(j,l)=min(nc1(1),nc2(1))+min(nc1(2),nc2(2))+min(nc1(1),nc2(1));
        EPS(j,l)=1-Vnon(j,l)./Vo(j,l);
        phi(j,l)=0;
        if t==3 && EPS(j,l)<0.93
            phi(j,l)=-19.5*EPS(j,l)+18.2;
        elseif t==3 && EPS(j,l)>0.93
            phi(j,l)=0;
        elseif t==2 && EPS(j,l)<0.93
            phi(j,l)= -21.7*EPS(j,l)+18.7; % for beta prime-2
        elseif t==2 && EPS(j,l)>0.93
            phi(j,l)=0;
        end
        if    phi(j,l)>8
            phi(j,l)=8;
        end
        end
end
end
```

5. MATLAB code of estimation of mass fraction of each component in each phase (Two α phases exist, total four phases)

```
% program to calculate two alpha one beta prime & liquid-four phase
function [Dn,xhatnew,yhatnew,SSE,SE]=mbtwoalpha(TAGMIX,H,T,MW,zhat,shat)
n=length(TAGMIX);
t=[1,3]; % choose which phase need to calculate (t=1 is alpha: gamma=1, t=3 is alpha: gamma~=1)
Dn=zeros(3*n,1);
xzero=zeros(3*n,1);
xone=ones(3*n,1);
for j=1:n
     xzero(j)=-zhat(j)*shat(2);
     xone(j)=zhat(j)*(1-shat(2));
     xzero(n+j)=-zhat(j)*shat(t(1));
   xone(n+j)=zhat(j)*(1-shat(t(1)));
     xzero(2*n+j)=-zhat(j)*shat(t(2));
   xone(2*n+j)=zhat(j)*(1-shat(t(2)));
end
b=zhat*shat(4);
A=sparse([eye(n),eye(n),eye(n)]);
Aeq=sparse([ones(1,n),zeros(1,n),zeros(1,n);zeros(1,n),ones(1,n),zeros(1,n);zeros(1,n),zeros(1,n),ones(1
    ,n)]);
beq=zeros(3,1);
options=optimoptions('fmincon','Algorithm','interior-point','MaxFunEvals',20000,'AlwaysHonorConstra
    ints','bounds','ScaleProblem','obj-and-constr','Display','iter');
Dn=fmincon(@error,Dn,A,b,Aeq,beq,xzero,xone,[],options);
  function [SSE]=error(Dn)
        [SSE,xhatnew,yhatnew,SE]=finalcalcu(Dn,TAGMIX,H,T,MW,zhat,shat,t);
   end
 [SSE,xhatnew,yhatnew,SE]=finalcalcu(Dn,TAGMIX,H,T,MW,zhat,shat,t);
end
% to do the final calculation using betaprime as a reference
function [SSE,xhatnew,yhatnew,SE]=finalcalcu(Dn,TAGMIX,H,T,MW,zhat,shat,t)
Rg=8.3145;
Tcc=0;
Tc=Tcc+273.15;
n=length(TAGMIX);
k=zeros(n,3);
for p=1:3
            for j=1:n
            k(j,p)=exp(-(H(j,p)*1000*((T(j,p))-Tc))/(Rg*(T(j,p))*Tc));
            end
end
I1=eye(n)*(-1);
IM=eye(3*n);     % eye((p-1)*n),
Z=sparse([I1,I1,I1;IM]);
Dn2=Z*Dn;
Dm=zeros(n,4);
Dm(1:n,2)=Dn2(n+1:2*n,1);     % beta prime difference
Dm(1:n,t(1))=Dn2(2*n+1:3*n,1);
Dm(1:n,t(2))=Dn2(3*n+1:4*n,1);
Dm(1:n,4)=Dn2(1:n,1);     % liquid difference
mo=zeros(n,4);
for j=1:n
      mo(j,t(1))=zhat(j)*shat(t(1));
      mo(j,t(2))=zhat(j)*shat(t(2));
```

```
        mo(j,2)=zhat(j)*shat(2);
        mo(j,4)=zhat(j)*shat(4);
end
mifer=mo+Dm;
xhatnew=zeros(n,3);
yhatnew=mifer(1:n,4)/shat(4);
xhatnew(1:n,t(1))=mifer(1:n,t(1))/shat(t(1));
xhatnew(1:n,t(2))=mifer(1:n,t(2))/shat(t(2));
xhatnew(1:n,2)=mifer(1:n,2)/shat(2);
%convert mass to mole
            for p=1:3
                [xnew_t]=masstomole(xhatnew,TAGMIX,MW,p);
                xnew(1:n,p)=xnew_t;
            end
   [ynew]=masstomole(yhatnew,TAGMIX,MW,1);
% calculate gamma and use xnew(2) to calculate y
        [gamma]=activitycoefficient(TAGMIX,xnew,T,Tcc);
     for j=1:n
                for j=1:n
                xnew1(j)=(xnew(j,t(1))*k(j,1))/(gamma(j,2)*k(j,2)); %alpha with small mass fraction
    gamma=1 (t(1)=1)
                xnew2(j)=(xnew(j,t(2))*k(j,1)*gamma(j,1))/(gamma(j,2)*k(j,2));
                ynew2(j)=gamma(j,2)*k(j,2)*xnew(j,2);
                ynew1(j)=k(j,1)*xnew(j,t(1));
            end
       %calculate SSE
       SE=zeros(n,4);
       SSE=0;
       for j=1:n
            SE(j,t(1))=xnew(j,2)-xnew1(j);
            SE(j,2)=ynew(j)-ynew2(j);
            SE(j,t(2))=xnew(j,2)-xnew2(j);
            SE(j,4)=ynew(j)-ynew1(j);
            SSE3=(SE(j,t(2))*10)^2;
            SSE2=(SE(j,2)*10)^2;
            SSE1=(SE(j,t(1))*10)^2;
            SSEL=(SE(j,4)*10)^2;
            SSE= SSE+SSE1+SSE2+SSE3+SSEL;
       end
% program to calculate activity coefficients
function [gamma]=activitycoefficient(TAGMIX,x,T,Tcc)
load TAG_LIST
Rg=8.3145;
Tc=Tcc+273.15;
n=length(TAGMIX);
%gamma(1:n,1)=1;
for t=1:2
for j=1:n
       for l=1:n
       TAG1=TAGMIX(j,1:3);
       TAG2=TAGMIX(l,1:3);
            TF(j)=T(j,t);
            TF(l)=T(l,t);
            TFbar(j,l)=(TF(j)+TF(l))/2;
       end
end
% calculate activity coefficients
       [phi]=interactionparameter(TAGMIX,t);
       tempphi=TFbar.*phi;
```

```
        gamma(1:n,t)=exp((1/Tc)*(tempphi*x(1:n,t)));
end
end
% program to convert mass fraction to mole fraction
function [z]=masstomole(zhat,TAGMIX,MW,t)
n=length(TAGMIX);
if zhat(1:n,t)~=0
        TM=sum(zhat(1:n,t)'./MW);
        for j=1:n
                z(j)= (zhat(j,t)'/MW(j))/TM;
        end
else
        z=zhat(1:n,t);
end
end
% program to convert mole fraction to mass fraction
function [xhat_t]=moletomass(x,TAGMIX,MW,t)
        n=length(TAGMIX);
      SM = MW * x(1:n,t);
        for j=1:n
                xhat_t(j)=x(j,t)*MW(j)/SM;
        end
end
function [phi]=interactionparameter(TAGMIX,t)
load TAG_LIST
n=length(TAGMIX);
for j=1:n
        for l=1:n
        TAG1=TAGMIX(j,1:3);
        TAG2=TAGMIX(l,1:3);
        for m=1:3
                FA1(m)=TAG1(1,m);
                id1(m)=find(TAG_LIST.letter==FA1(m));
                nc1(m)=TAG_LIST.nc(id1(m));
                FA2(m)=TAG2(1,m);
                id2(m)=find(TAG_LIST.letter==FA2(m));
                nc2(m)=TAG_LIST.nc(id2(m));
        end
        Vnon(j,l)=abs(nc1(1)-nc2(1))+abs(nc1(2)-nc2(2))+abs(nc1(3)-nc2(3));
        Vo(j,l)=min(nc1(1),nc2(1))+min(nc1(2),nc2(2))+min(nc1(1),nc2(1));
        EPS(j,l)=1-Vnon(j,l)./Vo(j,l);
        phi(j,l)=0;
        if t==2 && EPS(j,l)<0.93
                phi(j,l)=-19.5*EPS(j,l)+18.2;
        elseif t==2 && EPS(j,l)>0.93
                phi(j,l)=0;
        elseif t==3 && EPS(j,l)<0.93
                phi(j,l)=(-19.5*EPS(j,l)+18.2)*0.5; % for alpha-2
        elseif t==1 && EPS(j,l)>0.93
                phi(j,l)=0;
        end
        if    phi(j,l)>8
                phi(j,l)=8;
        end
  end
end
end
```

6. MATLAB code of estimation of melting enthalpy

```
% program to calculate the melting enthalpy
function [Hc,DHc]=enthalpy(TAGMIX,xhatnew,MW,H,T,shat)
load TAG_LIST
Rg=8.3145;
n=length(TAGMIX);
% convert mass to mole
xnew=zeros(n,3);
            for p=1:3
                  [xnew_t]=masstomole(xhatnew,TAGMIX,MW,p);
                  xnew(1:n,p)=xnew_t;
            end
for t=1:2
for j=1:n
      for l=1:n
      TAG1=TAGMIX(j,1:3);
      TAG2=TAGMIX(l,1:3);
            TF(j)=T(j,t);
            TF(l)=T(l,t);
            TFbar(j,l)=(TF(j)+TF(l))/2;
      end
end
% calculate activity coefficients
      [phi]=interactionparameter(TAGMIX,t);
end
for p=1:3
      A=Rg*TFbar.*phi;
    getc=0;
    Hpure=0;
    for j=1:n
          gec=0;
          for l=j+1:n
                gec=gec+A(j,l)*xnew(l,p);
          end
          getc=getc+xnew(j,p)*gec;
          if p==1 || p==3
                Hpure=Hpure+H(j,1)*1000*xnew(j,p);
          else
               Hpure=Hpure+H(j,2)*1000*xnew(j,p);
          end
    end
      Hc(p)=getc+Hpure;
end
% asumme there is 1 mole for each phase, so xnew=nnew; m=nnew*MW
      mnew=zeros(n,3);
      for t=1:3
      mnew(1:n,t)=xnew(1:n,t).*MW'; % units of MW is g/mol
      end
      Mtotal=sum(mnew); % units is g
      Hcm=zeros(1,3);
      for t=1:3
      if Hc(t)~=0
            Hcm(t)=Hc(t)/Mtotal(t);
      end
      end
      DHc=sum(Hcm.*shat(1:3));
```

```
end
function [phi]=interactionparameter(TAGMIX,t)
load TAG_LIST
n=length(TAGMIX);
for j=1:n
      for l=1:n
      TAG1=TAGMIX(j,1:3);
      TAG2=TAGMIX(l,1:3);
      for m=1:3
            FA1(m)=TAG1(1,m);
            id1(m)=find(TAG_LIST.letter==FA1(m));
            nc1(m)=TAG_LIST.nc(id1(m));
            FA2(m)=TAG2(1,m);
            id2(m)=find(TAG_LIST.letter==FA2(m));
            nc2(m)=TAG_LIST.nc(id2(m));
      end
      Vnon(j,l)=abs(nc1(1)-nc2(1))+abs(nc1(2)-nc2(2))+abs(nc1(3)-nc2(3));
      Vo(j,l)=min(nc1(1),nc2(1))+min(nc1(2),nc2(2))+min(nc1(1),nc2(1));
      EPS(j,l)=1-Vnon(j,l)./Vo(j,l);
      phi(j,l)=0;
      if t==2 && EPS(j,l)<0.93
            phi(j,l)=-19.5*EPS(j,l)+18.2;
      elseif t==2 && EPS(j,l)>0.93
            phi(j,l)=0;
      elseif t==3 && EPS(j,l)<0.98
            phi(j,l)= -35.8*EPS(j,l)+35.9;
      elseif t==3 && EPS(j,l)>0.98
            phi(j,l)=0;
      end
      if    phi(j,l)>8
            phi(j,l)=8;
      end
      end
end
end
% program to convert mass fraction to mole fraction
function [z]=masstomole(zhat,TAGMIX,MW,t)
n=length(TAGMIX);
if zhat(1:n,t)~=0
      TM=sum(zhat(1:n,t)'./MW);
      for j=1:n
            z(j)= (zhat(j,t)'/MW(j))/TM;
      end
else
      z=zhat(1:n,t);
end
end
```

The function to calculate the interaction parameters needed to change for the condition that same polymorph has different phase.